1996

Studies of structures and phase transitions in pyrrhotite

Fan Li
Iowa State University

INFORMATION TO USERS

This manuscript has been reproduced from the microfilm master. UMI films the text directly from the original or copy submitted. Thus, some thesis and dissertation copies are in typewriter face, while others may be from any type of computer printer.

The quality of this reproduction is dependent upon the quality of the copy submitted. Broken or indistinct print, colored or poor quality illustrations and photographs, print bleedthrough, substandard margins, and improper alignment can adversely affect reproduction.

In the unlikely event that the author did not send UMI a complete manuscript and there are missing pages, these will be noted. Also, if unauthorized copyright material had to be removed, a note will indicate the deletion.

Oversize materials (e.g., maps, drawings, charts) are reproduced by sectioning the original, beginning at the upper left-hand corner and continuing from left to right in equal sections with small overlaps. Each original is also photographed in one exposure and is included in reduced form at the back of the book.

Photographs included in the original manuscript have been reproduced xerographically in this copy. Higher quality 6" x 9" black and white photographic prints are available for any photographs or illustrations appearing in this copy for an additional charge. Contact UMI directly to order.

UMI

A Bell & Howell Information Company
300 North Zeeb Road, Ann Arbor MI 48106-1346 USA
313/761-4700 800/521-0600

Studies of structures and phase transitions in pyrrhotite

by

Fan Li

A dissertation submitted to the graduate faculty

in partial fulfillment of the requirements for the degree of

DOCTOR OF PHILOSOPHY

Major: Physical Chemistry

Major Professor: Hugo F. Franzen

Iowa State University

Ames, Iowa

1996

Graduate College
Iowa State University

This is to certify that the Doctoral dissertation of

Fan Li

has met the dissertation requirements of Iowa State University

Signature was redacted for privacy.

Major Professor

Signature was redacted for privacy.

For the Major Program

Signature was redacted for privacy.

For the Graduate College

TABLE OF CONTENTS

CHAPTER 1

GENERAL INTRODUCTION

The compounds in the $Fe_{1-x}S$ system (x=0-0.13), in mineralogy, are collectively called pyrrhotite, and the 1:1 stoichoimetric iron sulfide (FeS) with a $\sqrt{3} \times \sqrt{3} \times 2$ superstructure is particularly called troilite. Because of its important structural, electrical, magnetic and thermal properties, for over one century this system has been the subject of considerable interest for a wide range of disciplines. The prototypic structure of this system is NiAs-type, but a number of structure - and superstructure types resulting from the low-temperature vacancy ordering and structural distortions have been reported in this narrow composition range between room temperature and 700K. The most abundant pyrrhotites in nature are the monoclinic (4C), troilite (2C) and the intermediate pyrrhotites. The latter tend to be more wide-spread and can be generally categorized as nC type, of which the 5C, 6C and 11C types are special cases (in this thesis A and C refer to axial lengths of NiAs-type cell, A=3.44Å and C=5.70Å). Table 1 lists the superstructures reported for the natural pyrrhotites [1]. Apart from these crystallographic modifications, at least two magnetic transitions and one electrical transition are known to be involved in this system below 600K: At 600K the order-disorder transition (the so called β-transition) for magnetic spins occurs, which, in fact, is a Curie transition for the ferrimagnetic phases and a Neel transition for the antiferromagnetic phases. This magnetic transition is insensitive to composition. Below T_β, a second magnetic transition (called the Morin

Table 1. The structure types found in the naturally occurring pyrrhotites

Composition (at.% Fe)	Symmetry	Superstructure type (cell size, Å)	Remarks
50.0 (FeS)	Hexagonal	$\sqrt{3}$ A, 2C. a=5.96, c=11.75	natural troilite
~46.7 (Fe_7S_8)	Monoclinic	$2\sqrt{3}$ A, 2A, 4C. a=11.90, b=6.87, c=22.87, β=90°30′	magnetic pyrrhotite
~47.4 (~Fe_9S_{10})	Hexagonal	2A, 5C. a=6.88, c=28.7	5C pyrrhotite
~47.8 (~$Fe_{11}S_{12}$)	Hexagonal	2A, 6C. a=6.89, c=34.48	6C pyrrhotite
~47.6 (~$Fe_{10}S_{11}$)	orthorhombic	2A, 2B, 11C. a=6.89, b=11.95, c=63.18	11C pyrrhotite. In reality, it is a mixing of 5C and 6C
47.4→ 47.8 (Fe_9S_{10}→ $Fe_{11}S_{12}$)	orthorhombic or Monoclinic	2A, 2B, nC where n is a non-integer between 4.8 and 6	nC pyrrhotite.

transition) occurs for which the magnetic spins rotate from the orientation lying in the a-b plane for $T > T_M$ to the orientation parallel to c-axis for $T < T_M$. This change in spin orientation has been proved by neutron diffraction and the measurement of the anisotropy of the magnetic susceptibility as a function of temperature [2-4]. The temperature point for this transition is sensitively dependent on the composition. For FeS with the troilite structure type, T_M is found to be at 135°C, but theoretical and experiential investigations indicate that the transition temperature dramatically decreases with increasing iron deficiency [5-7]. On the other hand, the electrical properties also have a direct relationship with the compositions. At room temperature, troilite is considered to be a ferroelectric semiconductor, while Fe_7S_8 exhibits a high conductivity. The former undergoes a so-called α-transition at a temperature close to T_M (~120°C) for which the

material is transformed into a paraelectric conductor with a sharp increase of conductivity in the *c* direction. With an increase of x in $Fe_{1-x}S$, as for T_M, the temperature for this α-transition declines almost linearly [8,9].

In spite of the voluminous literature about the pyrrhotite system, a number of the most important properties have still remained open to interpretation. These questions involve (1) the nature of the transitions (α-, β- and γ-transitions discussed in the following papers), (2) the ordering of vacancies as a function of temperature and composition, and (3) the relation between structure and properties.

The understanding of structural properties and phase relations in pyrrhotite is of special significance for the metallurgical industry and mineralogy. The most common nickel- and copper-bearing minerals are pentlandite $(Fe, Ni)_9S_8$ and chalcopyrite ($CuFeS_2$), the former accounts for about three-quarters of the nickel mined in the world, the latter also accounts for most of copper mined. However these sulfide minerals are easily intergrown with pyrrhotite. From the outset, therefore, the separation of sulfide Ni/Cu ores from pyrrhotite has been central to the metallurgy of Ni and Cu [10, 11]. Figure 1 is a flowsheet showing the separation process performed in Inco as well as other Ni/Cu producers. As can be noted, two of the most important steps-- the magnetic separation and froth flotation-- depend critically on the structural characteristics of pyrrhotite. The former actually takes advantage of the magnetic properties in pyrrhotite, while the latter greatly relies on the surface chemical properties that are essentially determined by a variety of factors among which the most important are chemical composition, crystal structure and the morphology of the minerals.

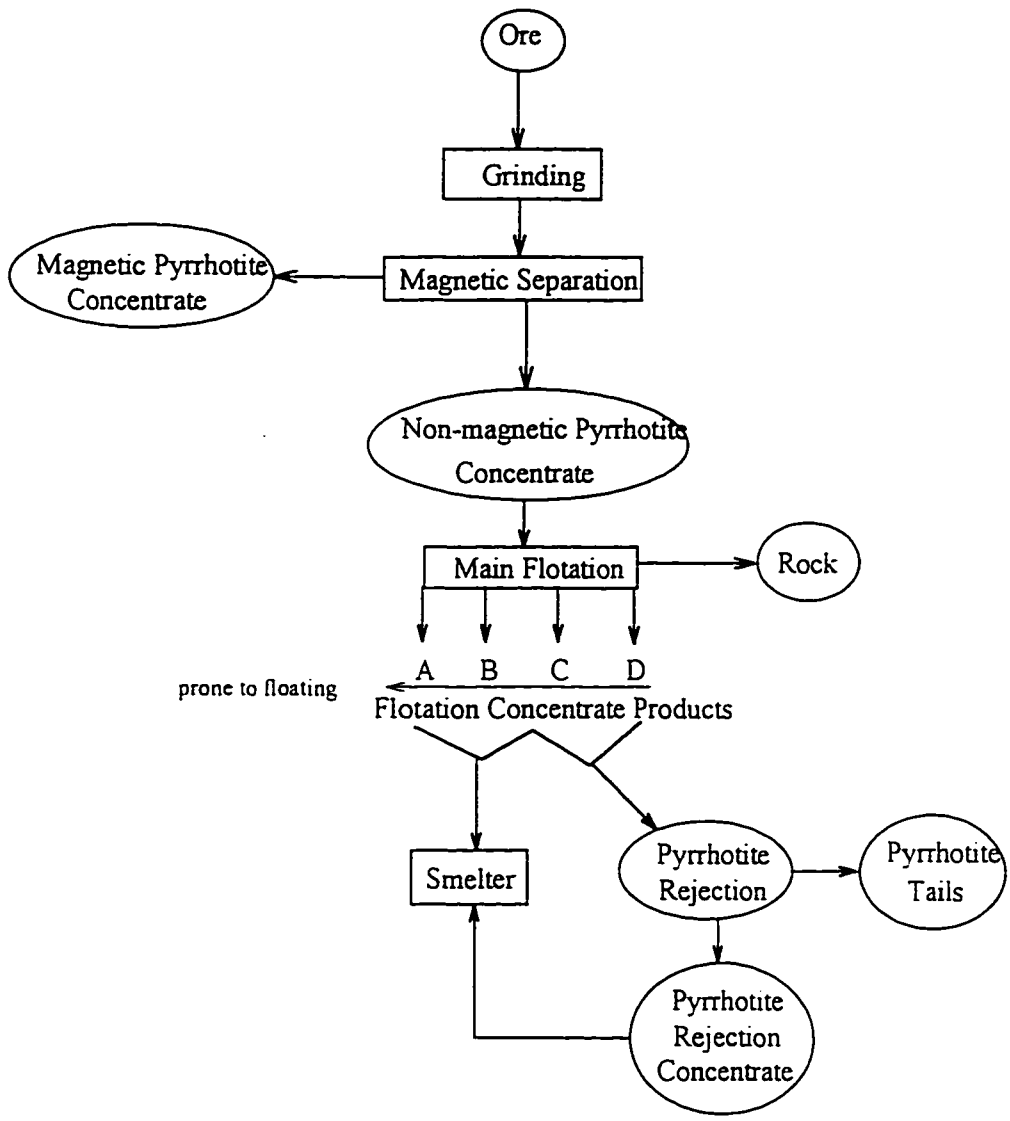

FIGURE 1. A flowsheet of extractive separation of pyrrhotite in Ni/Cu Metallurgy

In this research, we have undertaken a systematic investigation of various compositions of iron sulfide including high-temperature structure determination (x-ray and electron diffractions), thermal and thermomagnetic property characterization. It is the goal of the author to establish a thorough understanding of the phase relations as functions of both the temperature and composition, and thus to provide a basis for the consideration of pyrrhotite separations in minerals.

Dissertation Organization

This dissertation consists of four papers. Chapter 3 ("From Pyrrhotite to Troilite: An Application of Landau Theory of Phase Transition", which has been published in Journal of Alloy and Compounds) and Chapter 4 ("Phase Transitions In Near Stoichiometric Iron Sulfide", which has been published in JAC) mainly concern the theoretical and experimental investigation of phase transitions for the near 1:1 stoichoimetric iron sulfide. Chapter 5 ("Ordering, Incommensuration and Phase Transitions in Non-stoichiometric Iron Sulfides. Part I: A TEM Study of Fe_7S_8", which has been published in JSSC) will focus on the phase transitions in Fe_7S_8. Chapter 6 (Ordering, Incommensuration and Phase Transitions in Non-stoichiometric Iron Sulfides. Part II: A High-Temperature X-Ray Powder Diffraction and Thermomagnetization Study", which has been published in JSSC) will involve an investigation of the intermediate iron sulfides over the composition range between those two extreme cases, FeS and Fe_7S_8. Preceding these papers is a general experimental chapter (Chapter 2) and following these papers is a chapter in which general conclusions and a comprehensive phase diagram for this system are presented.

References

[1] Vaughan, D. J. and Craig, J. R., "Mineral Chemistry of Metal Sulfides", Cambridge University Press, New York (1978).

[2] Hirahara, E., and Murakami, M., Phys. Chem. Solid, **7**, 281 (1958).

[3] Sparks, J. T. Mead, W., Kirschbaum, A. J., and Marshall, W., J. Appl. Phys., **Suppl. 31**, 356S (1960).

[4] Sparks, J. T. Mead, W. and Komoto, T., J. Phys. Soc. Japan, **Suppl. 17**, 249 (1962).

[5] Andresen, A. F. and Torbo, P., Acta. Chem. Scand., **21**, 2841 (1967).

[6] Adachi, K., and Sato, K., J. Appl. Phys., **39 (2)**, 1343 (1968).

[7] Horwood, J. L., Townsend, M. G., and Webster, A. H., J. Solid State Chem., **17**, 35 (1967).

[8] van der Berg, C. B., Ferroelectrics, **4**, 117 (1972).

[9] Coey, J. M. D., Roux-Buisson, H., and Brusetti, R., J. de. Physique, C4, 1 (1976).

[10] Biswas, A. K., and Davenport, W.G., "Extractive Metallurgy of Copper" (3rd Ed.), Pergamon, Tarrytown, NY (1994).

[11] Joseph, R. B., Jr. and Queneau, P., "The Winning of Nickel: Its Geology, Mining and Extractive Metallurgy", Longmans Canada Limited, Toronto (1967).

CHAPTER 2

EXPERIMENTAL SECTION

Sample Preparation

The samples used for this project were synthesized from high-purity iron (Johnson-Matthey, 5N, -20 mesh) and sulfur powders (Aldrich, Sublimed, -100 mesh), the latter was pressed into pellets before mixing with iron powder. Carefully weighed quantities of iron and sulfur were sealed in evacuated silica-glass tubes which were then heated in a tube furnace. The samples were at first heated to 410°C and then gradually to 500°C. As sulfur boiled and vaporized over this temperature range, it diffused to the cooler end of the silica tube where the iron powder was placed so that the reaction between these two elements could take place. The temperature was controlled below 500°C until no yellow sulfur vapor was visible (approximately one week). The samples were annealed at 800°C for 20-30 days, and a very slow cooling followed. At the rate of -5°C/h, the samples were cooled to 600°C and annealed at this temperature for two weeks, and finally cooled down to room temperature at a rate of 3°C/h. After these steps the recovery percentage of products was determined to be 99-100%. If the samples were found to be non-homogenous, they were ground and re-loaded into the evacuated capsules for a second annealing. At this time the samples were first heated between 400-500°C for one day and then annealed at 800°C for 10 days. For some cases nonuniform samples were heated to

1200°C for a few hours before they were annealed at 800°C. Finally, the samples were cooled as described above.

The compositions of the final products were verified using the Electron Microprobe (ARL, SEMQ). The operating conditions were 20kV accelerating voltage and 25 nA beam current. Under these conditions both Fe and S were determined on WDS spectrometers (LiF crystal for Fe, PET crystal for S), and count rates were about 10,000s^{-1}. Three samples, $Fe_{0.885}S$, $Fe_{0.967}S$ and $Fe_{0.980}S$, prepared by Dr. Paul G. Spry [1] were used for standards. The theoretical error from counting statistics for a counting time of 10s was about 0.3%; the actual reproducibility as determined by a series of counts on the standards usually gave standard deviations of 0.6 to 0.8%. The compositional variations in different areas of the sample were found to be within these limits. Thus the standard deviation of the measured stoichiometry was less than 1%, and good sample homogeneity was further indicated by the absence of any significant anticorrelation between measured concentrations of Fe and S. The EMP analysis results and preparation conditions for the representative samples are listed in Table 2.

In addition to the synthetic samples, naturally occurring pyrrhotites were kindly provided by Inco Limited, Canada. The shipped samples were in the frozen slurry form. In our laboratory, they were heated to dry at 100-120°C in glass tubes under pure flowing nitrogen. Detailed descriptions of these natural samples are summarized in Table 3.

TABLE 2. The Representative $Fe_{1-x}S$ Samples Prepared in This Research

sample number	mixed Fe/S ratio	synthesis condition	the no. of points analyzed by EMP	actual Fe/S ratio (EMP result)
1	9:10	800°C, 20 days	8	0.887±0.010
16	7:8	800°C for 20 days; 1200°C for 12 hrs, then 700°C for 10 days	14	0.876±0.007
18	7:8	800°C for 10 days, and 700°C for 20 days.	60	0.875±0.004
21	11:12	same as no. 18	57	0.906±0.006
22	15:16	same as no. 18	43	0.925±0.004
52	1:1	800°C for 10 days, re-sealed and annealed at 800°C for another 10 days	34	1.002±0.012
53	1:1	same as no. 52	30	0.996±0.010

TABLE 3. A Description of the Natural Pyrrhotites Provided By Inco.

Name of sample	Inco 1	Inco 2	Inco 3	Inco 4	Inco 5	Inco 6
Source of Product	mag. concentrates after mag. separation	non-magnetic concentrates after mag. separation	fast flotation portion in floating separation (i.e., concentrates A and B)	slow flotation portion in floating separation (i.e., concentrates C and D	reject pyrrhotite tails	pyrrhotite rejection concentrate

In Situ High-Temperature Powder X-ray Diffraction (HTXRD).

The HTXRD experiments were carried out using a high-temperature powder diffractometer (Elliott GX21) with a multifunctional cylindrical chamber and a gas-flow proportional curved position sensitive detector (Inel CPS120 and Canberra ADC8715). V-filtered Cr radiation was used. The sample holder was a Ta-strip with a depression of 10mm x 6mm x 1.5mm in the center. Temperatures were measured with a chromel-alumel thermocouple that was spot welded to the bottom of the Ta-strip. The temperatures were controlled using a RE2400 thermocontroller with a precision of 0.01 mV. Temperature differentials in the sample region were determined to be less than 5°C. Using this diffractometer a satisfactory pattern can be obtained in about 1 minute, but the collection time for all patterns shown was set to 10 minutes in order to improve the counting statistics. The HTXRD measurements were performed under a vacuum of $\sim 10^{-4}$ Torr. The temperature measured during HTXRD was also calibrated using an organic sample, tris-(o-phenylenedioxy) cyclotriphosphazene, which has a melting point of 250^{0}C as determined by DSC and showed a melting transition at 251^{0}C on HTXRD.

Differential Thermal Analysis Experiment (DTA)

A Perkin-Elmer DTA 1700 with System 7/4 thermal controller was used for DTA studies. The sample powder was accurately weighed, and then loaded into an alumina crucible. The reference arm was loaded with Al_2O_3. The heating and cooling rates were usually 5K/min. The Ar-gas flow with O_2 impurity < 40ppm was maintained throughout the course of experiments. Finally, the differential temperature (ΔT) in all the DTA figures were consistently expressed as the degrees per milligram of sample.

High-Temperature Thermomagnetization Measurement (HTM)

Thermal magnetization measurements were carried out using a Vibrating Sample Magnetometer (VSM 4500, EG&G). The samples were accurately weighed and loaded into a BN sample holder. The applied magnetic field was between 1500 Oe and 22,000 Oe, depending on the magnetization of the sample. A pure argon atmosphere with O_2 impurity < 40ppm was maintained in the sample cylinder during the measurement.

Transmission Electron Microscopy (TEM)

For TEM observation the samples were crushed in a mortar and pestle into <400 mesh and mixed with ethanol. A single drop of the suspension was placed onto a holly carbon grid and allowed to air dry. Once dried, the sample was examined using a Philips CM30 TEM with a heating stage. All the selected area diffraction patterns in Fig. 3 of Chapter 5 were obtained from the same region of the crystal using a 50 μm aperture (i.e., the region near the tip of the crystal indicated by a arrow in Fig. 7(a)). In-situ heating was performed using a double tilt hot stage (Gatan, Model 628-0500) with a temperature monitor and a Pt/Rh thermocouple mounted at the edge of the sample. The heater current was manually adjusted, and the measured temperature, according to prior calibration, is within ±10°C of the sample temperature. Since the sample had been confirmed to have a Curie transition at 315°C, the highest heating temperature was 340°C.

References

[1] L. T. Bryndzia, S. D. Scott and P. G. Spry, *Econ. Geol.*, **83,** 1193 (1988).

CHAPTER 3

FROM PYRRHOTITE TO TROILITE: AN APPLICATION OF LANDAU THEORY OF PHASE TRANSITION

A paper published in the Journal of Alloy and Compounds

Fan Li and Hugo F. Franzen

FeS has been extensively studied because of the importance and complexity of its phase relations, structure and magnetic properties. Among numerous allotropes, representative are high-temperature pyrrhotite with the NiAS-type structure and troilite with space group $P\bar{6}2c$ and a unit cell of $a = \sqrt{3}\,A$ and $c = 2C$ (where A and C refer to unit cell parameters of the NiAs-type structure and are approximately 3.4 Å and 5.9 Å, respectively). The transition between these two related phases has been observed by various methods, and in some reports, has been suggested to be of second order [1-3]. The Landau theory has been, in previous studies, successfully applied to a number of phase transitions in structures with $P6_3/mmc$ symmetry [4-6]. In this report we contribute a new application of Landau theory to a symmetry breaking transition for NiAs-type ($P6_3/mmc$) in order to increase our understanding of this relatively high symmetry and its broken symmetries.

In the consideration of a second order phase transitions, the first condition of Landau theory requires that the space groups of the related structures be in the relation of a group and a subgroup [7]. Accordingly, in reciprocal space, a wave vector (**k**), or a set of equivalent wave

vectors in a star to which the distortion corresponds, need to be determined. The $\sqrt{3} \times \sqrt{3} \times 2$ superstructure characterizes the wave vector $\mathbf{k}=(\frac{1}{3},\frac{1}{3},\frac{1}{2})$ or its inverse $\mathbf{k}^{*}=(\frac{\bar{1}}{3},\frac{\bar{1}}{3},\frac{\bar{1}}{2})$. These two vectors are not equal modulo a reciprocal lattice vector and thus are separately in a star. All other wave vectors formed from **k** by rotations in D_{6h}, nevertheless, are equivalent to **k** or $\mathbf{k}^{*}$ modulo a reciprocal lattice vector **K** (see the figure 1). Therefore, **k** and $\mathbf{k}^{*}$ form a complete star (corresponding to the H-point in the Brillouin zone) which associates a subgroup with $P6_3/mmc$. In this case the two vectors in the star correspond to exactly the same lattice points and the same rotations, and not as more frequently occurs, to two different examples (different axial directions) of the same subgroup.

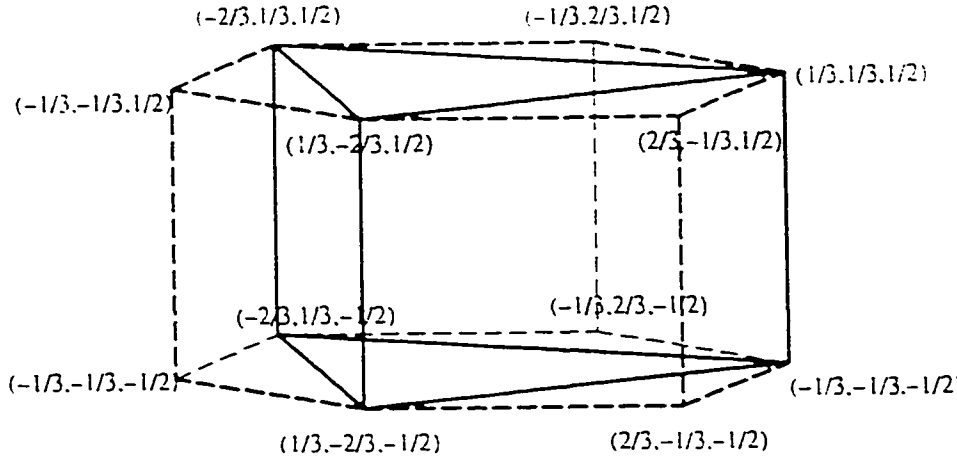

FIGURE 1. Hexagonal Brillouin zone showing H points (Trigonal prism connects points equal module a reciprocal lattice vector)

The second condition of Landau theory is that the transition should correspond to a single irreducible representation of the space group of higher symmetry. The significance of the correspondence is that the particle density function (ρ) for the low symmetry can be completely projected onto the basis functions (φ_i's) for a single irreducible representation which belongs to the space group of the particle density (ρ°) of the high symmetry, i.e.

$$\rho = \rho^\circ + \eta \cdot \Sigma \ \gamma_i \cdot \varphi_i$$

For the case of the H-point of $P6_3/mmc$ the small representations are two-dimensional. In light of the symmetry implied by the wave vectors to which the phase transition corresponds, two basis functions for an irreducible representation of $P6_3/mmc$ at the H-point are:

$$\varphi_1=\cos(\pi z)\times\{\sin[\tfrac{2}{3}\pi(x+y)]+\sin[\tfrac{2}{3}\pi(x-2y)\}+\sin[\tfrac{2}{3}\pi(y-2x)]\}$$

$$\varphi_2=\sin(\pi z)\times\{\sin[\tfrac{2}{3}\pi(x+y)]+\sin[\tfrac{2}{3}\pi(x-2y)\}+\sin[\tfrac{2}{3}\pi(y-2x)]\}$$

and a two-dimensional irreducible representation follows immediately. Table 1 lists a small irreducible representation together with the representations for R+**c**. This table facilitates finding the operations $\{\beta|\mathbf{t}\}$ and $\{\beta|\mathbf{t}+\mathbf{c}\}$ that remain (leave $\varphi_1 + \varphi_2$, φ_1 or φ_2 invariant) in the broken symmetry.

Use will be made of this irreducible representation later. First we consider the other two conditions of Landau theory. That the third condition of Landau is met follows from the fact that there are a number of representations which carry the two γ_i's into their negatives. It is impossible, therefore, to find a third-order invariant combination of these coefficients.

Furthermore, the fourth condition of Landau (called the Lifshitz criterion) is used to determine whether a minimum in the Gibbs free energy as a function of wave vectors is fixed at

TABLE 1. Small Representation of $P6_3/mmc$ at $k=(1/3, 1/3, 1/2)$ and the Symmetries of the Basis Functions and Their Sum

operation element $\{\beta\|t\}$	irr. rep. for φ_1 and φ_2 under $\{\beta\|t\}$	Present in distorted struc.? φ_1 φ_2 $\varphi_1+\varphi_2$	irr. rep. for φ_1 and φ_2 under $\{\beta\|t+c\}$	Present in distorted struc.? φ_1 φ_2 $\varphi_1+\varphi_2$
$\{\varepsilon\|000\}$	$\begin{pmatrix} 1 & 0 \\ 0 & 1 \end{pmatrix}$	yes yes yes	$\begin{pmatrix} \bar{1} & 0 \\ 0 & \bar{1} \end{pmatrix}$	no no no
$\{C_{6z}\|00\frac{1}{2}\}$	$\begin{pmatrix} 0 & \bar{1} \\ 1 & 0 \end{pmatrix}$	no no no	$\begin{pmatrix} 0 & 1 \\ \bar{1} & 0 \end{pmatrix}$	no no no
$\{C_{3z}\|000\}$	$\begin{pmatrix} 1 & 0 \\ 0 & 1 \end{pmatrix}$	yes yes yes	$\begin{pmatrix} \bar{1} & 0 \\ 0 & \bar{1} \end{pmatrix}$	no no no
$\{C_{2y}\|000\}$	$\begin{pmatrix} \bar{1} & 0 \\ 0 & 1 \end{pmatrix}$	no yes no	$\begin{pmatrix} 1 & 0 \\ 0 & \bar{1} \end{pmatrix}$	yes no no
$\{C_{2(x-y)}\|00\frac{1}{2}\}$	$\begin{pmatrix} 0 & \bar{1} \\ \bar{1} & 0 \end{pmatrix}$	no no no	$\begin{pmatrix} 0 & 1 \\ 1 & 0 \end{pmatrix}$	no no yes
$\{i\|000\}$	$\begin{pmatrix} 1 & 0 \\ 0 & \bar{1} \end{pmatrix}$	yes no no	$\begin{pmatrix} \bar{1} & 0 \\ 0 & 1 \end{pmatrix}$	no yes no
$\{\sigma_y\|000\}$	$\begin{pmatrix} \bar{1} & 0 \\ 0 & \bar{1} \end{pmatrix}$	no no no	$\begin{pmatrix} 1 & 0 \\ 0 & 1 \end{pmatrix}$	yes yes yes
$\{\sigma_{x-y}\|000\}$	$\begin{pmatrix} \bar{1} & 0 \\ 0 & \bar{1} \end{pmatrix}$	no no no	$\begin{pmatrix} 1 & 0 \\ 0 & 1 \end{pmatrix}$	yes yes yes

Table I. (continued)

$\{\sigma_z\|00\frac{1}{2}\}$	$\begin{pmatrix} 0 & 1 \\ 1 & 0 \end{pmatrix}$	no no yes	$\begin{pmatrix} 0 & \bar{1} \\ \bar{1} & 0 \end{pmatrix}$	no no no
$\{C_{2z}\|00\frac{1}{2}\}$	$\begin{pmatrix} 0 & \bar{1} \\ 1 & 0 \end{pmatrix}$	no no no	$\begin{pmatrix} 0 & 1 \\ \bar{1} & 0 \end{pmatrix}$	no no no
$\{C_{6z}^4\|000\}$	$\begin{pmatrix} 1 & 0 \\ 0 & 1 \end{pmatrix}$	yes yes yes	$\begin{pmatrix} \bar{1} & 0 \\ 0 & \bar{1} \end{pmatrix}$	no no no
$\{C_{6z}^5\|00\frac{1}{2}\}$	$\begin{pmatrix} 0 & \bar{1} \\ 1 & 0 \end{pmatrix}$	no no no	$\begin{pmatrix} 0 & 1 \\ \bar{1} & 0 \end{pmatrix}$	no no no
$\{C_{2x}\|000\}$	$\begin{pmatrix} \bar{1} & 0 \\ 0 & 1 \end{pmatrix}$	no yes no	$\begin{pmatrix} 1 & 0 \\ 0 & \bar{1} \end{pmatrix}$	yes no no
$\{C_{2(2x-y)}\|00\frac{1}{2}\}$	$\begin{pmatrix} 0 & \bar{1} \\ \bar{1} & 0 \end{pmatrix}$	no no no	$\begin{pmatrix} 0 & 1 \\ 1 & 0 \end{pmatrix}$	no no yes
$\{C_{2(x+y)}\|000\}$	$\begin{pmatrix} \bar{1} & 0 \\ 0 & 1 \end{pmatrix}$	no yes no	$\begin{pmatrix} 1 & 0 \\ 0 & \bar{1} \end{pmatrix}$	yes no no
$\{C_{2(x+2y)}\|00\frac{1}{2}\}$	$\begin{pmatrix} 0 & \bar{1} \\ \bar{1} & 0 \end{pmatrix}$	no no no	$\begin{pmatrix} 0 & 1 \\ 1 & 0 \end{pmatrix}$	no no yes
$\{\bar{C}_{6z}\|00\frac{1}{2}\}$	$\begin{pmatrix} 0 & 1 \\ 1 & 0 \end{pmatrix}$	no no yes	$\begin{pmatrix} 0 & \bar{1} \\ \bar{1} & 0 \end{pmatrix}$	no no no
$\{\bar{C}_{6z}^2\|000\}$	$\begin{pmatrix} 1 & 0 \\ 0 & \bar{1} \end{pmatrix}$	yes no no	$\begin{pmatrix} \bar{1} & 0 \\ 0 & 1 \end{pmatrix}$	no yes no

Table I (continued)

$\{\bar{C}_{6z}^{4}\|000\}$	$\begin{pmatrix} 1 & 0 \\ 0 & \bar{1} \end{pmatrix}$	yes no no	$\begin{pmatrix} \bar{1} & 0 \\ 0 & 1 \end{pmatrix}$	no yes no
$\{\bar{C}_{6z}^{5}\|00½\}$	$\begin{pmatrix} 0 & 1 \\ 1 & 0 \end{pmatrix}$	no no yes	$\begin{pmatrix} 0 & \bar{1} \\ \bar{1} & 0 \end{pmatrix}$	no no no
$\{\sigma_{x+y}\|00½\}$	$\begin{pmatrix} 0 & 1 \\ \bar{1} & 0 \end{pmatrix}$	no no no	$\begin{pmatrix} 0 & \bar{1} \\ 1 & 0 \end{pmatrix}$	no no no
$\{\sigma_{x}\|000\}$	$\begin{pmatrix} \bar{1} & 0 \\ 0 & \bar{1} \end{pmatrix}$	no no no	$\begin{pmatrix} 1 & 0 \\ 0 & 1 \end{pmatrix}$	yes yes yes
$\{\sigma_{2x+y}\|00½\}$	$\begin{pmatrix} 0 & 1 \\ \bar{1} & 0 \end{pmatrix}$	no no no	$\begin{pmatrix} 0 & \bar{1} \\ 1 & 0 \end{pmatrix}$	no no no
$\{\sigma_{x+2y}\|00½\}$	$\begin{pmatrix} 0 & 1 \\ \bar{1} & 0 \end{pmatrix}$	no no no	$\begin{pmatrix} 0 & \bar{1} \\ 1 & 0 \end{pmatrix}$	no no no

the wave vector under consideration. For this case, where **k** and **-k** ≠ **k** are in the star, the Lifshitz criterion has the form of [8]

$$\sum_{R} \{\chi_0(g)\,\chi_0(g_0^{-1}\cdot g\cdot g_1)\cdot V(R) - \chi_0(g_0\cdot g\cdot g_1\cdot g)\cdot V(R_1\cdot R)\} = 0$$

where the sum is over the elements of $G(\mathbf{k})$, $\chi_0(g)$ is the character of representation of the space group operation g, $V(R)$ is the character of the representation with respect to bases x, y and z under the point operations of the group and R_1 transforms **k** into **-k**, e.g. $g_1=g_1^{-1}=\{i|\mathbf{o}\}$ and $V(R\cdot i) = -V(R)$, so that the criterion can be written as

$$\sum_{R} \{\chi_0(g)\,\chi_0(g_0^{-1}\cdot g\cdot g_1) + \chi_0(g_0\cdot g\cdot g_1\cdot g)\}\cdot V(R) = 0$$

The results of analysis are given in Table 2. This criterion is not met . Thus it is concluded that the change from NiAs-type structure to a $\sqrt{3}$ x $\sqrt{3}$ x2 superstructure is not an allowed continuous process. Simply by looking at Table 1, it is revealed that there are two fates for the space group $P6_3/mmc$ after distortion at **k**=(1/3, 1/3, 1/2) and corresponding to the irreducible representation under consideration. The first one is that for which $\varphi_1+\varphi_2$ remains symmetric under those operations which stay in the distorted structure, but is non-symmetric under the others which are lost. This results in the space group $P\bar{6}2c$. The second one is that for which φ_1 (or φ_1 corresponding to a same symmetry) remains symmetric, which yields the space group $P\bar{3}1c$.

An important example for the transition from $P6_3/mmc$ to $P\bar{6}2c$ may be that known to occur between pyrrhotite and troilite. As mentioned at the beginning, high-temperature pyrrhotite and troilite have been individually refined as the space groups $P6_3/mmc$ and $P\bar{6}2c$, respectively. The above discussion shows that the second-order transformation from $P6_3/mmc$

TABLE 2. The Analysis of Lifshitz Criterion

g	$\chi_0(R\|t)$	$g_1^{-1}\cdot g\cdot g_1$	$\chi_0(g)\cdot\chi_0(g_1^{-1}\cdot g\cdot g_1)$	$g_1\cdot g\cdot g_1\cdot g$	$\chi_0(g_1\cdot g\cdot g_1\cdot g)$	$V(R)$
$\varepsilon\|000$	2	$g=\varepsilon\|000$	$(\chi_0(g))^2=4$	$g^2=\varepsilon\|000$	2	3
$C_{3z}\|000$	2	$g=C_{3z}\|000$	$(\chi_0(g))^2=4$	$g^2=C_{3z}^2\|000$	2	0
$C_{3z}^2\|000$	2	$g=C_{3z}^2\|000$	$(\chi_0(g))^2=4$	$g^2=C_{3z}\|000$	2	0
$C_{2x}\|000$	0	$g=C_{2x}\|000$	$(\chi_0(g))^2=0$	$g^2=\varepsilon\|000$	2	-1
$C_{2y}\|000$	0	$g=C_{2y}\|000$	$(\chi_0(g))^2=0$	$g^2=\varepsilon\|000$	2	-1
$C_{2(x+y)}\|000$	0	$g=C_{2(x+y)}\|000$	$(\chi_0(g))^2=0$	$g^2=\varepsilon\|000$	2	-1
$\overline{C}_{6z}\|00\frac{1}{2}$	0	$\overline{C}_{6z}\|00\overline{\frac{1}{2}}$	0	$C_{3z}\|00\bar{1}$	-2	-2
$\sigma_z\|00\frac{1}{2}$	0	$\sigma_z\|00\overline{\frac{1}{2}}$	0	$\varepsilon\|00\bar{1}$	-2	1
$\overline{C}_{6z}^5\|00\frac{1}{2}$	0	$\overline{C}_{6z}^5\|00\overline{\frac{1}{2}}$	0	$C_{3z}^2\|00\bar{1}$	-2	2
$\sigma_{x-y}\|00\frac{1}{2}$	0	$\sigma_{x-y}\|00\overline{\frac{1}{2}}$	0	$\varepsilon\|000$	2	1
$\sigma_{2x-y}\|00\frac{1}{2}$	0	$\sigma_{2x-y}\|00\overline{\frac{1}{2}}$	0	$\varepsilon\|000$	2	1
$\sigma_{x+2y}\|00\frac{1}{2}$	0	$\sigma_{x+2y}\|00\overline{\frac{1}{2}}$	0	$\varepsilon\|000$	2	1

Finally, the Lifshitz Criterion is equal to

$$\sum_R \{\chi_0(g)\,\chi_0(g_0^{-1}\cdot g\cdot g_1) + \chi_0(g_0\cdot g\cdot g_1\cdot g)\}\cdot V(R) = 24 \neq 0$$

to $P\bar{6}2c$ is not allowed by Lifshitz condition. According to Toledano and Toledano [8], violation of the Lifshitz conditions leads in most cases to a first-order transition for which the lock-in commensurate phase appears directly below the high-symmetry phase, but for the minority of cases the first-order transition may result in an incommensurate phase which remains stable within an interval of temperature. Hence this system is worthy of further experimental explorations. As for the second solution for which the $P\bar{3}1c$ symmetry structure results with the same lattice, hP24-type compound with the space group $P\bar{3}1c$ has been found for a Ni substituted TiS [9].

References

1.Hirone, T., Maeda, S., and Chiba, S. J. Phys. Soc. Japan **9** (4). 500(1954).

2.Nakazawa, H., and N. Morimoto, N., Mater. Res. Bull. **6**. 345 (1971).

3.Putnis, A., Science **186**, 439 (1974).

4. Franzen, H. F., Chem. Mater. **2**, 486 (1990).

5. Franzen, H. F., Cryst. Res. Technol. **28**(2), 169 (1993).

6. Franzen, H. F., "Physical Chemistry of Inorganic Crystalline Solid", Springer-Verlag, New York, 1990.

7. Landau, L. D.and Lifshitz, E. M., "Statistical Physics", Pergamon Press, London, 1958.

8. Toledano, J.-C. and Toledano, P., " The Landau Theory of Phase Transition", World Scientific, Singapore, 1987.

9. Villars, P., and Calvert, L. D., "Pearson's Handbook of Crystallographic Data for intermetallic Phases", 2nd Ed. ASM international, Materials Park, OH, (1991).

CHAPTER 4

PHASE TRANSITIONS IN NEAR STOICHIOMETRIC IRON SULFIDE

A paper published in the Journal of Alloy and Compounds

Fan Li and Hugo F. Franzen

Abstract

The phase transition between the NiAs-type structure ($P6_3/mmc$) and the troilite structure ($P\bar{6}2c$) in FeS has been examined in synthetic samples by high-temperature x-ray diffraction and DTA experiments, and reexamined by Landau theory. The low temperature spin-flip and para- to ferroelectric transition was also studied. It is found experimentally that the NiAs-type to troilite transition is first-order and, by reexamination of Landau theory, that this is required by the Lifshitz condition but not by the Landau conditions. The low-temperature transition is found to occur with no discontinuity in lattice parameters. It is therefore argued that the low-temperature phase, which is known to be ferroelectric, has a trigonal space group symmetry that is a polar subgroup of $P\bar{6}2c$, namely P31c.

Introduction

The $Fe_{1-x}S$ system has been extensively studied over almost one century. A large number of papers treating the transitions in near stoichiometric iron sulfide ($Fe_{1-x}S$, x=0-0.05) appeared between 1950 and 1980. Several good review articles were published in

the 1970s [1-3]. Crystallographically, it was established that iron sulfide in this composition range adopts the troilite structure ($P\bar{6}2c$ symmetry) with antiferromagnetic ordering at room temperature and transfers into the NiAs-type structure ($P6_3/mmc$) at high temperature (this has been called the α-transition). The temperature for this crystallographic transition is commonly believed to be at 120^0 - 135^0C based on measurements of the susceptibility vs. temperature and neutron diffraction experiments. In the latter an abrupt change in *a* and *c* cell parameters was observed [4-6]. The magnetic structure in FeS is characterized by two transitions up to 400^0 C: one is the magnetic moment spin-flip from $\|\mathbf{c}$ for $T<T_s$ (~140^0C to $\perp\mathbf{c}$ for $T>T_s$, i.e. so-called the Morin transition or α_s-transition; the other is the moment disordering at 315^0C, i.e. the Neel temperature at which the antiferromagnetic FeS transfers into the paramagnetic structure (so-called β-transition) [7-9].

However, the nature of the α-transition has, in fact, never been clearly established. In the early work, the α-phase denoted room-temperature FeS, and, correspondingly, the α-transition phase was thought to involve an abrupt change in volume found at 130^0C [10,11]. Later the troilite phase was identified by diffraction information obtained at room temperature [12-16]. The susceptibility, DTA and electrical resistivity measurements led to the attribution of the α-transition to a structural transformation from troilite symmetry to NiAs-type [4, 7, 17,18]. Although temperature dependent diffraction experiments by both neutron and x-ray often revealed an abrupt change in *a* and *c* cell parameters near T_α, these observations were commonly accompanied by either co-existence of two phases

in the temperature range below and/or above T_α, or by the appearance of an intermediate phase after α-transition [19-22].

These results led to uncertainties about transitions that appear in published phase diagrams. In most of the published Fe-S phase diagrams the phase below T_α is labeled troilite but the distinction between T_α and T_N is unclear [1, 23, 24]. The latest edition of "Binary Alloy Phase Diagrams" [25] extends the troilite phase up to 588K at which the Neel transition occurs. After the 1980s the majority of the research reported on near stoichiometric iron sulfide resulted in the identification of new intermediate phases. King Jr. et al. [26] and Kruse [27, 28] reported the existence of an MnP-type phase between the α- and β-transition temperatures. Fei [29] revealed five polymorphs in the naturally occurring sample. However, there is no commonly accepted transition sequence throughout these phases.

Our recent work using high-temperature x-ray diffraction and DTA has resulted in an understanding of phase transitions in synthetic FeS. In this paper, we present high-temperature x-ray diffraction patterns that are interpreted using restraints placed upon symmetry by the ferroelectric and antiferromagnetic ordering reported in the literature.

Results

Figures 1 and 2 show the XRD patterns at different temperatures when the sample $Fe_{0.996}S$ was heated and cooled, respectively. Below 300°C the sample yields a diffraction pattern that is in excellent agreement with that calculated for the troilite phase. On the other hand, it can be noticed that with temperature elevation the troilite superstructure

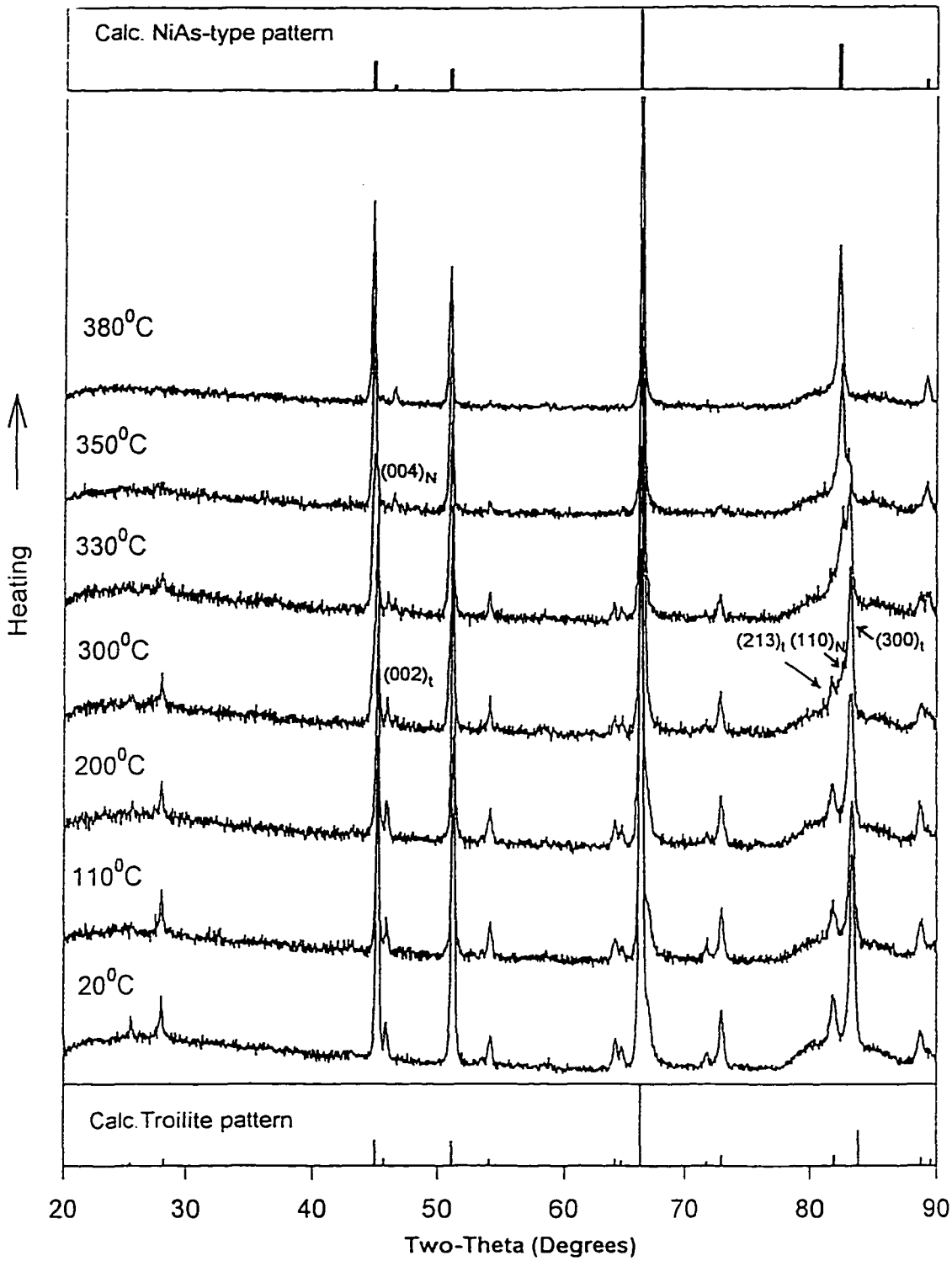

FIGURE 1. HTXRD patterns for $Fe_{0.996}S$ sample on heating ramp. $(\ )_N$: indices for NiAs-type; $(\ )_t$: indices for troilite.

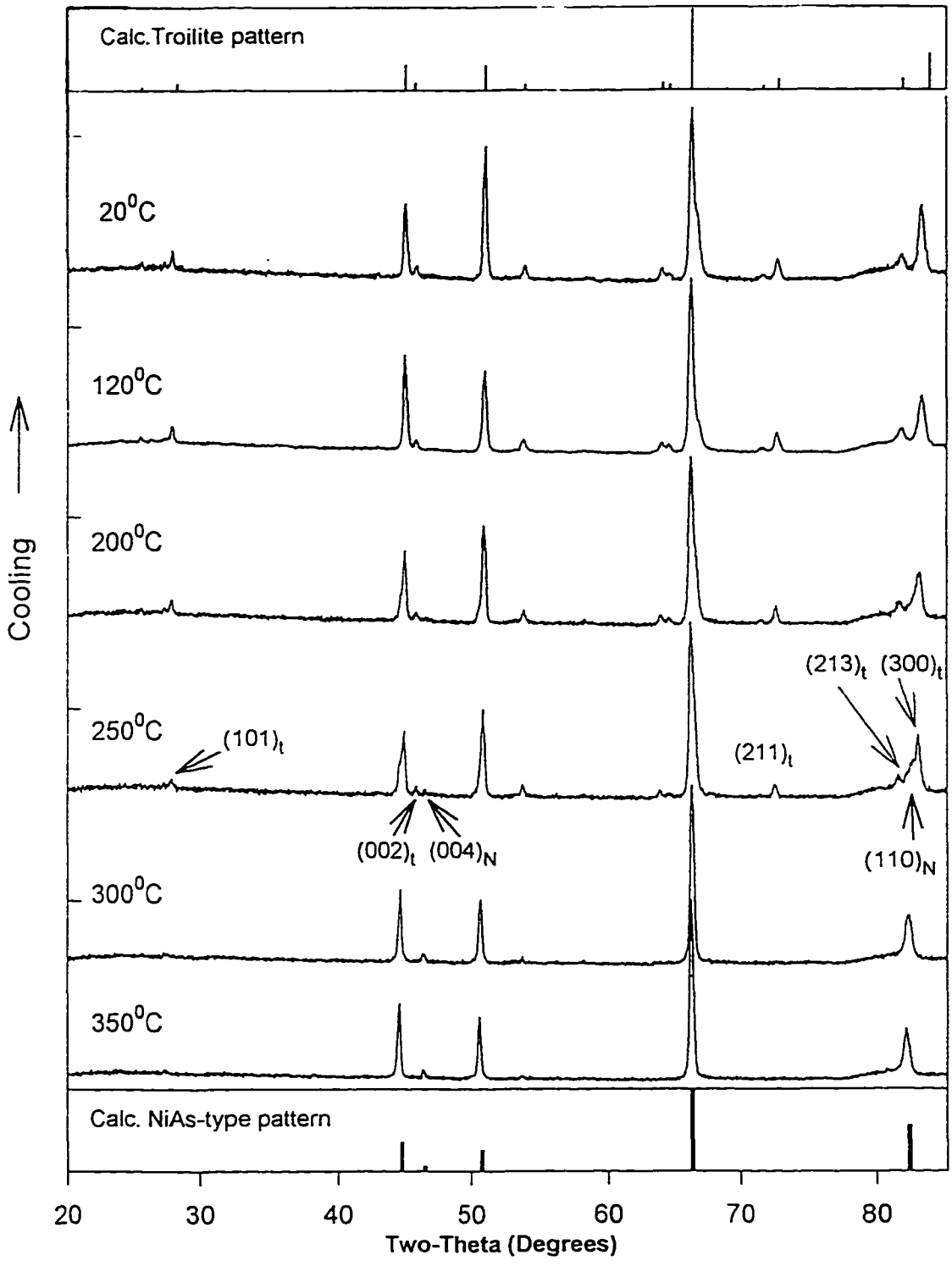

FIGURE 2. HTXRD patterns for $Fe_{0.996}S$ sample on cooling ramp.
$(\ )_N$: indices for NiAs-type; $(\ )_t$: indices for troilite.

peaks diminish in contrast to the substructure reflections. At about 300°C peaks which are consistent with the NiAs-type structure ($P6_3/mmc$) begin to appear. Thus, in the temperature range 300-350°C there occur two coexisting phases, troilite and NiAs-type, indicating that the transition is first order. Because of an abrupt change (discussed below) in lattice parameters from the troilite cell to the NiAs-type cell, a splitting between the troilite superstructure and NiAs-type substructure peaks is observed . Finally, above 350°C the sample was wholly transformed into the NiAs-type phase and only the NiAs-type XRD pattern is observed. When the temperature was decreased, this transformation process was reversed but lagged behind that on heating by about 30°C.

Figure 3, in which the change in the intensity of the 221diffraction peak with respect to that of 114 peak is plotted, illustrates this delay during the cooling ramp (-0.5K/min). The variations of cell parameters vs. temperature are plotted in Fig. 4. A discontinuous change in both *a* and *c* and a temperature region where two phases co-exist are displayed. At 330°C the transition from the troilite to NiAs-type phase gives rise to a expansion on *a*- and *b*-axes by 0.58% but a contraction on *c*-axis by 1.2%, and consequently there is an increase in the cell volume by 0.14%. The ratio *a/c* increases from 0.587 at room temperature for the troilite phase to 0.601 at 400°C for the NiAs-type phase.

In addition, when the temperature was changed from room temperature to 400°C, or vice versa, at a very rapid rate (within less than 20 s), both patterns at room temperature and at 400^0C as shown in Fig.1 changed before the patterns could be collected (less than one minute), indicating that this phase transformation occurs very rapidly.

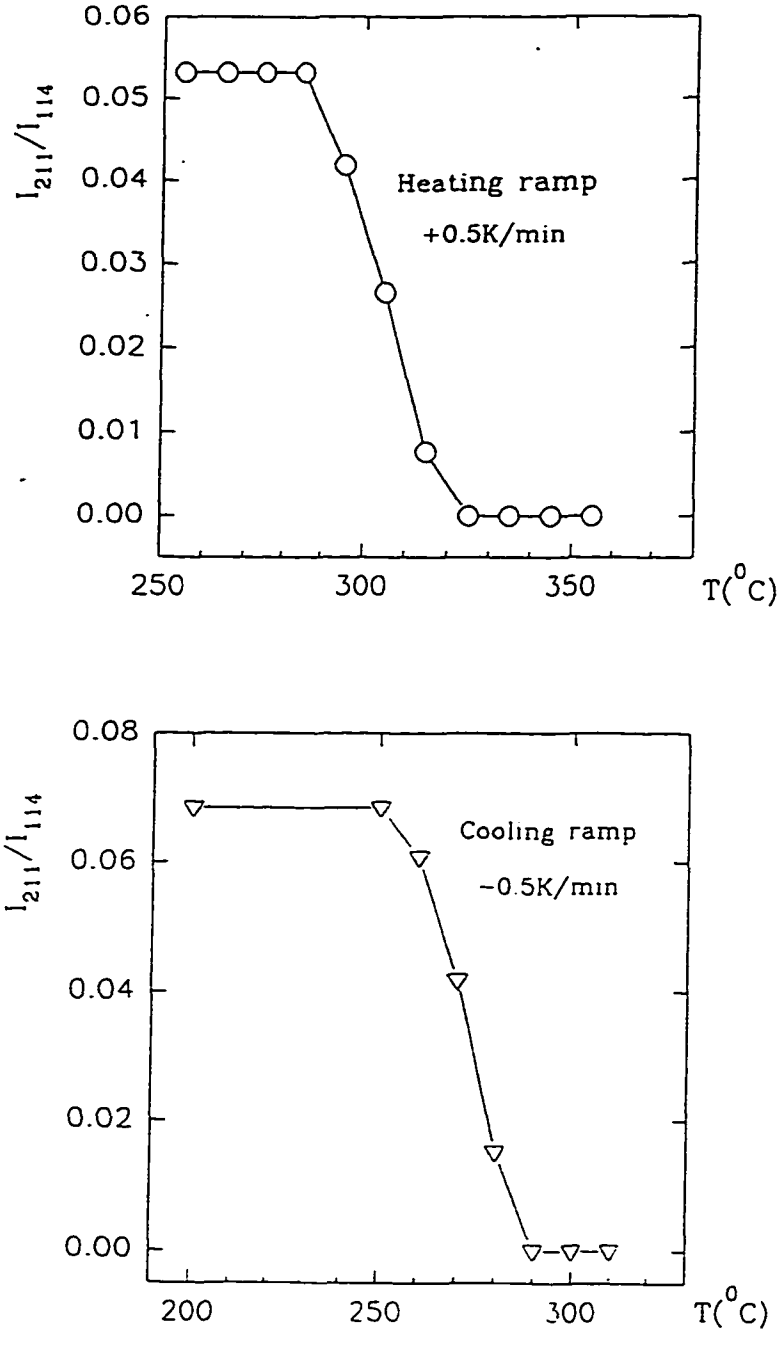

FIGURE 3. Intensity ratio of peak (211) to (114) as function of temperature, where (211) and (114) diffraction peaks refer to the troilite indices.

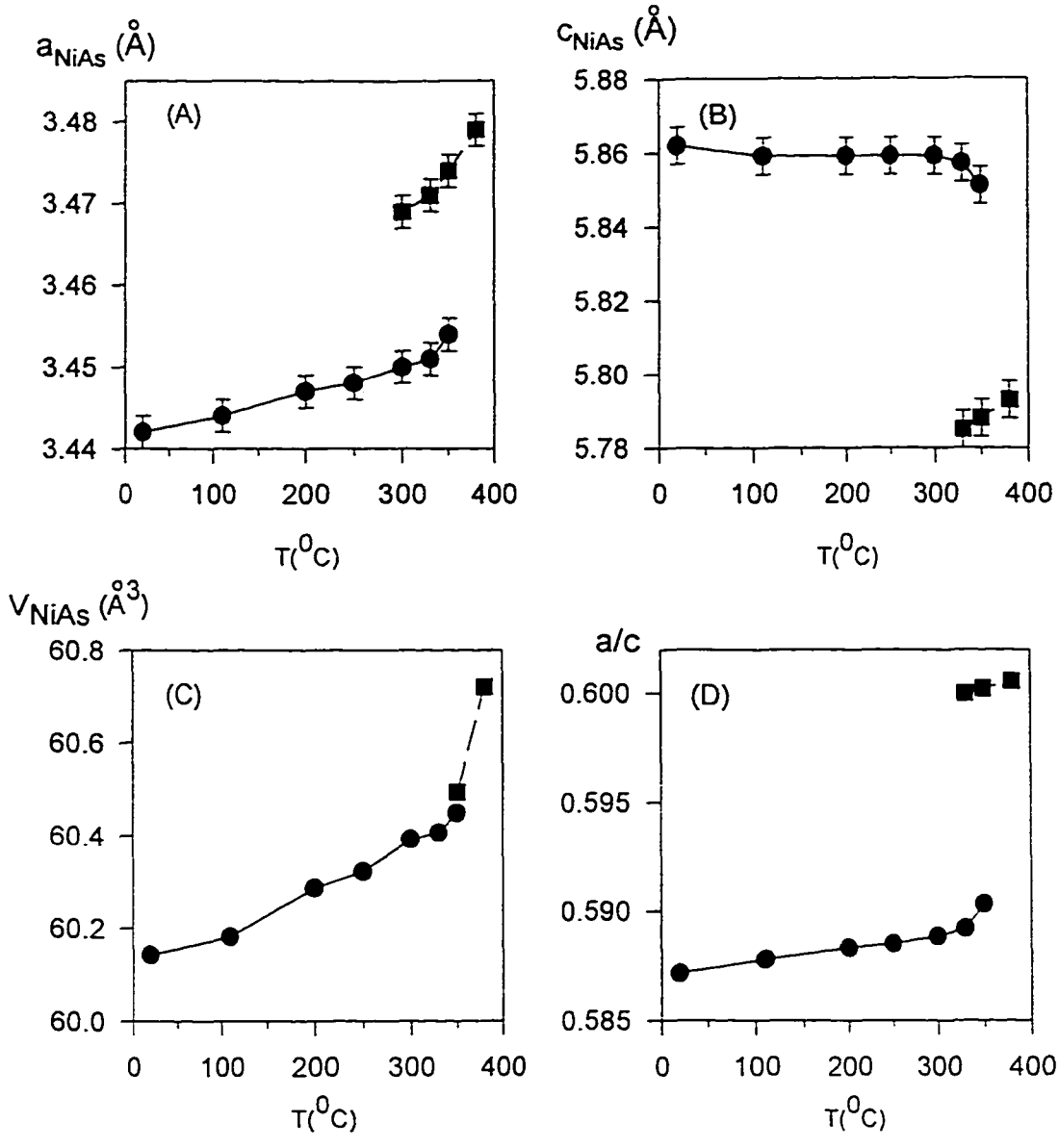

FIGURE 4. Lattice parameter changes with respect to temperature as computed from the XRD patterns on heating ramp shown in Fig. 1. Notice that all the cell parameters refer to the NiAs-type cell. (A) a_{NiAs} vs. temperature; (B) c_{NiAs} vs. temperature; (C) Cell volume V_{NiAs} vs. temperature; (D) Ratio a_{NiAs}/c_{NiAs} vs. temperature

● computed from $(110)_t$ and $(004)_t$ peaks

■ computed from $(100)_{NiAs}$ and $(002)_{NiAs}$ peaks

The DTA curves shown in Fig.5 displayed two peaks. For the heating ramp the peaks appear at 140^{0}C and at 315^{0}C, respectively, but for the cooling ramp they are at 120^{0}C and 300^{0}C, indicating that both the transitions reverse with a hysteresis. The DTA patterns obtained in this study are in good agreement with those found in literature [30]. Thus, the question arises, does the peak at low temperature (120-140^{0}C) correspond to a structural change? In order to search for a possible crystallographic transition in this temperature region, we carefully collected diffraction patterns in the temperature range 80-200^{0}C with 20K increments. The patterns were all found to be same as those obtained in the temperature range 20-200^{0}C shown in Fig.1. No significant difference from the troilite pattern was recognized. Therefore, this transition is attributed to one that occurs with no observable distortion from troilite in XRD pattern, and in particular no volume discontinuity.

On the other hand, the samples that have the ratio Fe/S=0.95-0.96 behaved differently. Figure 6 shows the temperature dependent diffraction patterns for the sample $Fe_{0.95}S$. It can be seen that at room temperature the sample is mainly characterized by the troilite pattern with superlattice peaks at positions (2θ) 25.62^0 (100), 28.03^0 (101), 64.15^0(203), 72.96^0 (211), 81.88^0 (213) and so on (indices in the brackets refer to the troilite structure). When the sample was heated, an abrupt change in the *a* and *c* parameters was identified. However, the troilite-like superlattice peaks started to disappear at temperatures as low as about 80^{0}C, and instead of yielding a simple NiAs-type pattern as observed in the $Fe_{0.996}S$ sample, several very weak diffraction peaks were

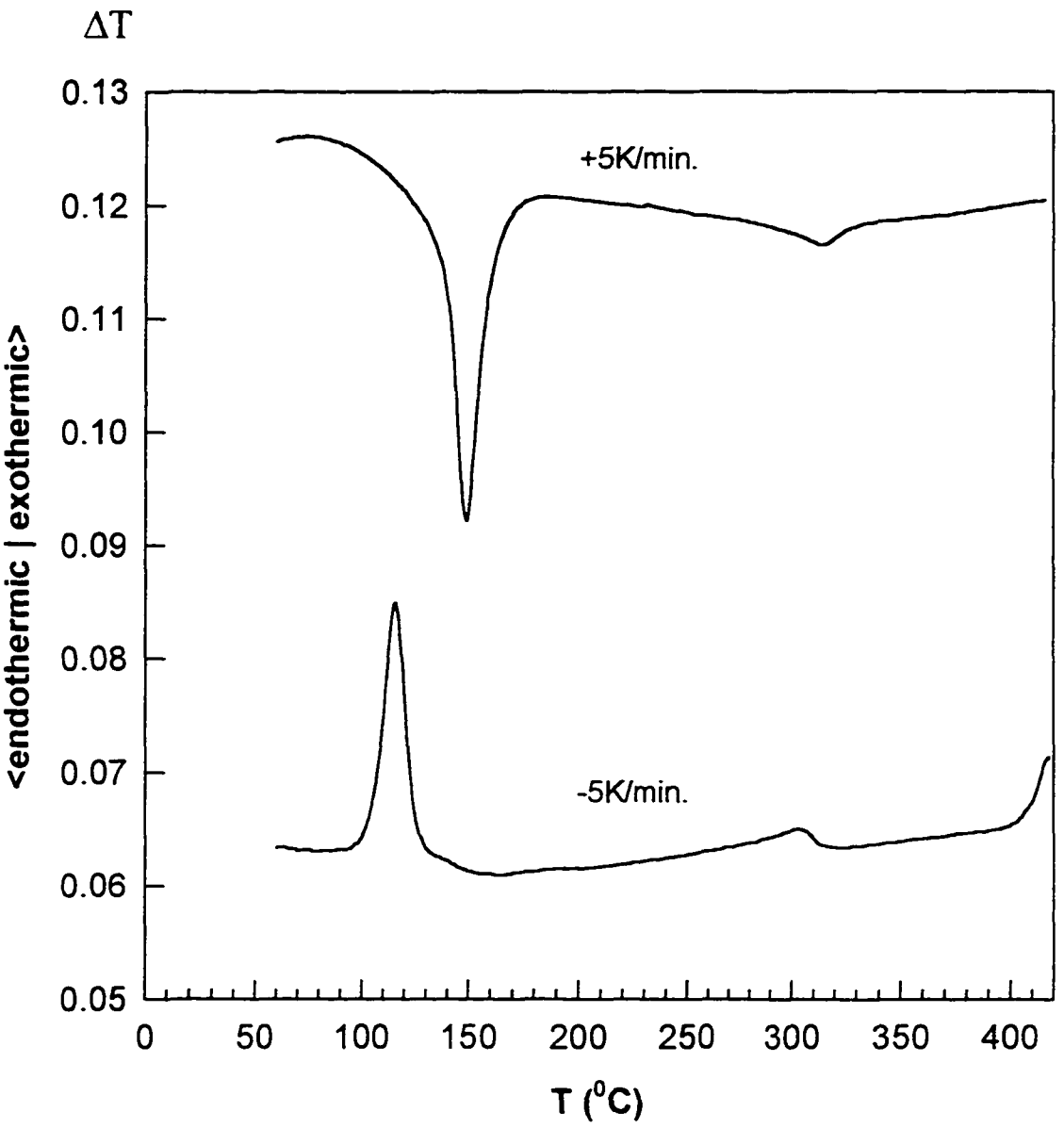

FIGURE 5. DTA curves for $Fe_{0.996}S$ sample.

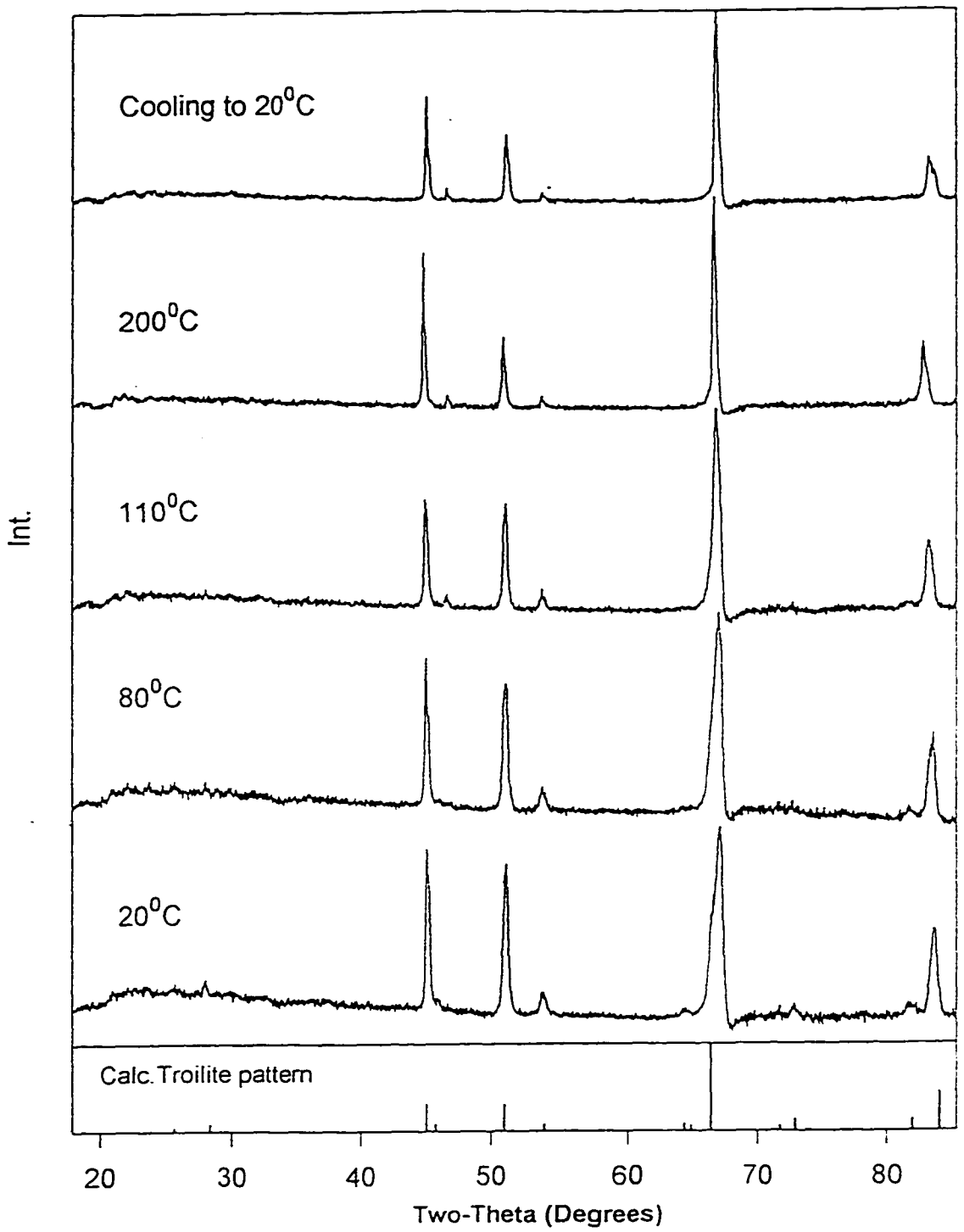

FIGURE 6. HTXRD patterns for $Fe_{0.95}S$ sample.

found in the low angle (2θ) range, corresponding to d≈6.70Å, 6.05Å and 6.20Å. This imperfect NiAs-type pattern with these low-angle diffractions was maintained up to 400°C. Furthermore, the change in XRD was not reversed upon cooling. The DTA heating curve as shown in Fig.7 displayed a similar feature as shown in Fig. 5, but the cooling curve, consistent with the XRD result, did not. Apparently, the phase that remains after loss of the $\sqrt{3} \times \sqrt{3} \times 2$ superstructure (troilite) is a distorted NiAs-type structure which gives evidence of being incommensurate. To assure the reproducibility of experiments, they were all repeated on other portions of samples.

Discussion

As mentioned earlier, there have been some contradictory results in the study of the transition sequence in the near stoichiometric iron sulfides ($Fe_{1-x}S$, x=0 - 0.05). One contradiction is assignment of the NiAs-type structure to the high temperature antiferromagnetic phase, for no magnetic space group associated with the crystallographic $P6_3/mmc$ symmetry can be found for which the magnetic moments lie in the basal plane, and the spin orientation at temperature above 140°C is known to be perpendicular to **c** [3, 6, 19]. In other words, the ordering with spins lying in the a-b plane is incompatible with $P6_3/mmc$ symmetry but is compatible with $P\bar{6}2c$ symmetry (crystallographically, troilite structure). Spin ordering in $P6_3/mmc$ is possible only if the spins are parallel to the c-axis as in NiS [31]. Furthermore, in the late 1960s, it was reported by van den Berg [32, 33] that at room temperature FeS is ferroelectric with uniaxial (c-axis) polarization and transfers into paraelectric at the temperature at which α-transition occurs. According to

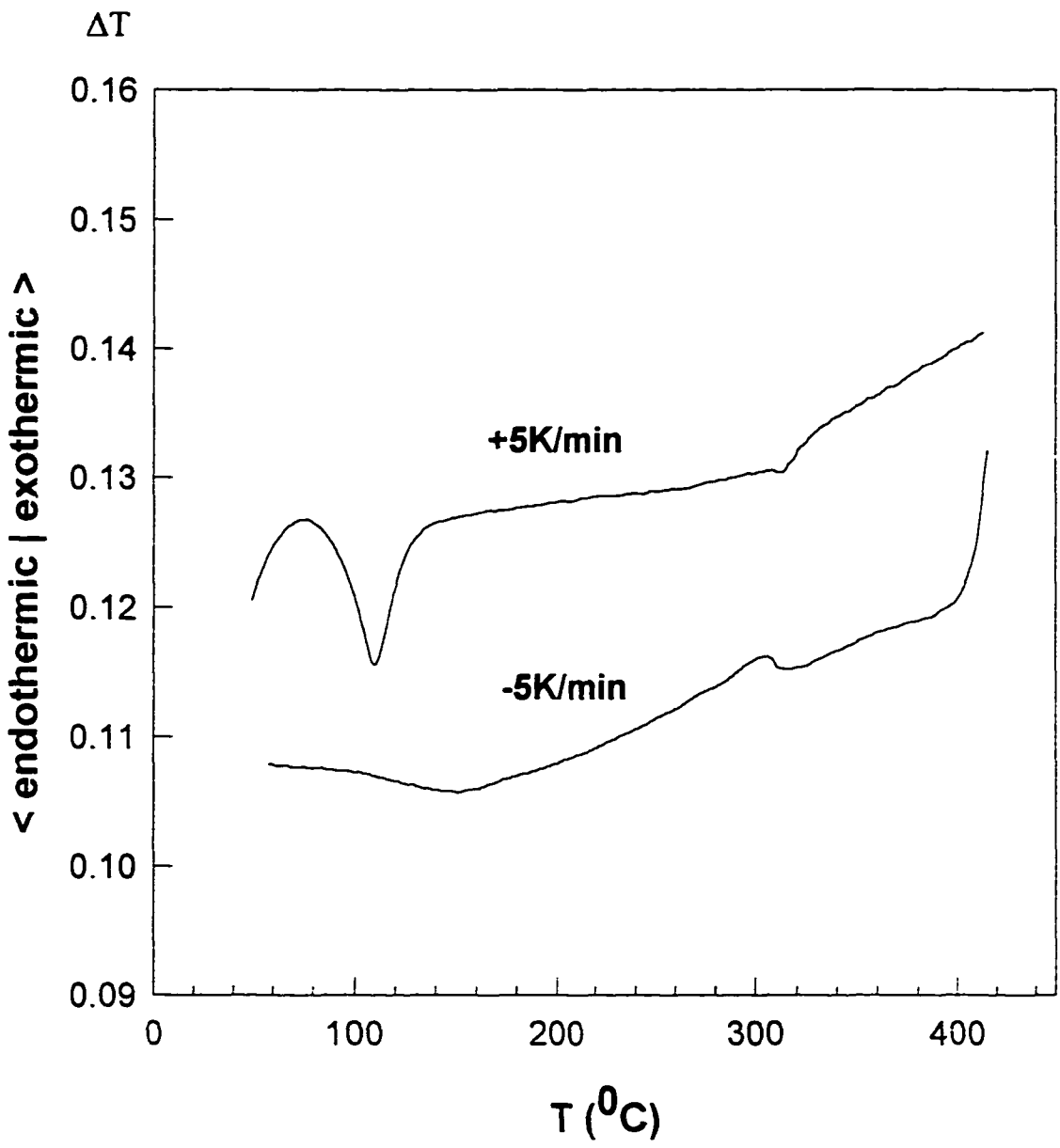

FIGURE 7. DTA curves for $Fe_{0.95}S$ sample.

group theory ferroelectric ordering in $P\bar{6}2c$ symmetry is inconsistent with the required vector invariance [34]. The ideal troilite structure therefore cannot be ferroelectric. Hence, by symmetry, troilite in $P\bar{6}2c$ symmetry can be realized only in a paraelectric state above the α-transition temperature, and the NiAs-type ($P6_3/mmc$) symmetry can only be achieved in the disordered paramagnetic state above the Neel temperature.

An interpretation that is consistent with symmetry requirements placed upon the observed ferroelectric ordering below 140^0C and the observed a-b spin orientation between 140^0C and 315^0C and the HTXRD and DTA results reported in this paper is: for $T>T_N$ (≅588K) FeS has $P6_3/mmc$ symmetry (NiAs-type) with paramagnetism. for $T_\alpha < T < T_N$ the material becomes antiferromagnetic with spins lying in the *a-b* plane and $P\bar{6}2c$ symmetry (troilite), and for $T< T_\alpha$ the symmetry is broken (with no discontinuity in the lattice parameters), a transition that occurs with a spin flip and the onset of ferroelectric ordering (two transitions probably take place independently, but the spin flip would not require broken symmetry). Since the observation that the low-temperature transition (in the α-transition temperature range) is accompanied by no discontinuity in lattice parameters (see Fig. 4) requires that the transition be structurally continuous, it is concluded that the low-temperature phase has space group symmetry that is a subgroup of that of troilite. The maximal uniaxial subgroups of $P\bar{6}2c$ are Amn2 and P31c . An orthorhombic symmetry would result in the splitting of diffraction lines, whereas the trigonal space group would not. No such splitting is noticed, therefore it is possible to conclude on the basis of the low-temperature pattern that the maximal subgroup

symmetry is probably P31c. Any other trigonal subgroup would result in additional diffraction lines relative to P31c - either superstructure lines or diffraction lines resulting from the loss the c-glide. The facts, that no additional lines are observed and that the lattice parameters change continuously, strongly suggest a second-order phase transition, and it follows that, since the transition from $P\bar{6}2c$ to P31c at the gamma point halves the number of symmetry elements, the transition can be second order according to Landau theory [34-37]. An earlier report from this group misinterpreted the symmetry requirements for the existence of a vector invariant and incorrectly stated the $P6_3/mmc \rightarrow P\bar{6}2c$ transition met the Lifshitz condition for a second order phase transition [35]. We subsequently found that a vector invariant had previously been reported [34], and a re-evaluation of our Lifshitz analysis revealed an error that led to our incorrect conclusion.

Considering the other composition, Fe/S = 0.95, of iron-deficient monsulfide, the previous research work on temperature dependent polarization and neutron diffraction has established a good model for the observed relation between the composition and the α-transition [19, 33, 38]. On the basis of the model proposed by van den Berg [38] , the α-transition, as illustrated as T_α in Fig. 8, possesses the following characteristics: 1).there exists an intermediate collapse from polar phase to paraelectric phase, correspondingly, there are intermediate phases, or Two Phase Structure (TPS) through this transition; 2). this collapse can be avoided in very nearly stoichiometric iron sulfide or by sufficiently slow heating and cooling; 3). the larger the x value for $Fe_{1-x}S$, the lower temperature at which the intermediate collapse occurs. In accordance with our observations on the

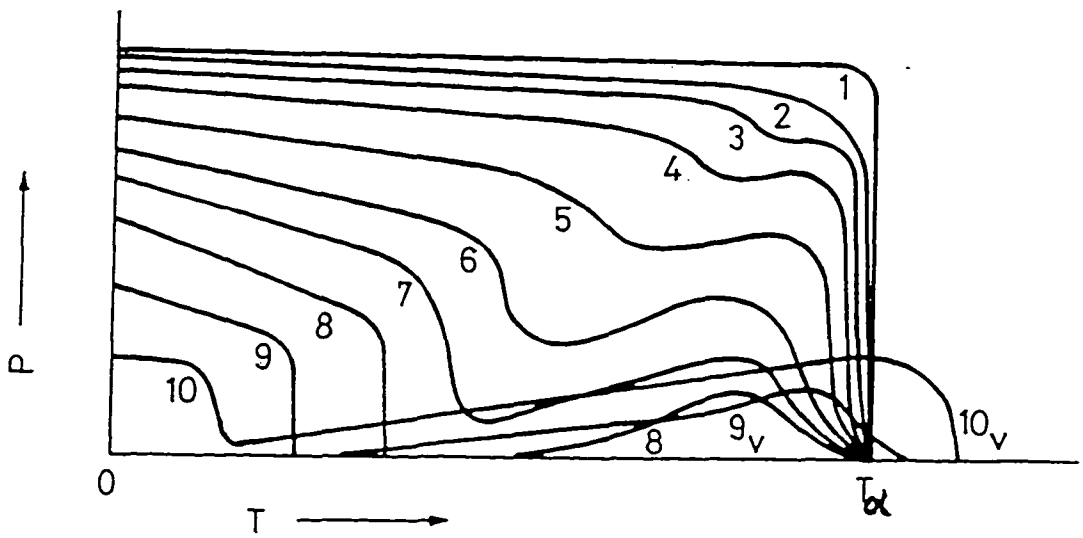

FIGURE 8. Polarization P versus temperature T for the semiconducting uniaxial ferroelectric $Fe_{1-x}S$ theoretically predicted by van den Berg [38]. The number from 1 to 10 on each curve corresponds to different x value from -0.02 to 0.125 (1/8) in $Fe_{1-x}S$. Notice that for the larger x a deeper dip is encountered during the transition in which the TPS is formed.

$Fe_{0.95}S$ sample, the iron sulfides in this composition range have a distorted troilite structure with a $\sqrt{3} \times \sqrt{3} \times 2$ cell at room temperature, but they follow a different transition track than does $Fe_{0.996}S$ upon heating. Under our heating conditions. the collapse has been avoided in the $Fe_{0.996}S$ case, even at a very rapid heating rate (according to van den Berg, it has a more effective polarization pumping), but in the $Fe_{0.95}S$ case an anomalous track is observed. The DTA (Fig. 7) show that the ferroelectric Curie transition in $Fe_{0.95}S$ occurs at 120°C, whereas the facts, that a simple troilite structure did not result and that the transition was not reversed upon recovery of temperature (notice that β-transition is not affected), indicate that the transition drifts off the reversible track during collapse. Based on van den Berg's model, TPS will result in a metastable. incommensurate domain structure. Our diffraction patterns for the $Fe_{0.95}S$ sample gave strong indication of the formation of incommensurate structure. The fact that for $Fe_{0.95}S$ there is a difference between the temperature at which the troilite phase disappears (~80-100^{0}C) on the HTXRD patterns and the temperature at which the DTA peak appears (~120^{0}C) supports the model that an intermediate collapse occurs at a low temperature below the ferroelectric Curie transition. The marked difference in transition behavior between $Fe_{0.996}S$ and $Fe_{0.95}S$ probably has contributed to the difficulty that has been encountered in reconciling results from different groups.

Conclusions

Experimentally, we have confirmed that the transition from $P6_3/mmc$ to $P\bar{6}2c$ at 588K is of first order. The transition sequence in near schoichiometric iron sulfide is

rationalized by symmetry requirements. It is concluded that the α-transition is the ferroelectric transition which is accompanied by a symmetry breaking transition which is second order if the composition is stoichiometric, but is first order for the non-stoichiometric composition.

Reference

[1] J. C. Ward, Rev. Pure and Appl. Chem. **20**, 175 (1970).

[2] J. M. D. Coey, H. Roux-Buisson and R. Brusetti, J. de Physique **C4**, 1 (1976).

[3] D. J. Vaughan and J. R.. Craig, "Mineral Chemistry of Metal Sulfides", Cambridge University Press, (1978).

[4] Haraldsen, Z. anorg. allg. Chem. **246**, 195 (1941).

[5] J. T. Sparks, W. Mead and T. Komoto, J. Phys. Soc. Janpan **17 (Suppl. B1)**, 249 (1962).

[6] E. Hirahara and M. Murakami, J. Phys. Chem. Solids **7**, 281-289 (1958).

[7] T. Hihara, M. Murakami and E. Hirahara, J. Phys. Soc. Japan **12**, 734 (1957).

[8] H. Horita and E. Hirahara, J. Phys. Soc. Japan **21**, 1447 (1966).

[9] E. J. Schwarz and D. J. Vaughan, J. Geomag. Geoeletr. **24**, 441-458 (1972).

[10] W. Treitschke and G. Tammann, Z. anorg. allg. Chem. **49**, 320 (1906).

[11] E. T. Allen, J. L. Crenshaw, J. Johnston and E. S. Larsen, Z. anorg. allg. chem. **76**, 201 (1912).

[12] R. Juza and W. Biltz, Z. anorg. Chem. **205**, 273 (1932).

[13]G. Hagg and I. Sucksdorff, Z. Phys. Chem. **22**, 444 (1933).

[14] H. Haraldsen, Z. anorg. allgem. chem. **231**, 78(1937).

[15] E. F. Bertaut, Bull. Soc. Fr. Mineral. Cristallogr. **79**, 276 (1956).

[16] A. Putnis, Science **186**, 439 (1970).

[17] M. Murakamai, J. Phys. Soc. Japan **16**, 187 (1961).

[18] W. Moldenhauer and W. Bruckner, Physica Status Solidi A **34**, 565 (1976).

[19] A. F. Andersen and P. Torbo, Acta Chem. Scand. **21**(10), 2841 (1967).

[20] J. T. Sparks, W. Mead, A. J. Kirschbaum and W. Marshall , J. App. Phys. **31 (5) (Suppl.)**, 356S (1960).

[21] M.E. Fleet and N. Macrae, Canad. Min. **9**, 699 (1969).

[22] R. G. Arnold, Econ. Geol. **64**, 405 (1969).

[23] G. A. Desborough and R. H. Carpenter, Economic Geology **60**, 1431-1450 (1965).

[24] W. G. Moffatt (ed.), "The Handbook of Binary Phase Diagrams" Vol.3, General Electric, New York (1984).

[25] T. B. Massalski (Ed.), "Binary Alloy Phase Diagrams" (2nd ed.), AMS International (1990).

[26]H. E. King Jr and C.T.Prewitt, Acta Cryst. **B38**, 1877-1887 (1982).

[27] O. Kruse, American Mineralogist **75**, 755-763 (1990).

[28] O. Kruse, American Mineralogist **77**, 391-398 (1992).

[29] Y. Fei, presented on MRS Meeting, Fall 1995, Boston, abstract p.534.

[30] T. Hirone, S. Meada, S. Chiba and N. Tsuya, J. Phys. Soc. Japan **9**(4), 500 (1954).

[31] J. T. Sparks and T. O. Komoto, Rev. Moden Phys. 40(4), 752 (1968).

[32] C.B. van den Berg, J. E. van Delden and J. Bouman, Phys. Stat. Sol. **36**, K89 (1969).

[33] C.B. van den Berg, Phys. Stat. Sol. **40**, K65 (1970).

[34] J.-C. Toledano and P. Toledano, "The Landau Theory of Phase Transitions", World Sci., Singapore (1987).

[35] F. Li and F. H. Franzen, J. Alloy and Compounds **215**, L3-L6 (1994).

[36] L. D. Landau and E. M. Lifshitz, Statistical Physics, Pergamon Press. London, (1958).

[37] H. F. Franzen, "Physical Chemistry of Solid", C. Y. Ng, ed., World Sci. , New Jersey (1993).

[38] C.B. van den Berg, Ferroelectics **4**, 103-116 and 195-212 (1972).

CHAPTER 5

A ORDERING, INCOMMENSURATION AND PHASE TRANSITIONS IN PYRRHOTITE. Part I: A TEM STUDY OF Fe_7S_8

A paper published in the Journal of Solid State Chemistry

Fan Li , Hugo F. Franzen and Matthew J. Kramer

Abstract

Vacancy ordering in synthetic Fe_7S_8 at elevated temperature was studied using transmission electron microscopy. Two known idealized structures of Fe_7S_8 are monoclinic and trigonal based upon ABCD and ABC stacking of Kagome nets, respectively. The TEM results indicate a tendency for Fe_7S_8 to transform from monoclinic to trigonal between 200°C and 300°C. A disordering of vacancies occurs above 300°C and yields a partially filled CdI_2-type structure. The Curie magnetic transition is associated with this vacancy-ordering transition. On slow cooling, it was found that the vacancies are ordered such as to tend to restore the Kagome nets and lead to ABCD and ABC layering.

Introduction

A primary feature of the vacancy ordering in defect NiAs-type iron sulfides is the formation of Kagome nets, partially vacant hexagonal planes of iron atoms within which vacancies are ordered such that they occupy the alternate sites in alternate rows (see Fig.1a). Therefore an understanding of the structures of the nonstoichiometric iron sulfides ($Fe_{1-x}S$) can be based upon consideration of the stacking sequences of Kagome

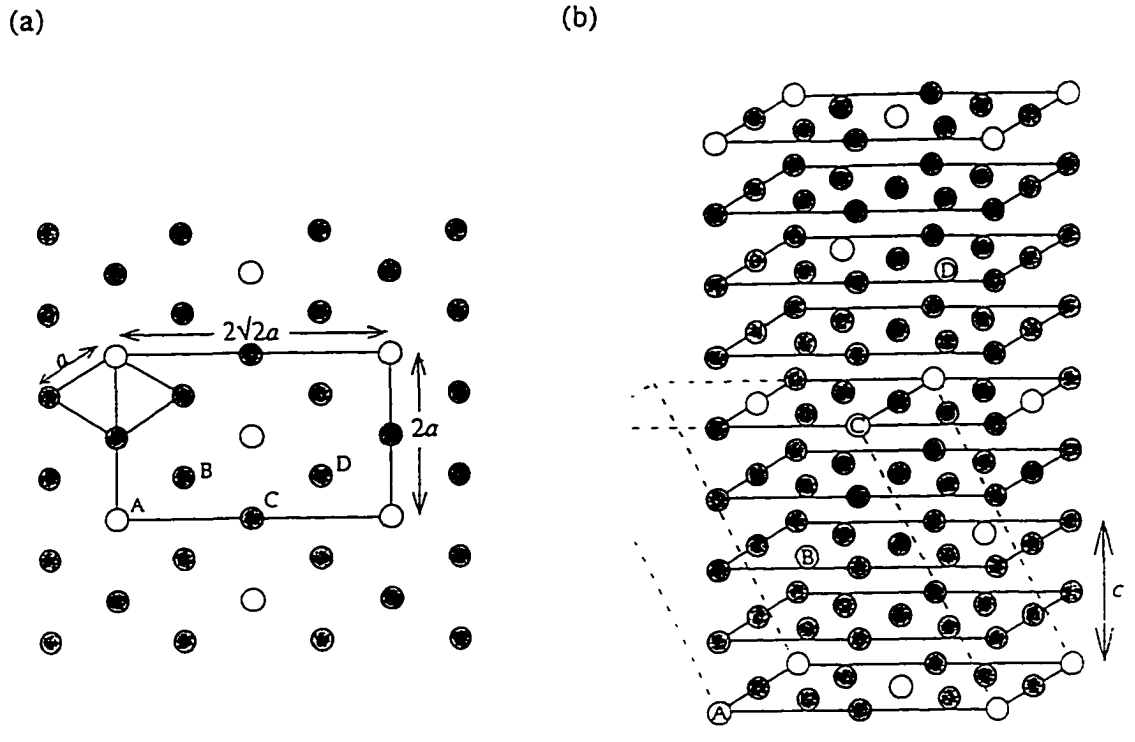

FIGURE 1. (a) A schematic Kagome net in NiAs-type $Fe_{1-x}S$. The open circles represent the vacancy sites and the solid circles represent the iron-filled sites. Notice that for a subcell shown by the bold lines there are four unequavalent sites as labeled as A, B, C and D for which the vacancies could be placed. The superstructure derived from such a Kagome net will have the lattice parameters $A=2\sqrt{2}a$ and $B=2a$ (a and c refer to the lattice parameters of a NiAs subcell) as illustrated by the lighter lines. (b) In Fe_7S_8, the Kagome nets are stacked alternately with the iron filled layers along the c-axis and the A, B, C and D nets are staggered such that a 4C monoclinic structure results. The dash lines show such a monoclinic unit cell where the sulfur atoms are omitted for simplicity.

nets along the c-axis of NiAs-type substructure. Here the stacking sequence refers to two variations: (1) permutation of filled Fe and Kagome nets (at this point the origins of the Kagome net are considered as randomly located in the a-b plane); (2) ordering of Kagome nets in the [001] direction (at this point the four possible origins in the Kagome nets are considered to be ordered along [001] direction when layering, i. e., the Kagome nets are labeled as A, B, C and D).

Among the defect iron sulfides that can be described as ordered vacancies in the NiAs-type structure, Fe_7S_8 is an extreme. This composition corresponds to Kagome nets alternating with filled planes, with the 1/8 of the iron positions completely empty. As for the ordering of Kagome nets, although a variety of possible stacking sequences can be generated with little energy preference [1], only two sequences in Fe_7S_8, $D_AFD_BFD_CFD_DF...$ and $D_AFD_BFD_CF...$ (F: iron-filled layer, D_A, D_B, D_C and D_D stand for the four Kagome nets unequivalent with respect to the origin) have been identified by x-ray diffraction studies. The former yields an ideal monoclinic symmetry with c = 4C (see Fig. 1b), while the latter yields a trigonal structure with c = 3C (A and C in this paper will refer to the a- and c-length of NiAs-type structure, respectively). It is noteworthy that the ideal 4C monoclinic structure with ABCD stacking has been found only in natural pyrrhotite minerals that have undergone processes over geological time [2], and the 3C trigonal structures were only found in quenched samples [3, 4]. The relationship of these two structures has not been studied, so it has remained unclear whether the 3C stacking is an intermediate superstructure phase stable at certain temperatures or forms as a metastable phase. As for the laboratory-grown samples mixed stacking of both ABC and

ABCD is most often encountered. The mixing of stacking sequences of Kagome nets can vary from random through incommensurate to complete order in domains of the dimensions appropriate to x-ray or TEM investigation, and this disorder can be of thermodynamic or kinetic origin. Even though a 4C structure can occur in a short range, the stacking of Kagome nets in Fe_7S_8 can do so in different fashions, such as ABDC, BACD and so on. Thus the monoclinic "structure" is probably significantly distorted in a long range. These complications have hindered the understanding of phase relations in this system. In order to refine the x-ray diffraction of a single crystal of Fe_7S_8, Keller-Besrest et al. [5] introduced a fault rate for the 4C stacking sequence to rationalize the partial occupancy variable and in this way obtained a very good solution.

In the study of structural imperfection, electron diffraction is of special interest due to its high sensitivity in comparison with x-rays, allowing the examination of a thin section of specimen and providing evidence of ordering on a smaller scale (by a factor of 10^3 or more). In the last decades, several attempts have been made to shed further light on the pyrrohtite structures using TEM [6-8], but almost all the crystals studied were naturally occurring $Fe_{1-x}S$. The samples invariably gave evidence for twinning, heterogeneity or composition gradients. It is known that Fe_7S_8 is ferrimagnetic because of vacancy ordering within the alternate layers along *c*-axis and an antiferromagnetic coupling between the adjacent planes at room temperature, and it is further known that this material transforms to paramagnetic at about 315^0C. It has, however, not been demonstrated whether this transformation results from disordering of vacancies or from a magnetic moment disordering process.

The present paper reports the results of a TEM study that was carried out on a synthetic Fe_7S_8 sample in order to improve our understanding of the relationship between the monoclinic and trigonal forms of pyrrhotite, and of the relationship between the magnetic transition and the ordered structure.

Results and Discussions

The Structure at Room Temperature

The alternation of partially filled Kagome net layers with the fully filled iron layers can be clearly seen in the high resolution transmission electron micrography (HRTEM). Figure 2 depicts a layer image from the Fe_7S_8 sample at room temperature with the electron beam perpendicular to the *c*-axis. The fringes show a contrasting alternation of a dark strip with a light strip, indicating a two-layer periodicity. The distance between two dark strips was estimated to be d=5.6 - 5.7Å which corresponds to one *c*-length of the NiAs-type substructure. From this view, however, the monoclinic and trigonal orderings are indistinguishable, as, in fact, are the projected Kagome nets. Figure 3 displays a series of the $[001]_{NiAs}$ selected area diffraction patterns (SAD) at various temperatures. The pattern, when the sample was at room temperature, showed no weak superstructure reflections (Fig.3a), and all the diffraction maxima in this projection corresponded to the NiAs substructure, suggesting that *a*- and *b*-axes are not doubled as they would be in the projected 2Ax2Ax3C trigonal structure. On the other hand, the convergent beam electron diffraction (CBED), as shown in Fig.4, reveals a deviation from the hexagonal and trigonal

FIGURE 2. A HRTEM image of Fe_7S_8 at room temperature with the electron beam perpendicular to c-axis.

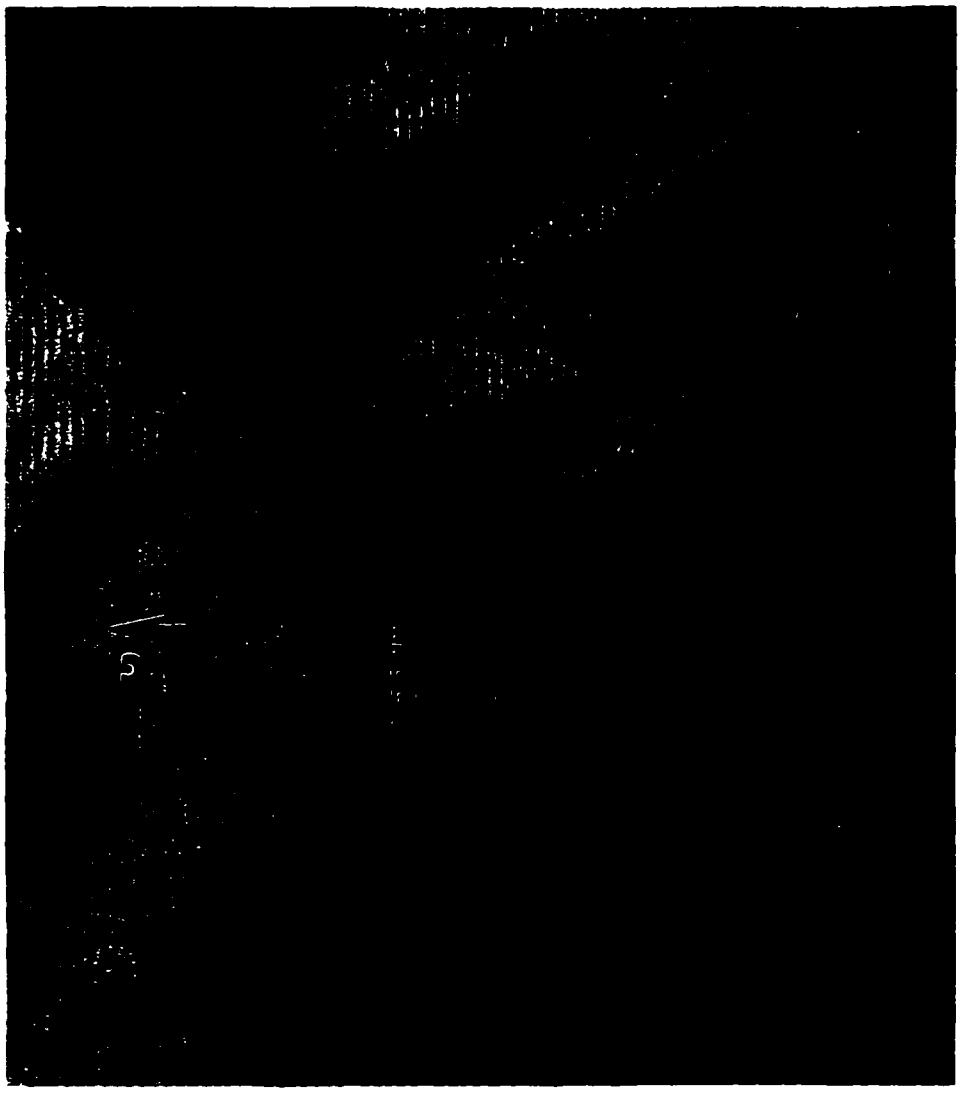

FIGURE 3. SAD patterns for $[001]_{NiAs}$ zone. All the patterns were obtained from the same region of the crystal (i.e., the region near the tip of the crystal as indicated by an arrow in Fig. 8A). (a) at room temperature; (b) at 210°C; (c) at 340°C; (d) when cooled to room temperature.

(a)

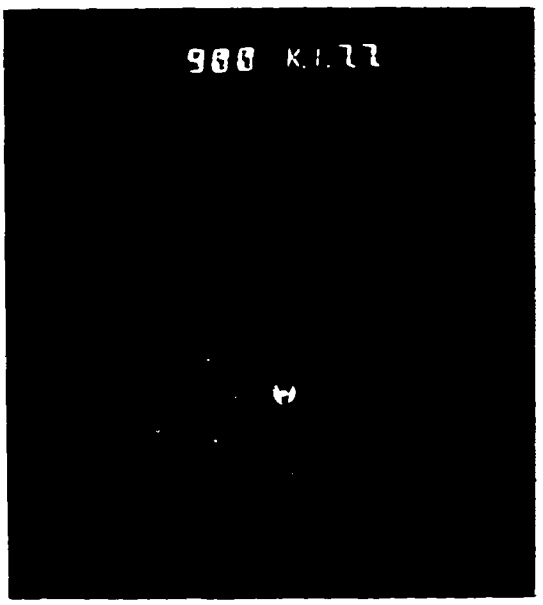

(b)

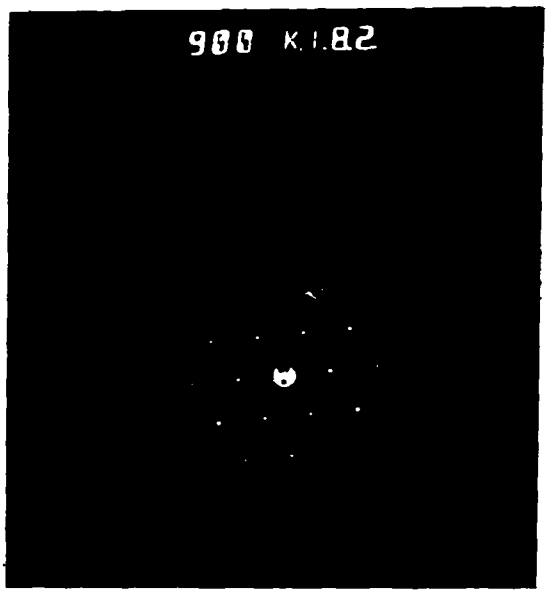

(c)

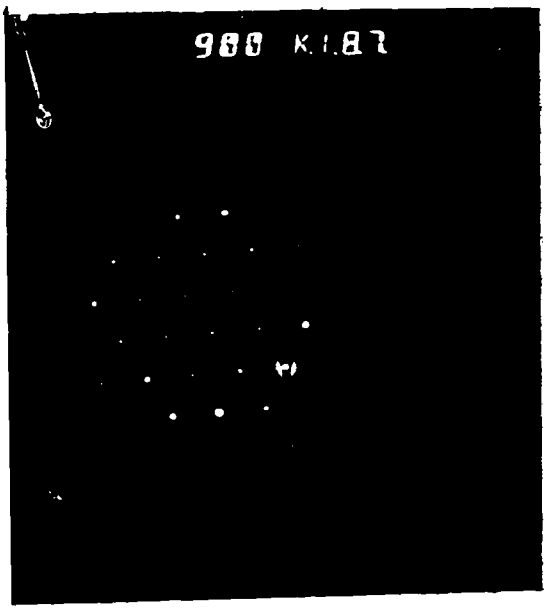

(d)

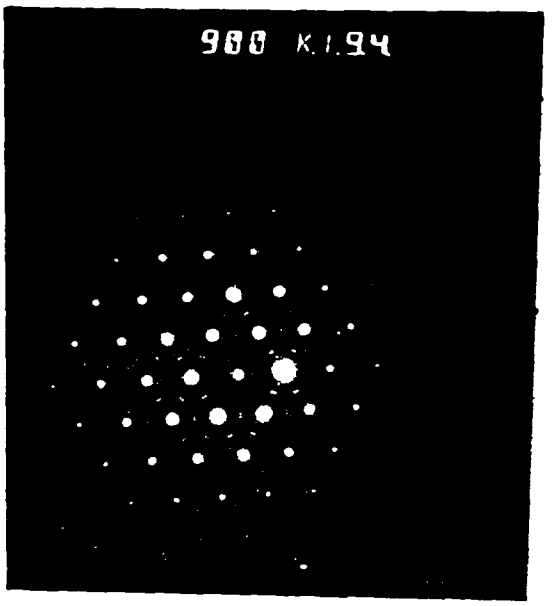

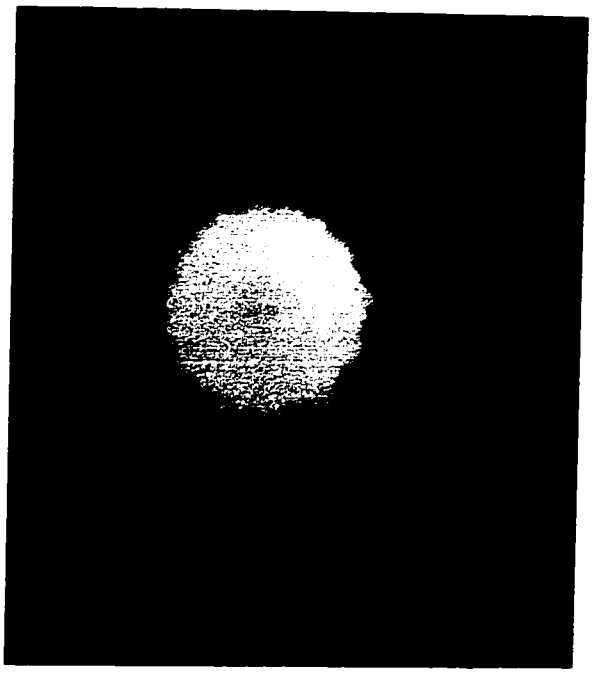

FIGURE 4. CBED pattern of Fe_7S_8 from $[001]_{NiAs}$ zone direction.

symmetries in this direction. The observation that both the zero order Laue zone (ZOLZ) (central bright area) and the first order Laue zone (FOLZ) (outer thin ring) are coaxial indicates that the beam direction lies along the $[001]_{NiAs}$ axis. By inspecting the changes in the intensity of ZOLZ and FOLZ, it can be found that the brightness of FOLZ is not uniform and the $(0\bar{4}40)_{NiAs}$ reflection in ZOLZ is very weak in comparison with $(40\bar{4}0)_{NiAs}$ and $(\bar{4}400)_{NiAs}$ reflections. This distribution in the reflection intensity implies the absence of hexagonal/trigonal symmetry, but the occurrence of a two-fold axis whose direction is arrowed in Fig. 4. We were unable to orient the sample for a good quality SAD in any $[hk0]_{NiAs}$ zone direction due to the restrictions on the degree of tilting the crystal, but the SAD for the $[012]_{NiAs}$ zone axis clearly exhibited a 4C superstructure (notice that 3 weak reflection spots lie between NiAs-type sublattice maxima $(0000)_{NiAs}$ and $(20\bar{2}\bar{1})_{NiAs}$) and all the reflections could be indexed according to the monoclinic structure (Fig. 5). The sublattice parameters measured from these SAD patterns are a=3.44 ± 0.03Å and c=5.68 ± 0.04Å which are in very good agreement not only with the spacing between the dark strips in Fig. 2, but also with what has been observed using XRD techniques.

A basic distinction between the monoclinic and trigonal structures of Fe_7S_8 is the difference in the vacancy density projected down the NiAs-type c-axis. In the case of the ideal ABCD monoclinic structure the doubling of $\bar{a}$ and $\bar{b}$ inherent in the Kagome net is lost in the projection. Thus, the projections of ideal monoclinic pyrrhotite in this zone show no superstructure; whereas in the ideal ABC trigonal case a doubling of the cell

(a)

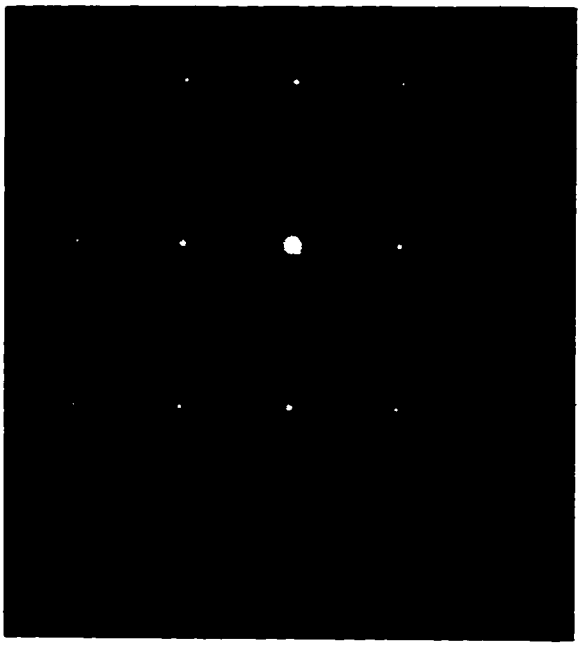

(b)

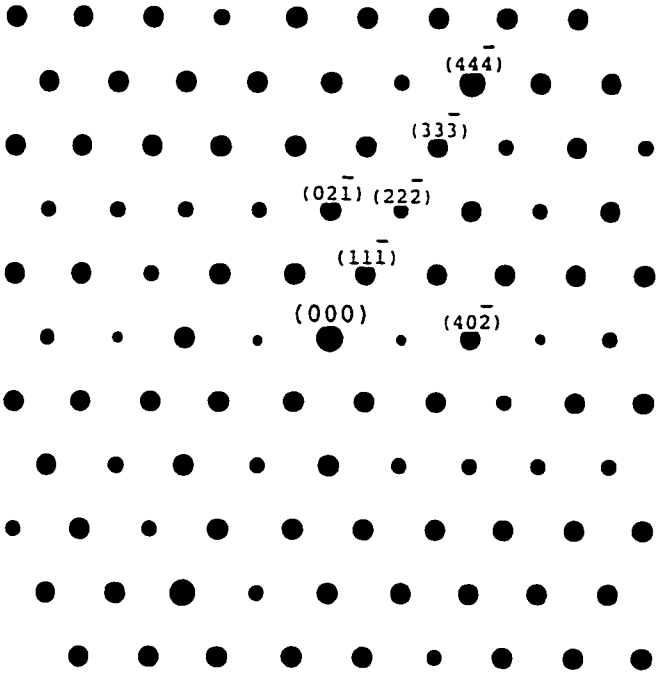

FIGURE 5. (a) The SAD pattern for $[012]_{NiAs}$ zone; (b) the computer-generated pattern (x1.5) from the same zone axis based on the monoclinic structure where the indices refer to the monoclinic structure.

edges would be observed. This feature of the distinct SAD patterns was simulated very well by the computer program (Microscopist). Figure 6 displays the computer-generated SAD patterns for both the ideal ABCD and ABC stacking cases on the basis of the structural information provided in literature [2, 4].

Thus the above observations, i.e.(1) alternating density along the c-axis, (2) no superstructure in projection down c-axis and (3) 4C superstructure reflections in the $[012]_{NiAs}$ zone direction, are all consistent with the interpretation that the known monoclinic structure of Fe_7S_8 is the stable modification at room temperature. It can be concluded that, however, the extent of monoclinic distortion in the synthetic sample is significantly lower than that found in natural samples, i.e., the lattice distortion is minimal and the observed monoclinic structure is present on a nearly undistorted hexagonal lattice.

Order-Disorder Transition at Elevated Temperature

When the sample temperature was raised to 210^0C, and the $[001]_{NiAs}$ SAD pattern observed, in spite of presence of some randomly distributed reflection spots, a set of very weak spots was found to appear systematically between pairs of reflection maxima of the NiAs-type substructure. This observation can be interpreted as the formation of superstructure with doubled *a*- and *b*-length over a depth suitable for diffraction. However these weak superlattice spots were no longer observed when the temperature reached 340^0C (Fig. 3b and 3c). These changes show that some superlattice with doubled *a*- and *b*-axes was developed and subsequently destroyed in the course of heating the sample. This development and destruction of 2Ax2A superlattice in projection upon heating indicates

(a)

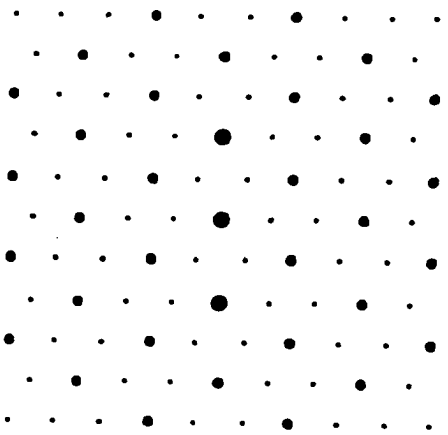

(b)

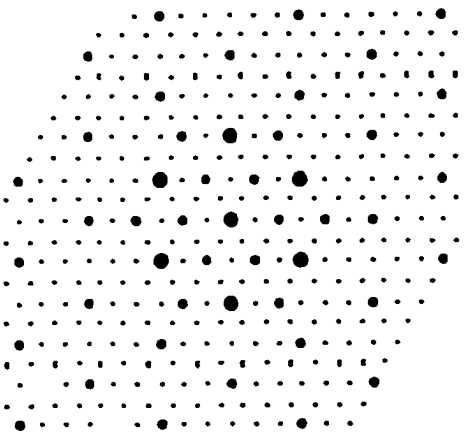

FIGURE 6. (a) A SAD pattern from $[001]_{NiAs}$ direction simulated for the monoclinic structure with the ABCD stacking. The space group is C2/c, and the structural information reported in Ref. [2] is used. Notice that this pattern shows no superlattice reflection. (b). A SAD pattern from the $[001]_{NiAs}$ direction simulated for the trigonal structure with the ABC stacking. The space group is $P3_121$, and the structural information reported in [3] is used. Notice that this pattern shows superlattice spots resulting in a doubling of a- and b-axis length.

that some trigonal ABC ordering in Fe_7S_8 are formed between room temperature, where the monoclinic is stable, and 340^{0}C, where the vacancies disorder. These observations also show that at these relatively low temperatures a two-phase equilibrium mixture is not achieved, but rather a mixing of stacking sequences occurs. Because the XRD patterns at 350^{0}C showed superstructure diffraction peaks at low angle of 2θ and because a rapid increase of magnetization was found upon cooling samples heated to 340°C [10], it is concluded that the vacancies do not disorder to yield a NiAs-type structure at this temperature but rather remain in a · · · DFDFDFDF · · · stacking sequence (D: iron deficient plane with randomly distributed vacancies; F: iron filled plane) along *c*-axis that results in a partially filled CdI_2-type symmetry. Therefore, the proposed transition sequence along the temperature scale is: monoclinic (ABCD) → trigonal (ABC) → defect CdI_2-type with a DFDF stacking.

The heat effects accompanying these transitions were observed during a DTA experiment on this synthetic Fe_7S_8 sample. Figure 7 shows the DTA curves corresponding to heating from 50°C to 400°C and subsequent cooling from 400°C to 50°C. A small peak can be found at about 240^{0}C, and a large peak follows at about 310°C. These results indicate that at the DTA heating and cooling rates the sample undergoes two changes in structural modification, one corresponding to, as proposed, the monoclinic → trigonal transition (or better disordered monoclinic → disordered trigonal) probably in a wide temperature range between 200°C and 250°C, the other corresponding to the vacancy-disordering transition in a narrow temperature range from 305°C to 320°C. Also, the

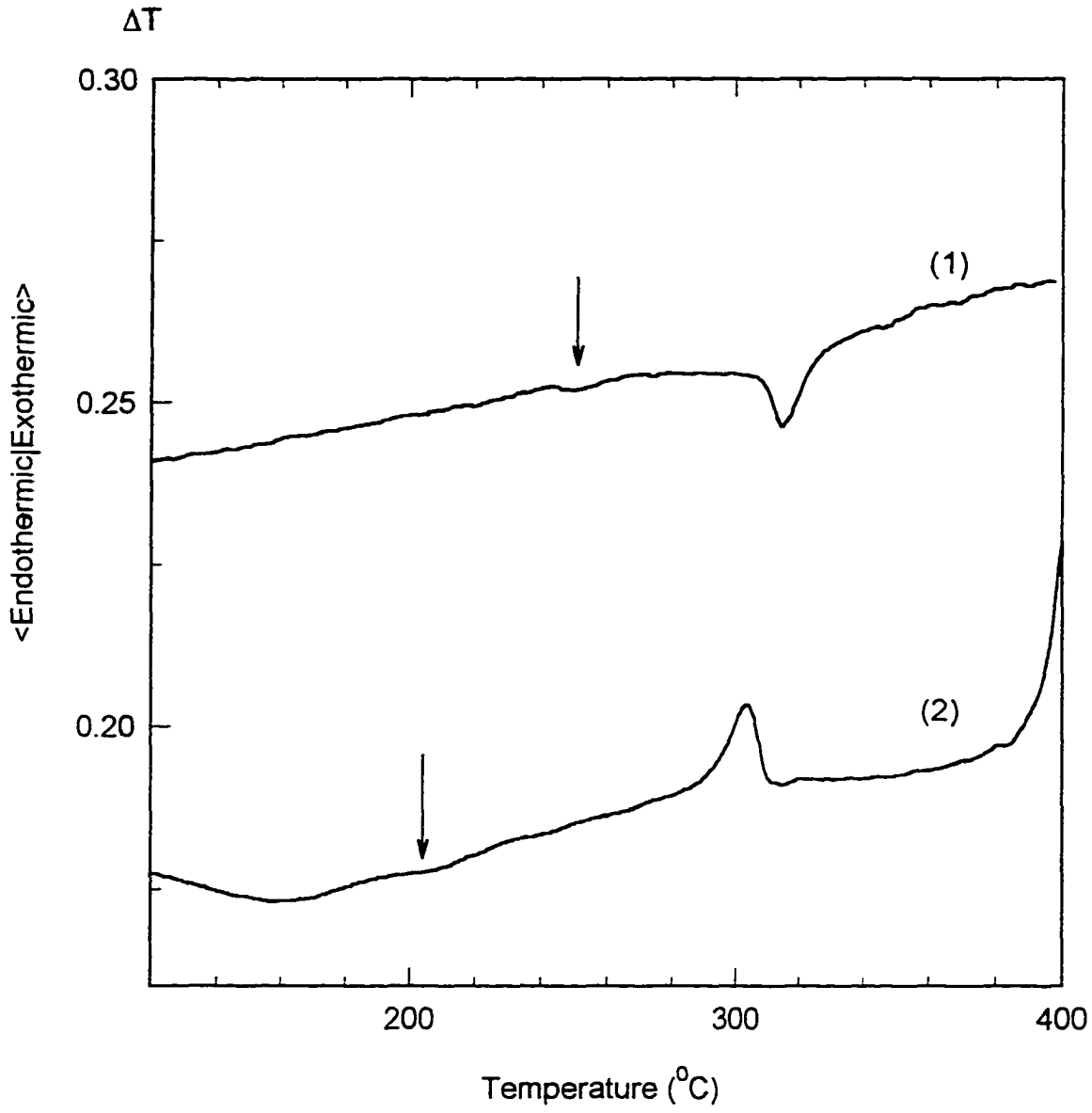

FIGURE 7. DTA curves of the synthetic Fe_7S_8 sample.
Curve 1: heating from 50°C to 400°C at +5K/min.
Curve 2: cooling from 400°C to 50°C at -5K/min.
The small anomalies are indicated by arrows.

transitions in these two temperature ranges were observed from the thermal-magnetization and high-temperature x-ray diffraction investigations as will be reported in a separate paper.

SAD Pattern after Quenching Samples

When the sample was quenched from 340^{0}C to room temperature in a few minutes, the SAD in the projection down the $[001]_{NiAs}$ direction demonstrated a relatively complicated Kagome pattern (Fig. 3d). A set of split spot pairs is displayed symmetrically at 1/2 ($\boldsymbol{a}^* + \boldsymbol{b}^*$) $\pm\delta$ relative to n/2 $\boldsymbol{a}^*$ and n/2 $\boldsymbol{b}^*$ (n=odd). These split diffraction spots indicate that a discommensuration occurs in the [001] plane when the sample is quenched on this time scale. The absence of this discommensuration in the as prepared samples shows that the annealing procedures used in the preparation yields predominantly the monoclinic ordered structure (although not ordered to the extent of natural samples). The doubling of *a*- and *b*-axes in the $[001]_{NiAs}$ projection in the quenched sample indicates the formation of Kagome net within the vacancy containing layers without formation of the monoclinic ordering along the $[001]_{NiAs}$ direction, while the discommensuration suggests the existence of domains at relative long intervals along the $[110]_{NiAs}$ and $[1\bar{2}0]_{NiAs}$ directions. Such domains would result from periodic mixing of ABC trigonal stacking adjacent to ABCD monoclinic stacking with boundaries perpendicular to the $[110]_{NiAs}$ and $[1\bar{2}0]_{NiAs}$ directions and period appropriate to the length of 1/2 ($\boldsymbol{a}^* + \boldsymbol{b}^*$) $\pm\delta$ (δ was measured to be 5.91×10^{-3} Å^{-1}, which corresponds to a length of 169Å (~ 50a)).

Quenching the disordered structure from high temperatures shows the strong tendency toward the formation of Kagome nets. The subsequent stacking of the Kagome nets depends on the temperature and cooling rate. However, it seems that the ABC sequence is more favored by rapid cooling . By using x-ray diffraction Fleet [3] investigated the structure of Fe_7S_8 samples prepared by quenching from 500^0C, and found that crystals were twinned in such a way that domains were rotated by multiples of 60^0 about the *c*-axis, as is the case with mixing of ABC and ABCD stacking. Thus, the results from both the x-ray and electron diffraction support the transition sequence proposed above, and are consistent with a kinetic barrier in the course of the transition from ABC stacking to ABCD stacking that was partially overcome in the samples annealed in the preparation of materials for this study, and as they are frequently found in natural occurring samples.

Transmission Electron Micrographs

On the other hand, TEM images reveal a change of microstructure with temperature. At room temperature the grains in the sample are highly faulted, most likely due to annealing and slow cooling during sample preparation (Fig. 8a). As discussed above, the stacking sequence probably varied from one domain to another. As the temperature was raised, the observed strain contrasts became diffuse and vanished with the disappearance of the defects (Fig. 8b-c), implying that the disordering of vacancies has developed, so that the microstructure tends to reach a unified stacking sequence. After the sample is quenched, large size domains with the uniform microstructure are maintained, but some dislocations were observed (Fig. 8d).

FIGURE 8. TEM images: (A) at room temperature; (B) at 210°C; (C) at 340°C; (D) when the sample was cooled to room temperature.

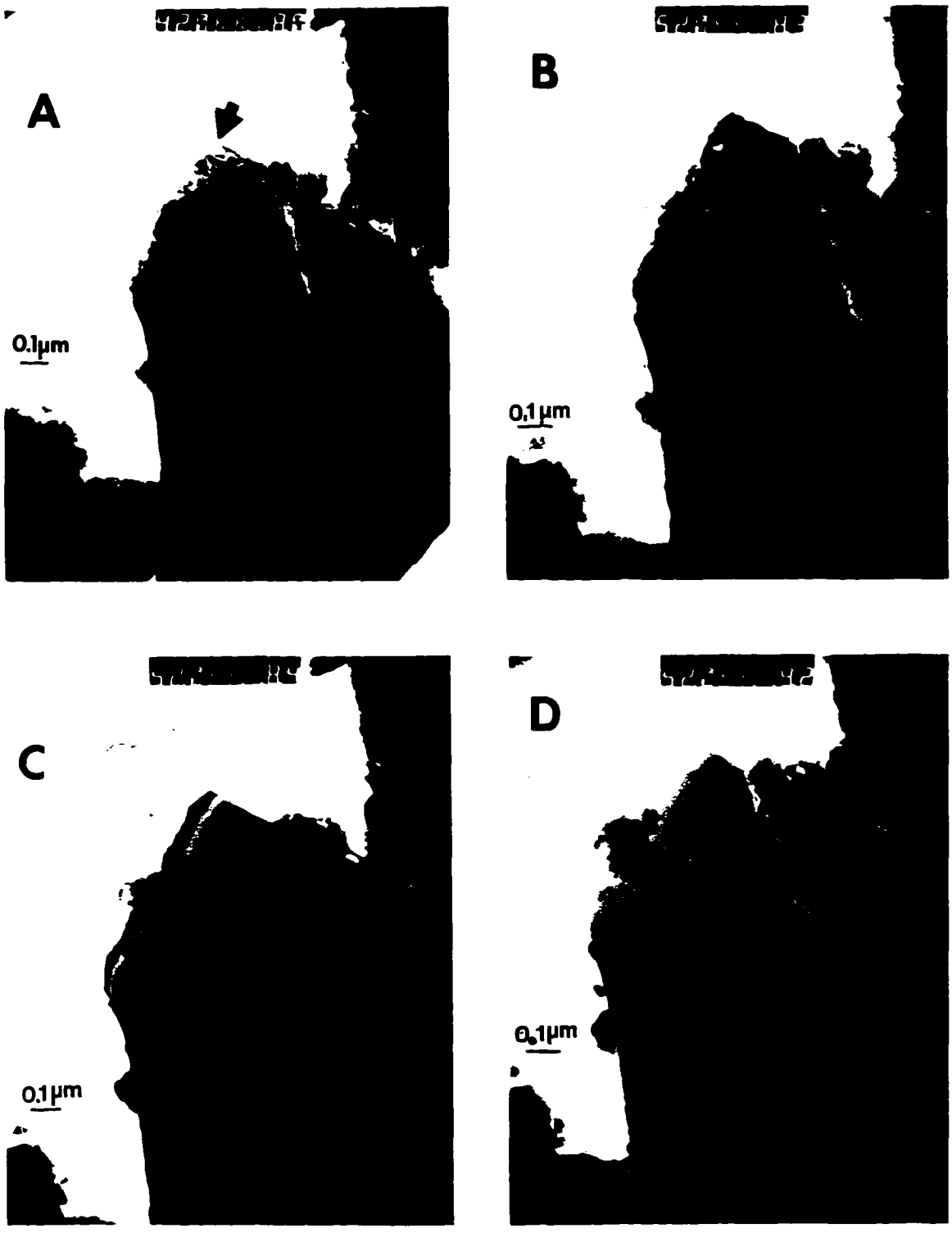
A
0.1μm
B
0.1μm
C
0.1μm
D
0.1μm

Conclusion

The structures in Fe_7S_8 result from closely related stacking sequences of Kagome nets in alternate metal-containing layers along *c*-axis. In this work we have attempted to attach significance only to what can be readily distinguished. Among the stacking sequences described above, only the trigonal (ABCABC...) doubles the basal plane periods in the projection down the *c*-axis. A crystal that was generally expected, and on the basis of diffraction patterns and lattice images confirmed, to be the monoclinic structure was observed via diffraction pattern to transform at 205°C to yield diffraction maxima that double *a* and *b* in projection down the *c*-axis. At this temperature an endothermic effect was correspondingly observed (i.e., from DTA) upon heating a bulk sample and the sample is known to be ferrimagnetic. Taken together these structural and property observations point to, at least partial, ABCABC... ordering with increasing temperature, and thus to reversible development of this ordering in pyrrhotite.

References

[1] M. Posfai and I. Dodony, *Eur. J. Mineral.* **2**, 525 (1990).

[2] M. Tokomi, K. Nishiguchi and N. Morimoto, *Am. Mineral.* **57**, 1066 (1972).

[3] M. E. Fleet, *Acta Cryst. B* **27** ,1864 (1971).

[4] A. Nakano, M. Tokonami and N. Morimoto, *Acta Cryst. B* **35**, 722 (1979).

[5] F. Keller-Besrest, G. Collin and R. Comes, *Acta Cryst. B* **38**, 296 (1982).

[6] H. Nakazawa, N. Morimoto and E. Watanabe, *Acta Cryst. B* **35**, 722 (1979).

[7] H. Nakazawa, N. Morimoto and E. Watanabe, *Acta Cryst. A* **Suppl. 31**, 722 (1975).

[8] I. Dodony and M. Posfai, *Eur. J. Mineral.* **2**, 529 (1990).

[9] F. Li and H. F. Franzen, *J. Solid State Chem.* **126**, 108-120 (1996) (Chapter 6).

CHAPTER 6

ORDERING, INCOMMENSURATION AND PHASE TRANSITIONS IN PYRRHOTITE. PART II: A HIGH-TEMPERATURE X-RAY POWDER DIFFRACTION AND THERMOMAGNETIC STUDY

A paper published in the Journal of Solid State Chemistry

Fan Li and Hugo F. Franzen

Abstract

High-temperature x-ray diffraction (HTXRD) has been combined with thermomagnetic measurements to study synthetic and natural pyrrhotites. The temperature dependence of the properties observed in DTA, thermomagnetic and diffraction measurements indicates that transitions consistently occur upon heating and cooling so long as the sample is kept below 400°C, but if the ultimate heating temperature is higher than 550°C the transitions are altered, probably due to the loss of sulfur. The previously proposed transition sequence for Fe_7S_8 was supported by HTXRD observation, especially on natural monoclinic pyrrhotite. For intermediate pyrrhotite, the principal ordering was found to be the formation of Kagome nets, and it was found that the vertical stacking sequences that are commensurate along the *c* axis yield antiferromagnetic characteristics. Based on the changes observed in the HTXRD patterns it is proposed that the mechanism for an observed magnetic λ-transition between the temperatures 150°C and 250°C is the transformation of a commensurate structure with

ABCD layering of Kagome nets into a vacancy-disordered structure with the same *c*-modulation.

INTRODUCTION

Studies of vacancy and magnetic spin orderings have been of special importance in solid state research because they lead directly to an understanding of crystallographic and magnetic structures, nonetheless, two complications make such studies difficult: First, there is no method to directly probe the individual vacancies and magnetic spins. The macroscopic observations are averages over correlations among the vacancies and spins. Second, because the temperature, cooling rate and other factors usually influence the resultant ordering, it is difficult to achieve nearly perfect ordering in a crystal. Different experimental conditions often alter the ordering path during property measurements. Thus it is frequently necessary for either thermodynamic or kinetic reasons to study an imperfect or incomplete ordering process.

Pyrrhotites, which are iron sulfides with the general composition $Fe_{1-x}S$ (x=0-0.125), are typical defect compounds. The prototypical structure for this system is NiAs-like with antiferromagnetically coupled iron-layers. At low temperature (below 400°C) most pyrrhotites exhibit some degree of superstructure development as the result of vacancy ordering, which, in turn, results in varied magnetic, thermal and electric properties and complicated phase relations.

In previous studies [1-2], we have discussed the structural aspects and phase transitions for the two extreme cases of pyrrhotite, FeS and Fe_7S_8. In the FeS case, the transition

sequence along the temperature scale is concluded to be: distorted troilite (antiferromagnetic with spins || c) → troilite (spins rotated to ⊥c) → NiAs-type (paramagnetic with random spins). We have found that this transition sequence can be extended to the composition range, at least, from $Fe_{1.002}S$ to $Fe_{0.996}S$. When x reaches 0.05, pyrrhotite comes into a two-phase region where the troilite phase co-exists with a hexagonal phase. The α-transition for this region does not reverse upon cooling at the usual laboratory rates due to a transition collapse [3], and intermediate hexagonal phases result. In the Fe_7S_8 case, a perfect ordered structure can be achieved by the maximum separation of iron vacancy sites. This ordered structure has a stacking sequence of iron layers, as in the ideal model proposed by Bertaut [4], of $D_AF\ D_BF\ D_CF\ D_DF$ along the c-axis of the NiAs structural type (F stands for the iron filled layer; D_A, D_B, D_C and D_D stand for the four Kagome nets unequivalent with respect to the origin). Based on the results of a TEM investigation, the idealized transition sequence was found to be: monoclinic ABCD stacking (ferrimagnetic) → trigonal ABC stacking (ferrimagnetic) → hexagonal structure with vacancies disordered within alternate planes (paramagnetic) → NiAs-type structure with disordered vacancies.

On the other hand, the pyrrhotites with intermediate compositions (x=0.05-0.12) have also received considerable attention because this composition range is widely found among the natural pyrrhotite minerals, and because the order-disorder processes in this group of pyrrhotites remain unexplained. The main efforts regarding this composition range have focused on the following aspects:

1. Possible discrete phases. A number of stable NC superstructures (A and C are the axial lengths of the NiAs-type unit cell, and N is an integer) have been discovered by powder x-ray and electron diffraction experiments, such as 5C for Fe_9S_{10} [5], 6C for $Fe_{11}S_{12}$ [6] and 11C for $Fe_{10}S_{11}$ [7,8]. Their structures are generally based on the Fe_7S_8 structure, i.e., partially filled Kagome net layers and iron-filled layers that are stacked in such a way that long-range ordering is established along the *c*-dimension, and these structures commonly have 2A repeats (inherent in Kagome nets) within the planes. Although these idealized superstructure types are theoretically possible, there is still a lack of evidence concerning structural details and information concerning transition sequences. On the other hand, evidence has revealed that some pyrrhotites over this composition range have hexagonal structures which have, in fact, integral $A_{NiAs\text{-}type}$ repeats but non-integral $C_{NiAs\text{-}type}$ repeats. Apparently, this implies that incommensurate ordering also occurs in this system.

2. Magnetic properties. The magnetic behavior of pyrrhotite is sensitively altered by changes of composition. In addition to the antiferromagnetism found in stoichiometric or near stoichiometric iron sulfide ($Fe_{0.92}S$ - FeS), other magnetic behaviors have been discovered and were categorized according to the following three types [9]: (1) Weiss-type, that is, ferrimagnetic. This behavior corresponds to the composition ranging from $Fe_{0.87}S$ to $Fe_{0.88}S$, including Fe_7S_8. It has been widely accepted that this ferrimagnetism arises from unbalanced antiferromagnetic coupling, and that the Curie transition takes place at 315°C; (2) Peak-type, i.e. a so-called anti-Curie transition (because ferrimagnetism disappears as the temperature decreases) or a λ-transition (because of the peak shape). The pyrrhotites showing this

behavior have compositions between $Fe_{0.91}S$ and $Fe_{0.92}S$. In this case the magnetization is characterized by an abrupt rise and fall of a ferrimagnetic peak in a narrow temperature range (from 200°C to 250°C), while elsewhere the pyrrhotite is antiferromagnetic; (3) mixed-type. The pyrrhotite for this magnetic type is actually a mixture of Weiss-type and peak-type pyrrhotite, and hence the thermomagnetic behavior is a combination of the first two types.

Nevertheless, the mechanism of the anti-Curie transition has remained unexplained, even though the later discovery of the various NC superstructures seems to shed further light on the mechanism giving rise to its formation. One hypothesis proposed by Lotgering [10,11] considered a competition between vacancy ordering and spin ordering. Since the spin ordering is a second-order transition but vacancy ordering is first order, Lotgering argued that it was possible for the free energy of a magnetically ordered but vacancy disordered phase to be less than that of a magnetically and vacancy ordered phase at some temperature below the Curie point. Thus the transition was proposed to be: a phase with ordered spins and disordered vacancies at the Neel point (315°C) $\xrightarrow{300^\circ C}$ spins disordered and vacancies ordered $\xrightarrow{265^\circ C}$ vacancies disordered and spins ordered (gradually to reach the maximum ferrimagnetization) $\longrightarrow$ vacancy disordering at low temperature. This competitive ordering mechanism was not supported by the neutron diffraction experiments later conducted by Andersen and Torbo [12,13]. Another interpretation was proposed by Hirone et al. [14,15]. They suggested that there may be two vacancy-ordered phases, one that is ferrimagnetic stable at higher temperature, the other, stable at lower temperature, is antiferromagnetic, and

that they transform at T_λ (220°C). Since the magnetic transition occurs at about 280°C on a cooling ramp, rather than at 315°C, at which temperature the spin ordering is supposed to occur, an extra vacancy disordered structure was proposed to follow the high-temperature ferrimagnetic structure. However, the DSC experiment carried out by the same authors revealed only two transitions at 220°C and 315°C, instead of three transitions, and there was no experimental evidence to identify the two phases with different orderings on either side of T_λ. On the other hand, detailed thermodynamic data for the anti-Curie transition were acquired by Townsend's group [16]. However, from the structural information obtained using Mossbauer spectroscopy at high temperature, they have not succeeded in identifying the structure that supports the ferrimagnetic superlattice over the temperature range of 150°C - 250°C. Therefore, an inherent relationship between the revealed NC superstructures and anti-Curie transition has not yet been established.

In the present work, we have performed high-temperature XRD, thermomagnetic and DTA measurements on pyrrhotites with a variety of compositions with special attention paid to the intermediate pyrrhotites. These studies provide new insight into the phase relations in this system.

RESULTS AND DISCUSSION

1. Thermomagnetic Behaviors

The thermomagnetic measurements on our synthesized samples demonstrated all three types of magnetic behavior described in the introduction. Figures 1, 2 and 3 display Weiss-

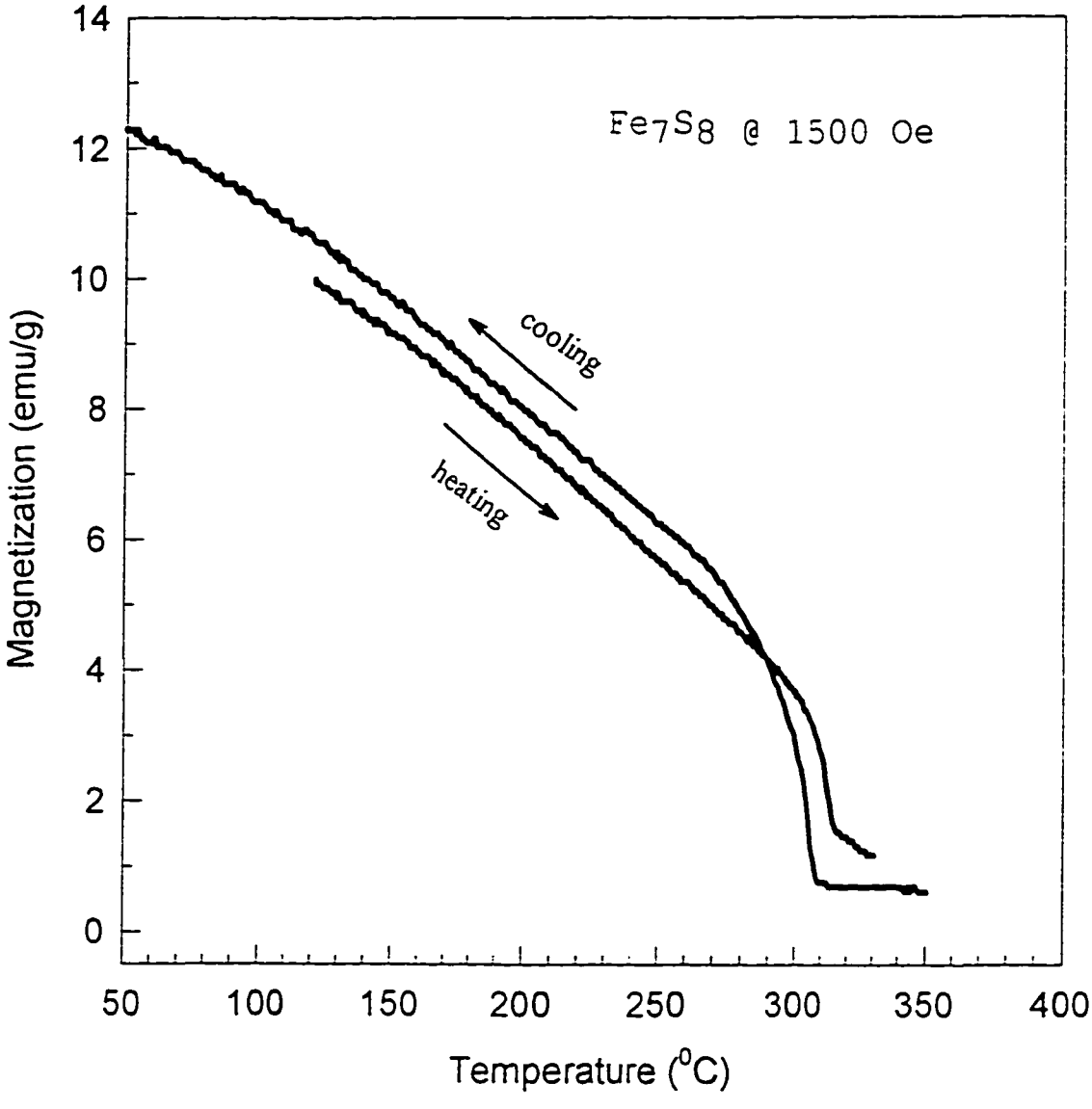

FIGURE 1. Temperature dependence of magnetization for a Weiss-type pyrrhotite (Fe_7S_8).

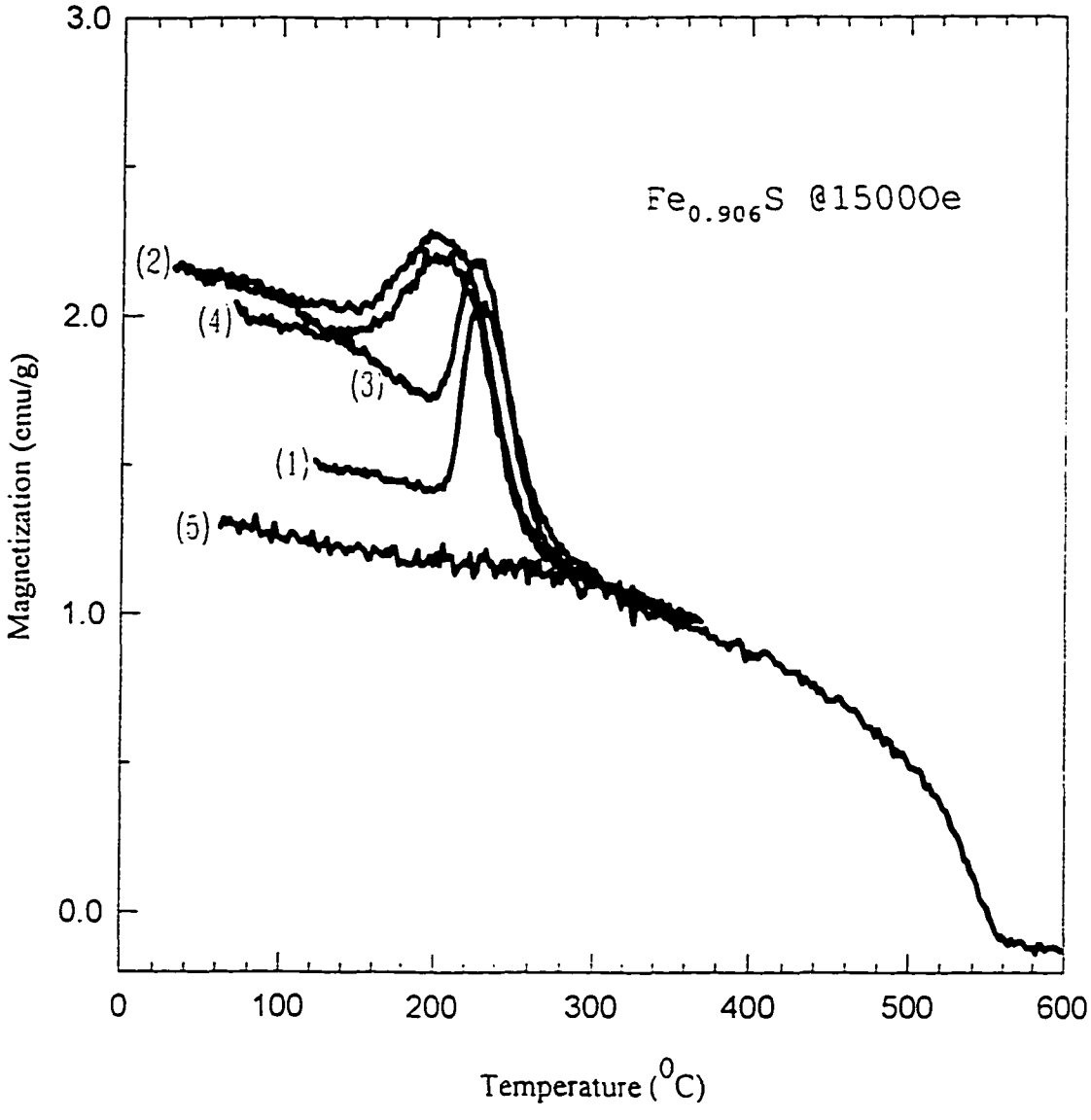

FIGURE 2. Temperature dependence of magnetization for a peak-type pyrrhotite subjected to three sequential heating-cooling cycles.
curve 1: heating from 100°C to 350°C;
curve 2: cooling from 350°C to 30°C;
curve 3: heating from 30°C to 350°C;
curve 4: cooling from 350°C to 30°C;
curve 5: cooling from 600°C to 50°C.
Notice that on curve 5 only the magnetization contributed by magnetite was maintained when the sample was cooled from 600°C.

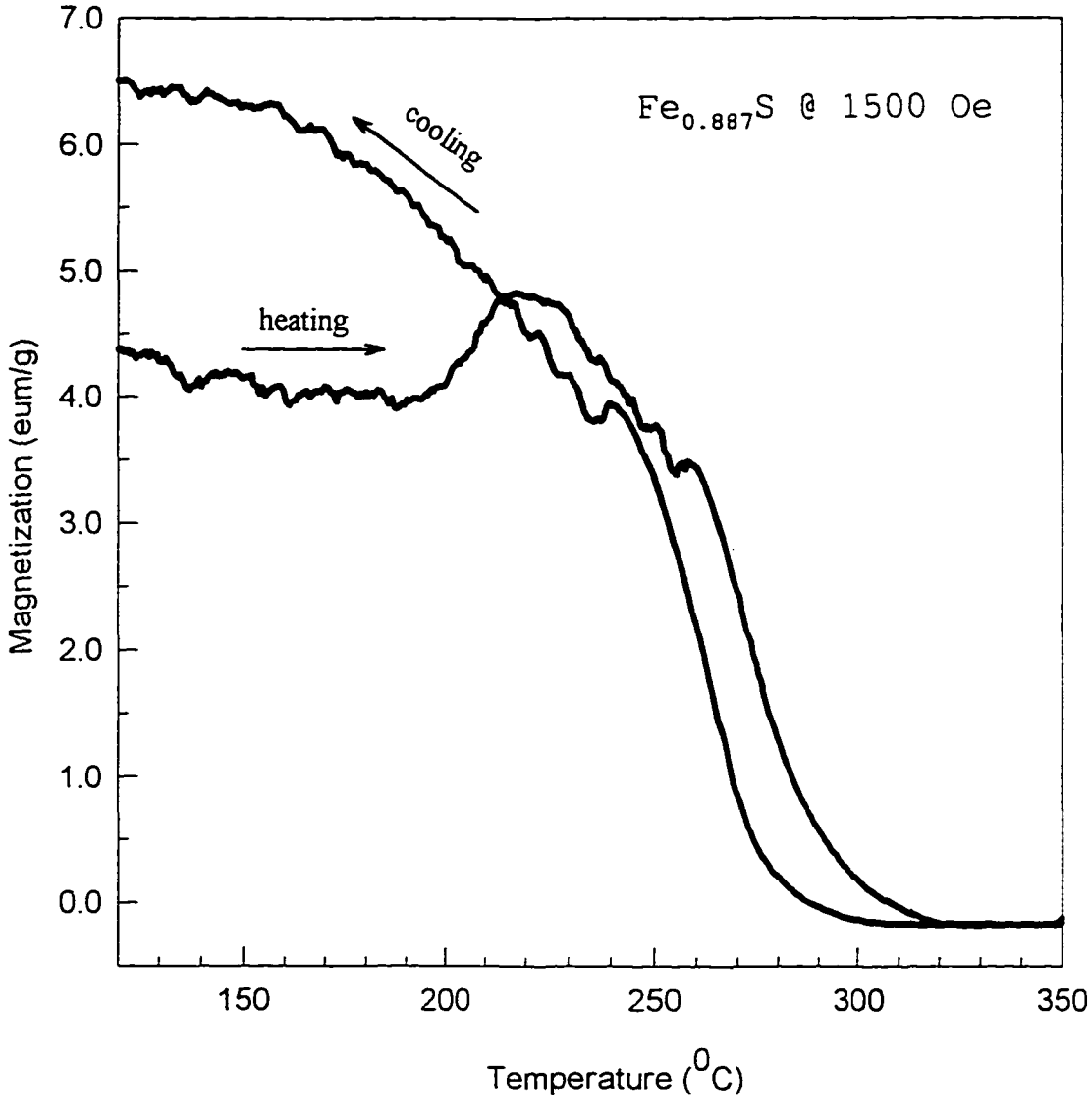

FIGURE 3 Temperature dependence of magnetization for a mixed-type pyrrhotite

type curve from an Fe_7S_8 sample, the peak-type curve from an $Fe_{0.906}S$ sample and a mixed-type curve from an $Fe_{0.887}S$ sample, respectively. Notice that since some of the samples contain traces of magnetite (by weight about 0-1.5%) formed during synthesis, the magnetization curves in the figures show a contribution from magnetite as demonstrated by its characteristic Curie transition (=585°C). Nevertheless, some important features were observed and are summarized as follows:

1). Saturation magnetization. For Fe_7S_8, the saturated magnetization can be reached when the external field exceeds 10,000 Oe (M=15.9 emu/g at 20,000 Oe). However, the atomic magnetic moment could not be directly determined because of the anisotropy in polycrystalline pyrrhotite. In order to estimate the corrected saturation magnetization, a comparative experiment was carried out on a polycrystalline magnetite (Fe_3O_4) sample. The result showed that for Fe_3O_4 the experimental magnetization was 78% of that calculated. Hence the saturation magnetization for Fe_7S_8 was estimated to be 20.4 emu/g at room temperature, corresponding to a net magnetic moment J= 9.5 m_B per unit cell (a 4C structure containing four Fe_7S_8). This magnitude, though in a good agreement with the values measured by Schwarz and Hayase et al. [9, 17], is still less than that calculated according to Bertaut's model. Ideally, if all the spontaneous spins are assumed to lie exactly in the *a-b* plane and the antiferromagnetic coupling occurs only between the iron-filled layers and the iron-deficient layers, the net uncompensated moment will be 16.5 m_B per unit cell (according to J= $4m_B$ for Fe^{++} and J=$5m_B$ for Fe^{+++}). Accordingly, approximately 57% of the iron vacancies yield a net ferrimagnetism. In other words, out of the possible 1/8 of the vacant iron sites that could be

uncompensated (assuming parallel ordered spins in the plane), only 57% contribute to the net ferrimagnetization, indicating that residual disorder or other factors such as canting of magnetic moment off the c-plane have to be taken into account. As for the $Fe_{0.906}S$ sample, the maximum ferrimagnetization at the anti-Curie transition point is estimated to be approximately 1/5 of that in Fe_7S_8. This magnitude is compatible with the proportion of iron vacancies because cancellation of ferrimagnetism between the defect layers inevitably exists for this case.

2). Magnetic reversibility. In the temperature range between 20°C and 400°C, the thermomagnetic behavior for all the samples can be reversed upon change from heating to cooling. The ferrimagnetization in Weiss-type pyrrhotite was recovered with a hysteresis of 10-20K upon cooling (Fig. 1). For peak-type pyrrhotite, the λ-shaped peak was also reversed on the cooling ramp, but is accompanied by the production of a Weiss-type component, indicating that the peak-type has been partially converted into Weiss-type at high temperature (see the cooling curve and the 2nd run curves in Fig. 2). On the other hand, heating mixed-type pyrrhotite also gave rise to an increase of Weiss-type component, and a decrease of peak-type component as shown in Fig. 3. This feature suggests that the peak-type pyrrhotite (with the antiferromagnetic structure) has the same structure as the high-temperature form of the Weiss-type (with the ferrimagnetic ordering), and that this structure is maintained at least, in part, when a relatively fast cooling is performed.

When the samples were heated to temperatures higher than 550^{0}C and subsequently cooled to room temperature, the magnetic behaviors were not recovered in any of the three

types of pyrrhotite, however. If the heating process proceeds in a relative short term and the cooling is at a slow rate, the reversal of ferrimagnetization is possible. This loss of ferrimagnetism can be attributed to the decomposition of samples. At the highest experimental temperatures sulfur may evolve from the pyrrhotite samples so that the stoichiometry of the samples and accordingly the magnetic properties are altered. Figure 4 illustrates a magnetization measurement for mixed-type pyrrhotite, in which the sample was rapidly heated to 500°C, 550°C or 600°C (in 10 minutes) and then slowly cooled to record its magnetization. It is interesting to notice that the mixed-type pyrrhotite can be transformed into pyrrhotite with more Weiss-type at 500°C, as did when cooled from 400°C, but with more peak-type at 550°C, and finally into almost complete peak-type at 600°C.

3). Natural pyrrhotites. No matter from which ore separation processing stage the natural pyrrhotite was derived, the magnetization curves consistently showed all three transitions—the anti-Curie, Curie transitions in pyrrhotite and the Curie transition in magnetite (Fig. 5). It is not surprising that sample Inco1 (magnetic portion) contains more Weiss-type component as well as magnetite, while sample Inco2 (non-magnetic portion) contains more antiferromagnetic component. The magnetization in all natural pyrrhotites was found to perish very easily upon heating the samples to 550°C. This is interpreted as related to the occurrence of impurities in the natural products which take over the excess sulfur from pyrrhotite at high temperature. It is noticed that the proportion of Weiss-type to peak-type pyrrhotite varies from the fast flotation samples (sample Inco 3) to slow flotation sample (sample Inco 4). As seen later in the XRD observations, the change of magnetic type that has its origin in changes

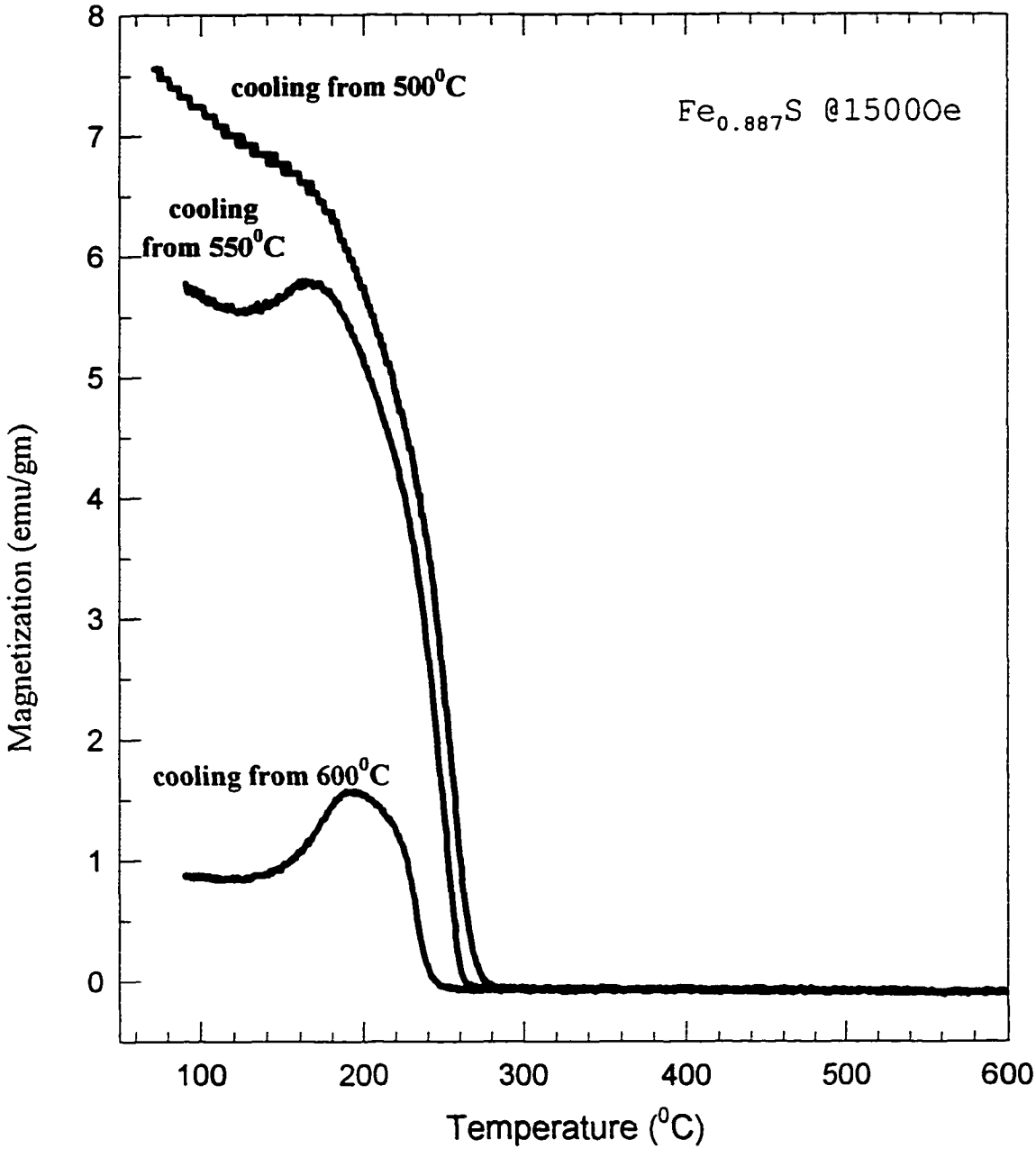

FIGURE 4. The change of magnetization when the mixed-type pyrrhotite was cooled from different temperatures.

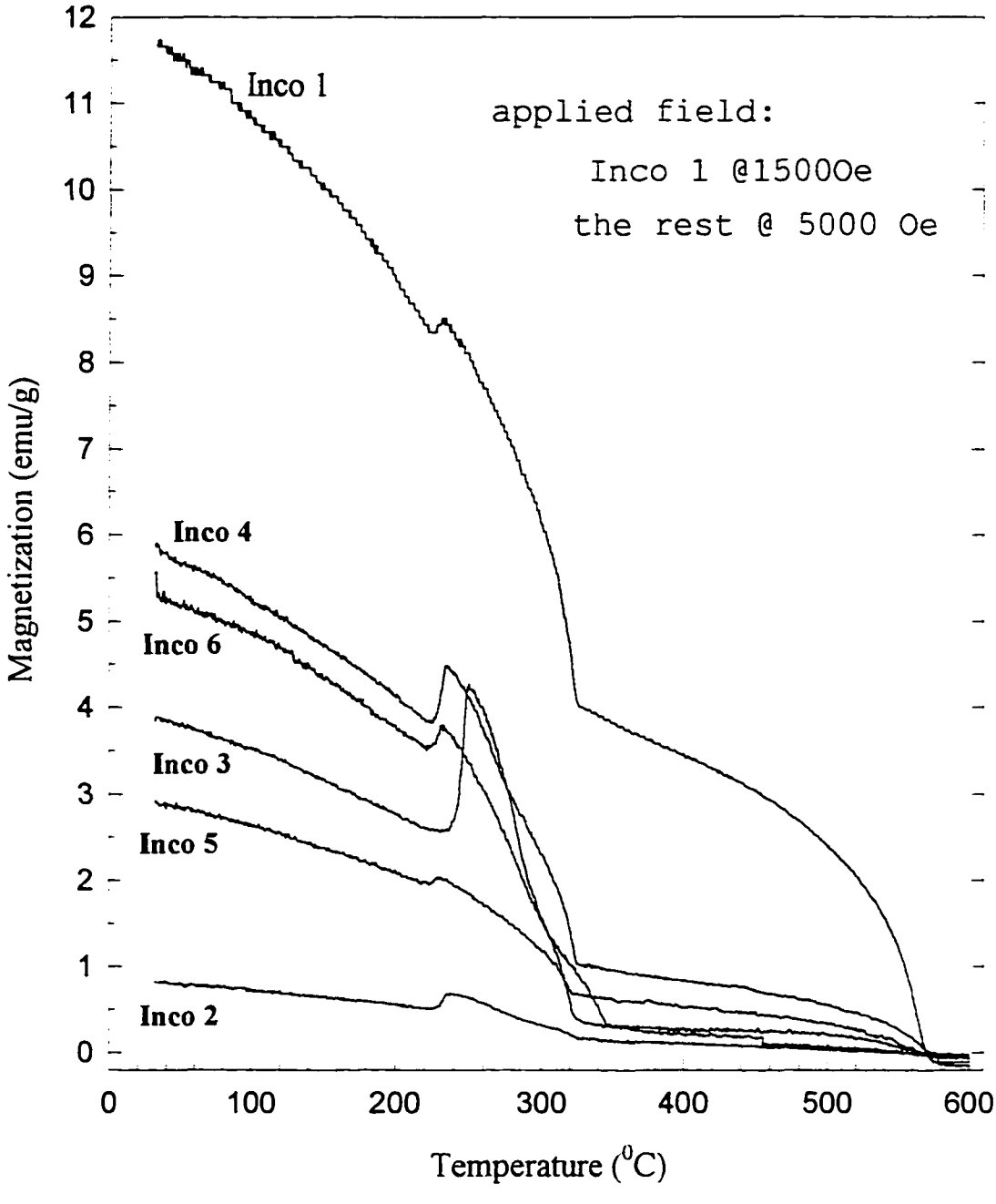

FIGURE 5. Thermomagnetic curves for natural pyrrhotites provided by Inco. All the curves correspond to the heating process. Note the magnetization contribution from magnetite which is characterized by its Curie transition at 580°C.

in the composition and structure results in the density order: Weiss-type > peak-type > non-magnetic-type (mainly, antiferromagnetic type). This may be important for the floating rate in separation process of the mineral.

2. DTA and HTXRD Results

In order to understand the magnetic behaviors illustrated above, DTA and HTXRD experiments were performed in two sequential heating-cooling cycles of 25°C-400°C and 25°C-600°C.

2.1. Weiss-type pyrrhotite.

The ideal ordered structure for Fe_7S_8 as proposed by Bertaut is monoclinic [4]. Its XRD pattern is characterized by significant peak splitting in the NiAs-type substructure diffraction [19]. This signature, especially in the $(102)_{NiAs}$ peak, was clearly manifested in natural magnetic sample (Inco1) in spite of the presence of a number of weak peaks originating from impurity phases (see Figure 6). For the synthesized sample, however, this kind of splitting is not obvious even though a broadening of the peak can be recognized (see Fig.7). At low angles (2θ), weak superstructure peaks can be identified and indexed according to the monoclinic structure, but they can as well be indexed as arising from the trigonal 3c superstructure because the powder XRD patterns of the two structure types are not strongly differentiated. Attempts to refine single-crystal diffraction from a synthetic Fe_7S_8 sample according to either the trigonal or monoclinic structure were unsuccessful. When diffuse diffraction between any two integer *l* reflections in the reciprocal space of the NiAs subcell was scanned, weak diffuse reflections were observed at $l = 1/3$ and $2/3$ implying a 3C

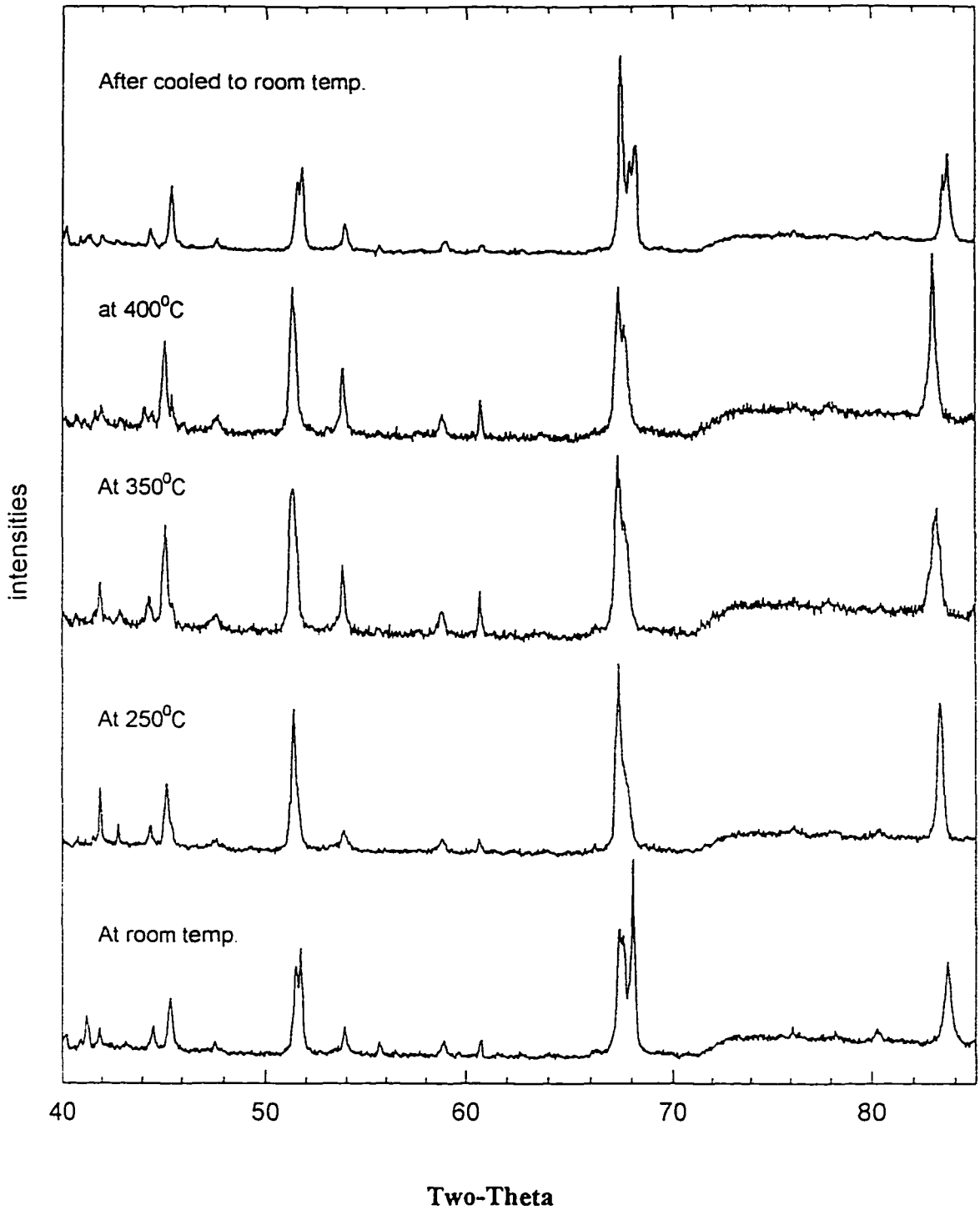

FIGURE 6. HTXRD patterns for natural magnetic pyrrhotite (Inco 1).

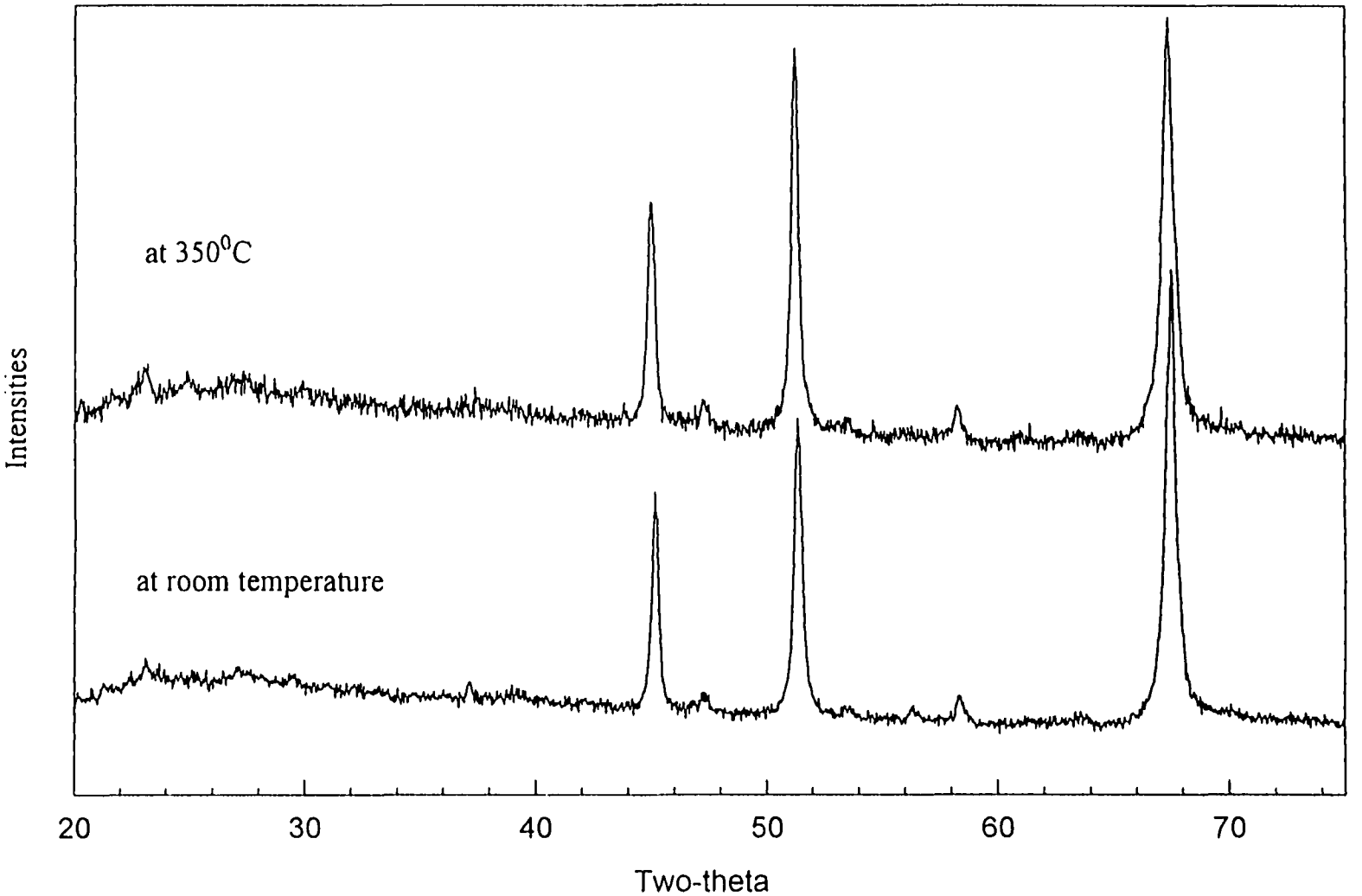

FIGURE 7 HTXRD pattens for the synthetic Fe_7S_8 sample.

supercell, and also at $l = 1/2$ implying a 4C supercell (see Fig. 8). This evidence indicates that the synthetic sample at this resolution yields not single crystals, but regions with mixed stacking sequences. A bulk sample contains stacking faults leading to different regions of 4C stackings (ABCD, BACD, CABD, and so on) such that the monoclinic symmetry is lost in the x-ray averaging. At the single crystal level, on the other hand, electron diffraction yields evidence of partially ordered "monoclinic" structures.

When the natural occurring Fe_7S_8 sample (Inco1) was heated to 150°C - 250°C, the split peaks in the XRD pattern were clearly seen to converge, and then a diffraction pattern closely approximating that expected from the trigonal structure was formed (Fig. 6). The monoclinic pattern was recovered on cooling to room temperature. This observation supports the transition sequence proposed for this type of pyrrhotite in a previous study [1]. On the other hand, the synthetic samples do not show a significant change in the XRD patterns until 550°C. This lack of differentiation results from the similarity in the patterns for the monoclinic and the trigonal structures and the greater extent of disorder relative to the natural samples.

When the temperature exceeded 550°C, a loss of sulfur from the synthetic sample was indicated by the resultant modification of the XRD patterns (see Fig. 9). Initially at 550°C, almost all the substructure diffraction peaks showed some splitting with time, indicative of sulfur loss relative to the original 7:8 ratio. As the sample was kept in the temperature range between 550° - 600°C, the split peaks converged, and finally transformed into a nearly ideal NiAs-type pattern with the disappearance of superstructure peaks at low angles. For the natural pyrrhotite samples, because chemical reactions between the pyrrhotite and impurities

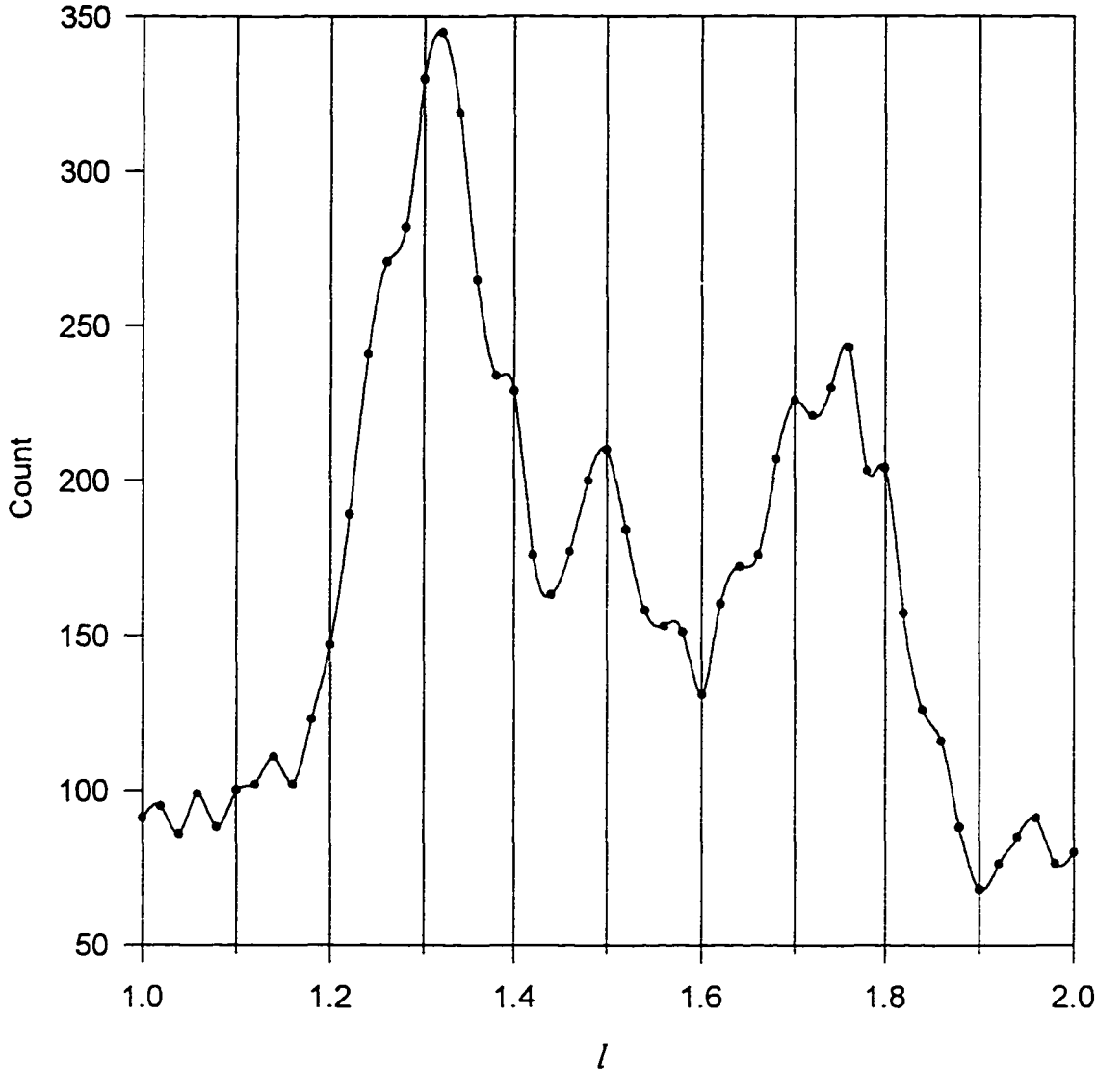

FIGURE 8. The x-ray diffuse diffraction scanned between indices (031) and (032) of NiAs-type cell. Notice that reflection maxima approximately appear at 1/4, 1/3, 1/2, 2/3 and 3/4 of integral *l*.

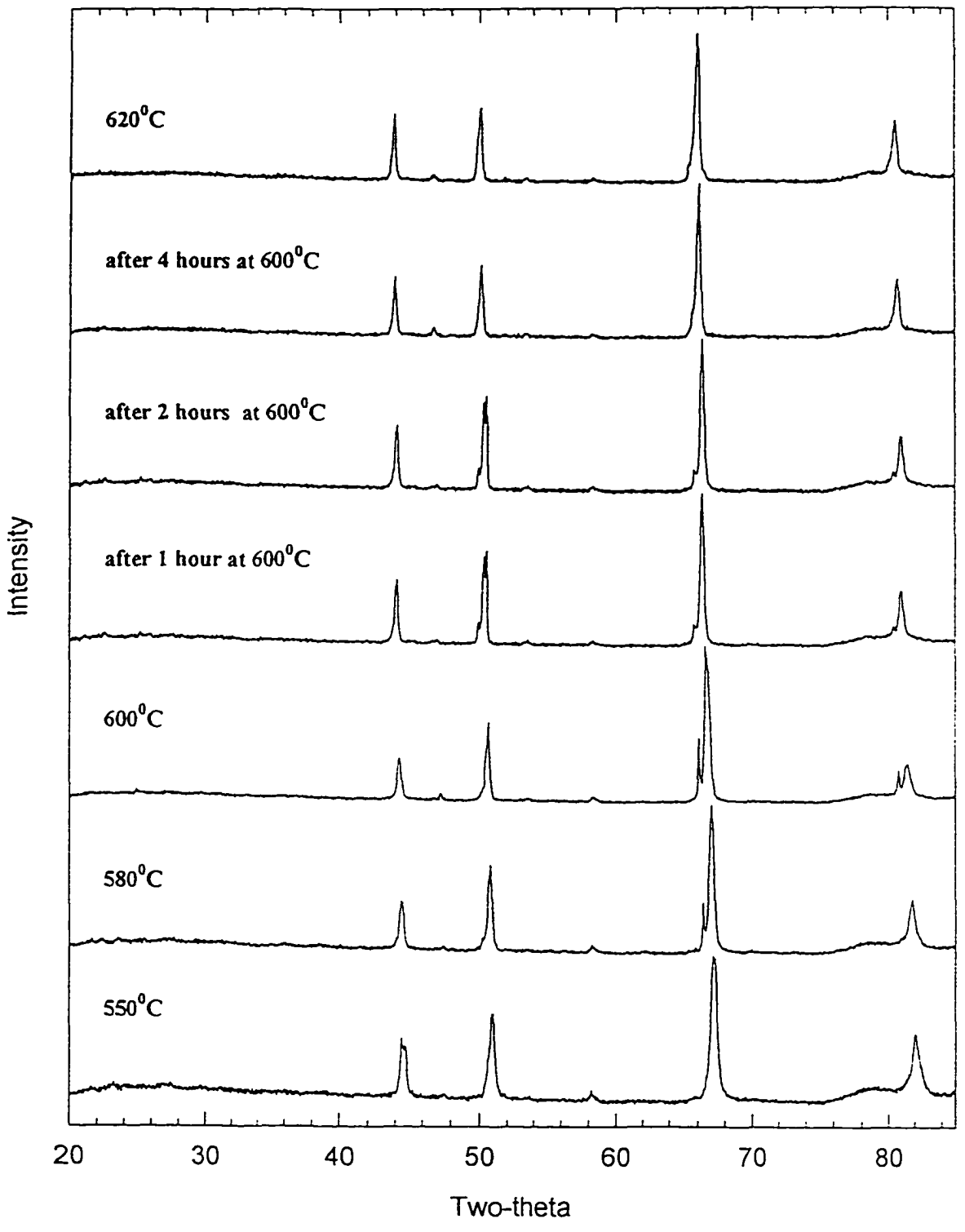

FIGURE 9. HTXRD patterns of the synthetic Fe_7S_8 sample for T>550°C.

may occur, it is difficult to identify the decomposition process by XRD patterns. Since the samples cooled from 600°C have been found to show no ferrimagnetism, the loss of ferrimagnetism can be attributed to the loss of sulfur (and hence of vacancies) accompanied by a disordering of the vacancies (i.e., all sites equally occupied) at high temperature, and inadequate time for ordering during cooling. On the other hand, there is a noticeable volume expansion of the unit cell from Fe_7S_8 to FeS in excess of the background thermal expansion. Therefore, the change in XRD pattern with time at T >550°C was such that a set of diffraction lines corresponding to the larger cell parameters appeared and eventually replaced the original pattern, which corresponded to the smaller cell and thus the simple NiAs structure was observed to grow through loss of sulfur above about 550°C.

A large peak was clearly observed on the DTA curves for both the natural and synthesized samples (see Fig. 10 and 11) at the temperatures at which the Curie transition is known to occur: at 315°C on the heating ramp and at 305°C on the cooling ramp, provided that the sample was not heated to a temperature at which noticeable decomposition occurred. In addition, a small thermal anomaly was identified at temperatures between 200°C and 240°C. This thermal anomaly was reversed when the samples were cooled from 400°C. The whole process was repeated in a subsequent heating up to 620°C. However, only a small peak at 305°C and a wide kink at 260°C were observed when the samples were cooled from the temperature of 620°C. These DTA observations are consistent with the thermomagnetic and HTXRD observations. The small anomaly at temperatures between 200°C and 240°C, as interpreted in the previous report [1], results from the tendency to order from the ABCD 4C

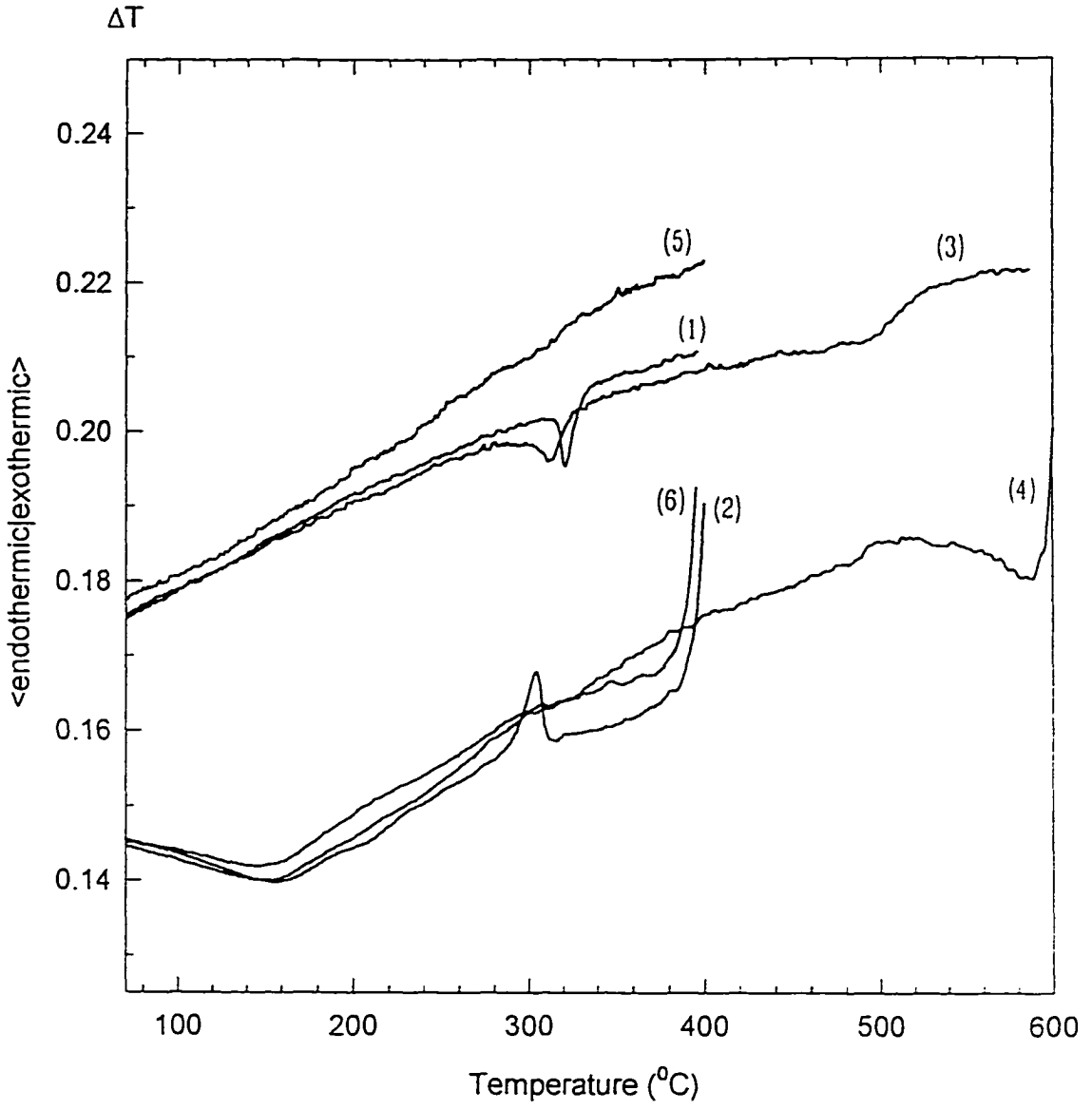

FIGURE 10. DTA curves of the natural magnetic pyrrhotite (Inco 1) subjected to three sequential heating-cooling cycles.

(1)heating from 50°C to 400°C; (2)cooling from 400°C to 50°C;

(3)heating from 50°C to 600°C; (4)cooling from 600°C to 50°C;

(5)heating from 50°C to 400°C; (6)cooling from 400°C to 50°C.

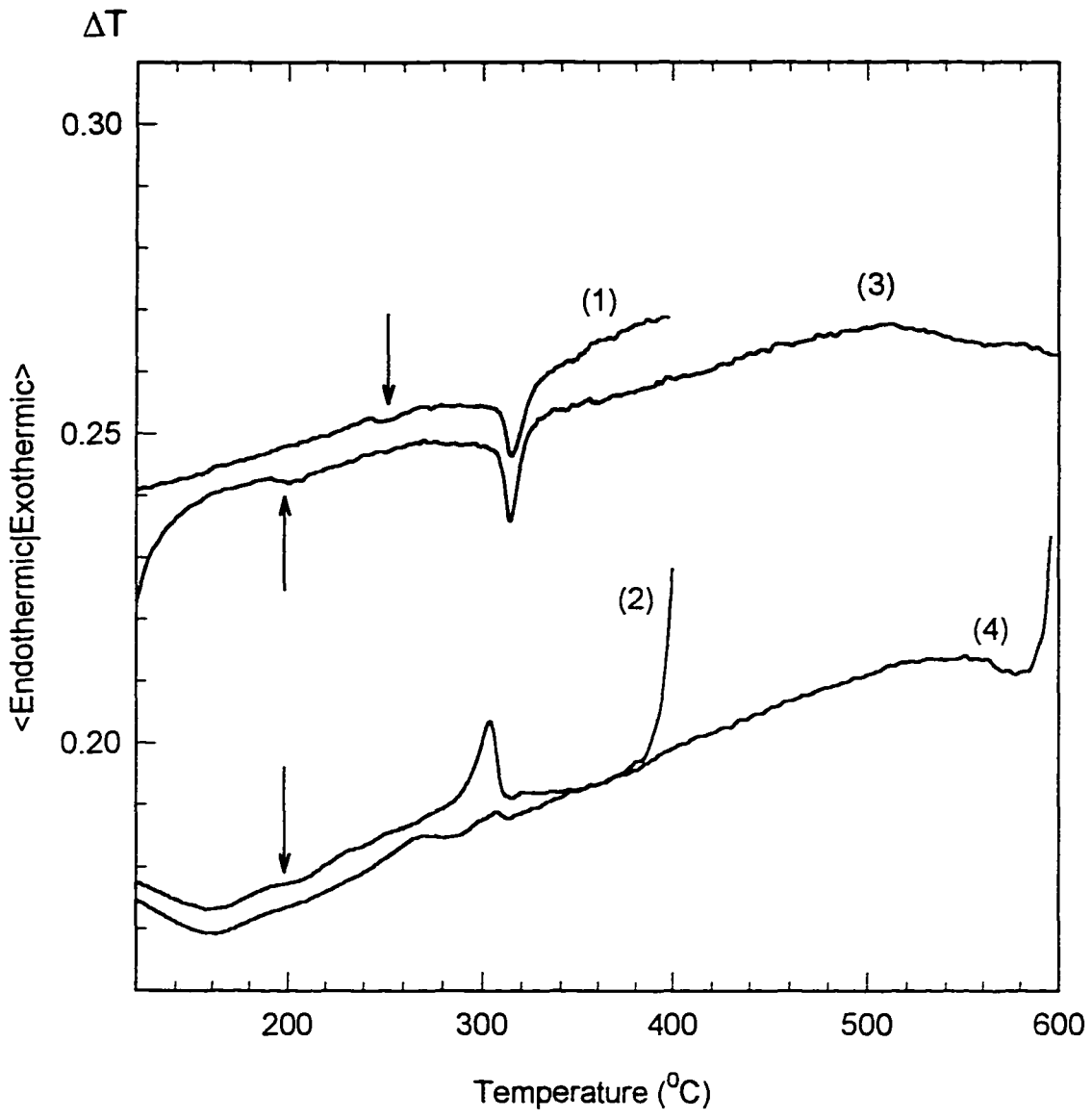

FIGURE 11. DTA curves of the synthetic Fe_7S_8 sample subjected to two sequential heating-cooling cycles. (1) heating from 50°C to 400°C; (2) cooling from 400°C to 50°C; (3) heating from 50°C to 600°C; (4) cooling from 600°C to 50°C. The small anomalies are indicated by arrows.

structure to ABC 3C structure and vice versa. Although the large peak can be attributed to the Curie transition, its intensity and the decrease of intensity brought about by heating up to 620°C are particularly worthy of notice. Since the ordering of magnetic spins is essentially independent of composition, the small peak on the DTA curve 4 as shown in Figs. 10 and 11 is considered to represents a "net" spin order-disorder process. This kind of small thermal anomaly also appeared in the DTA experiments for other samples, such as the antiferromagnetic FeS sample reported earlier [2] and the peak-type $Fe_{1-x}S$ sample as shown later. Hence it is concluded that the unusual intensity found at 300° - 320°C for the Fe_7S_8 sample results from significant contributions from vacancy disordering. Since TEM observations have shown that the disordering of vacancies has developed to a significant extent by 340°C, it can be concluded that this intense thermal anomaly corresponds to a transition for which the disordering of spins is associated with the disordering of vacancies. Once the vacancies have been removed from the lattice, or if the vacancies remain disordered such that adjacent planes are equivalent, the ordering of magnetic spins will proceed as a pure spin ordering.

2.2. Peak-type pyrrhotite

Figure 12 shows the DTA curves obtained from three sequential heating-cooling cycles for the $Fe_{0.906}S$ pyrrhotite showing the peak-type magnetic anomaly. A small peak invariably appeared at 315°C on heating curves and at 305°C on cooling curves. This peak corresponds to the magnetic moment order-disorder transition (Néel point), and, as expected, it is not affected by the ultimate heating temperature. In addition, curves 1 (from 50 to 400°C), 2

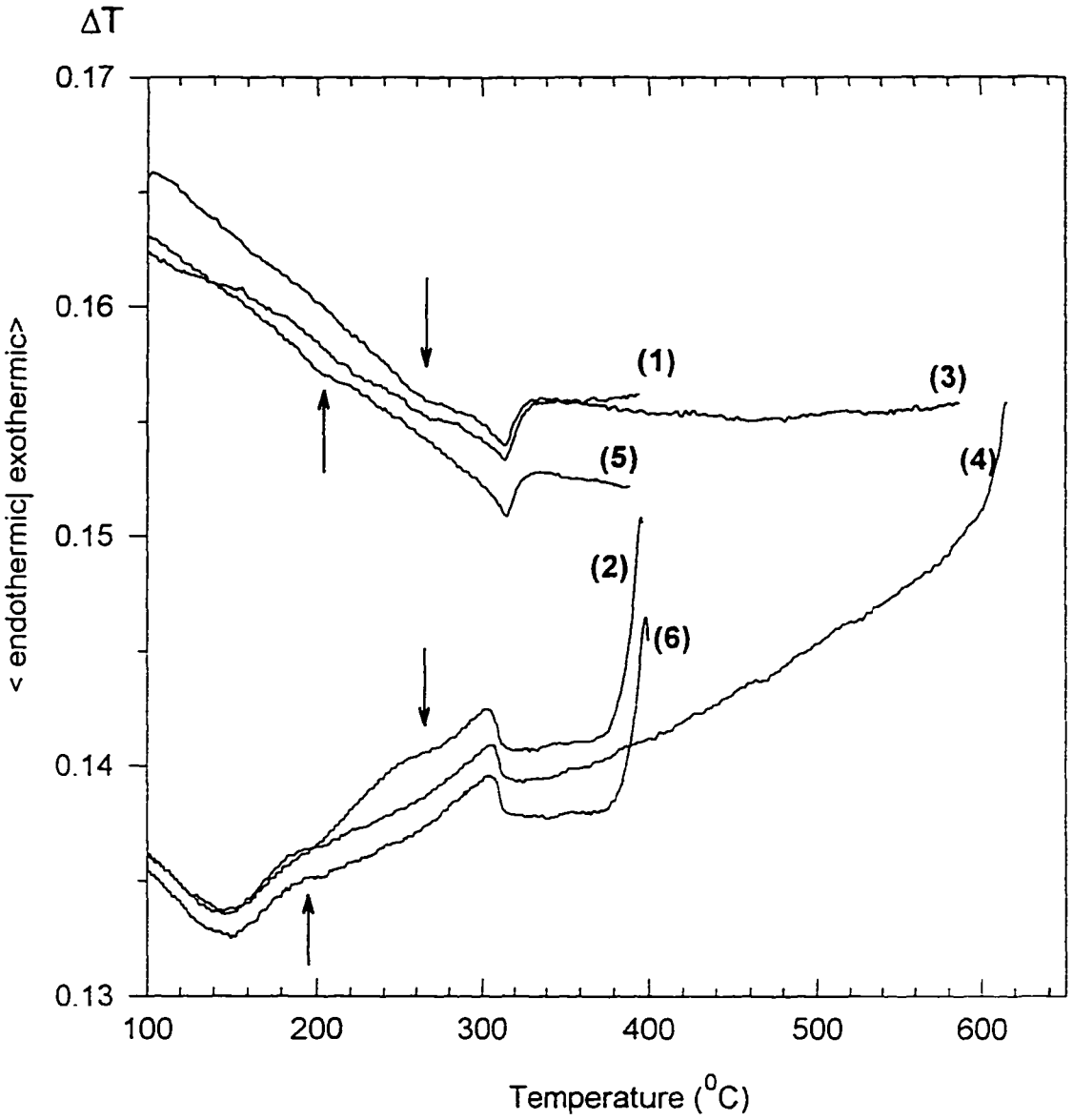

FIGURE 12. DTA curves of the peak-type sample ($Fe_{0.906}S$) subjected to three sequential heating-cooling cycles (5K/min under Ar-gas flow)
(1):Heating from 50°C to 400°C; (2) Cooling from 400°C to 50°C,
(3):Heating from 50°C to 600°C; (4) Cooling from 600°C to 50°C,
(5):Heating from 50°C to 400°C; (6): Cooling from 400°C to 50°C
The arrows indicate the small anomalies.

(from 400°C to 50°C) and 3 (from 50° to 600°C) show a thermal anomaly at temperatures between 230°C and 280°C (pointed by down arrows); while curves 4 (from 600°C to 50°C), 5 (a subsequent second run from 50°C to 400°C) and 6 (a subsequent second run from 400°C to 50°C) show an anomaly at temperatures between 200°C and 180°C (pointed by up arrows). It appears that the former (between 230°C and 280°C) corresponds to the anti-Curie transition, while for the latter, observed at temperature lower than 200°C, it is suggested that this transition has been modified, probably as a result of change in the composition at 600°C. These results indicate that all the transition processes in this type of pyrrhotite, except the spin disordering, have relatively low integral enthalpy changes.

Since peak-type pyrrhotite occurs in the composition region in which the various NC (N=5, 6 and 11) superstructures were discovered, XRD patterns were examined to determine whether an NC structure could be identified in the synthetic sample. As can be seen in Fig. 13, several superstructure diffractions can be recognized in the low angle region along with the NiAs-type substructure reflections. Three relatively intense peaks (they will be named peak 1, peak 2 and peak 3, and indicated by arrows in Fig.13) correspond to d=5.85 ± 0.01Å (at 22.56°), d=6.14 ± 0.01 Å (21.48°) and d=6.79 ± 0.01 Å (19.40°), respectively. Based on the XRD information reported in the literature [20], the room-temperature pattern for the $Fe_{0.906}S$ sample seems to fit the reported 5C superstructure quite well, though the 6C and 11C may be possible due to their very similar diffraction patterns and the limited diffraction evidence (The other diffraction pattern was taken using Cu-radiation. As shown in Figs. 14 and 15, the pattern is in a good agreement with patterns of 5C, 6C and 11C structures,

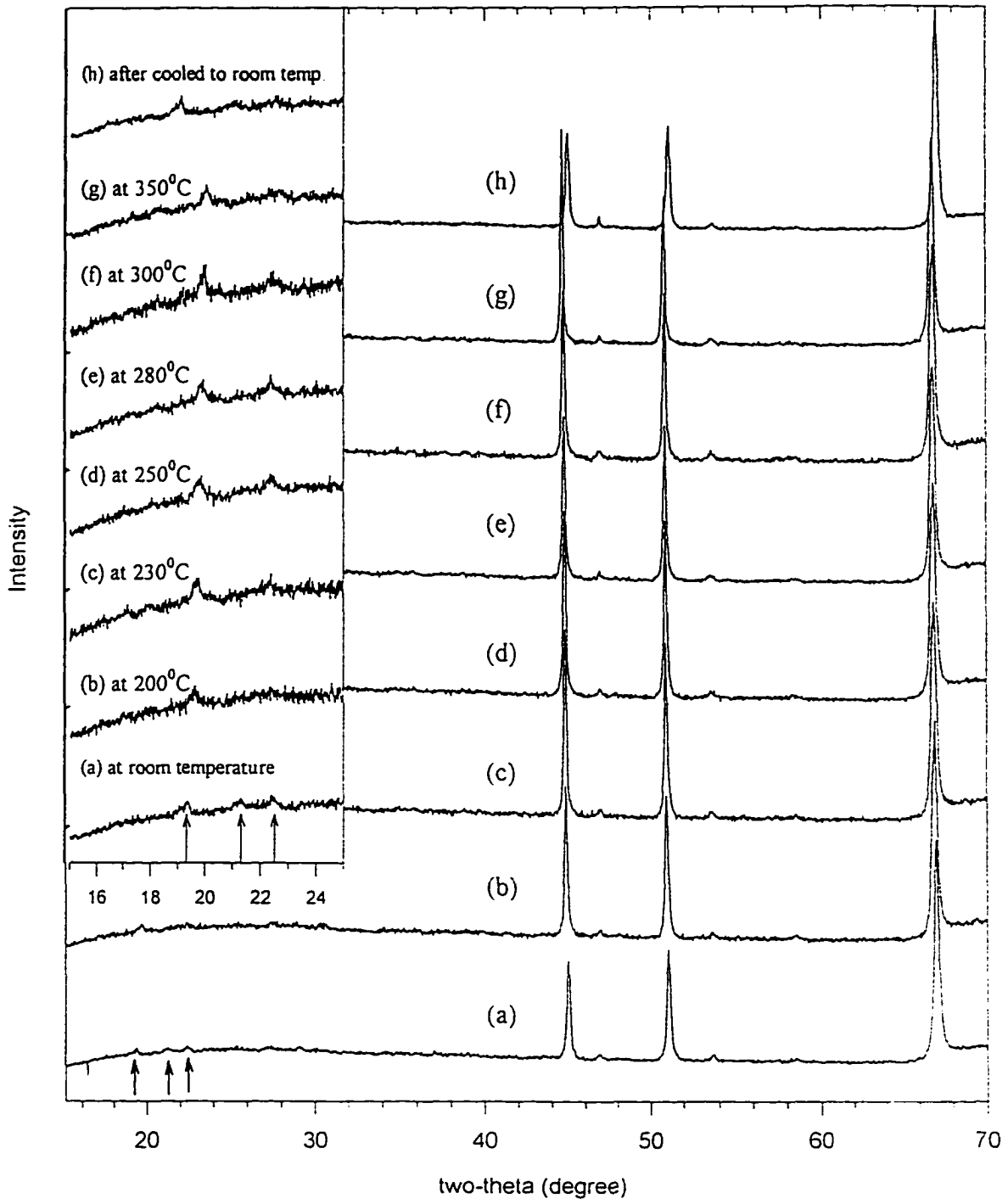

FIGURE 13. HTXRD patterns of the sample $Fe_{0.906}S$ (peak-type).
The inset is the low-angle region with an enlarged scale.
The superstructure peaks are arrowed.

FIGURE 14 and 15. The XRD patterns for the sample $Fe_{0.906}S$ (peak-type) taken using the CuKα radiation (Scintag diffractometer, 2000), below which are the patterns from JCPDS-ICDD database (1990) for the 5C, 6C and 11C structure of pyrrhotite, respectively.

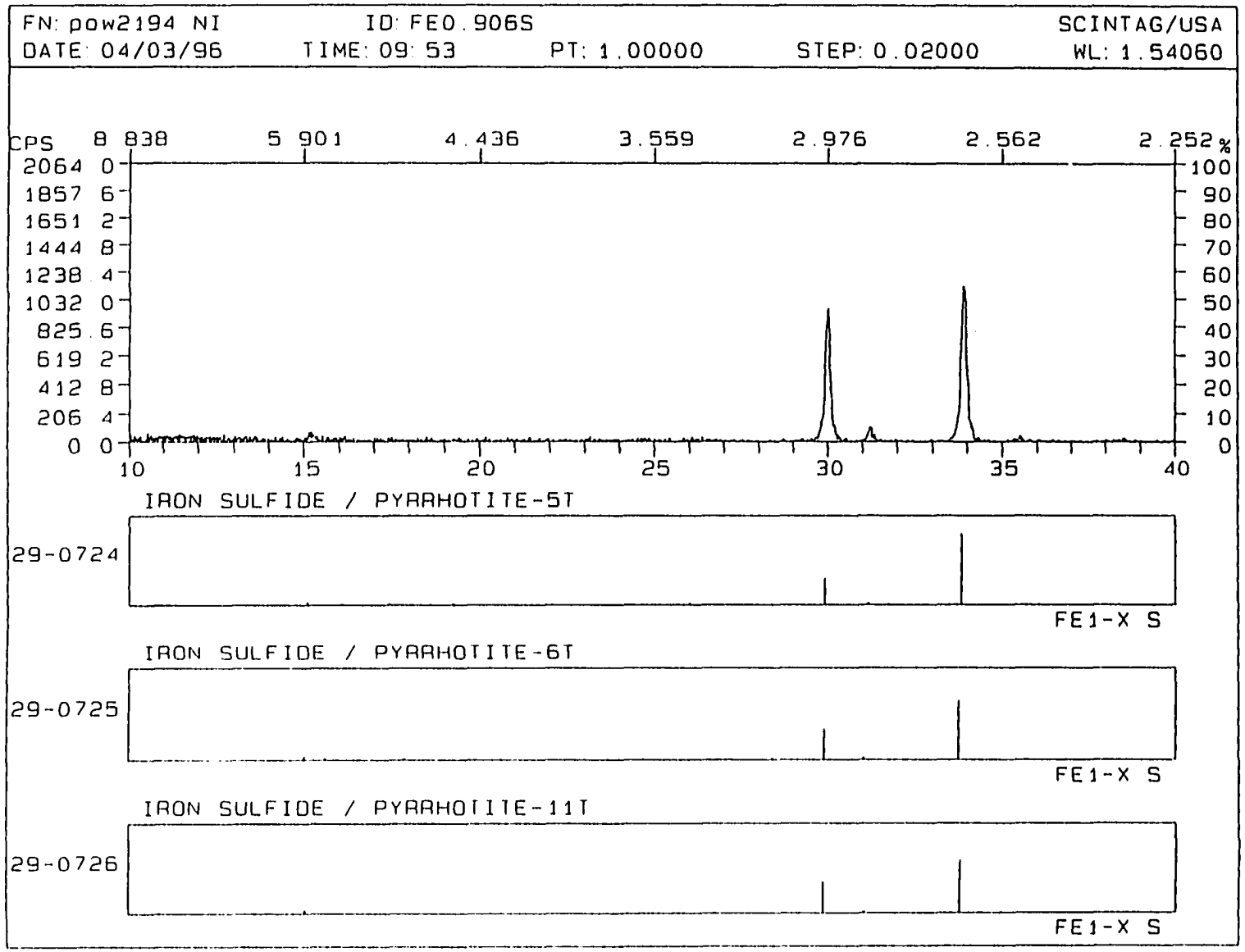
FN: pow2194 NI
ID: FE0.906S
SCINTAG/USA
DATE: 04/03/96
TIME: 09:53
PT: 1.00000
STEP: 0.02000
WL: 1.54060
CPS
8.838
5.901
4.436
3.559
2.976
2.562
2.252
%
2064.0
1857.6
1651.2
1444.8
1238.4
1032.0
825.6
619.2
412.8
206.4
0.0
100
90
80
70
60
50
40
30
20
10
0
10
15
20
25
30
35
40
IRON SULFIDE / PYRRHOTITE-5T
29-0724
FE1-X S
IRON SULFIDE / PYRRHOTITE-6T
29-0725
FE1-X S
IRON SULFIDE / PYRRHOTITE-11T
29-0726
FE1-X S

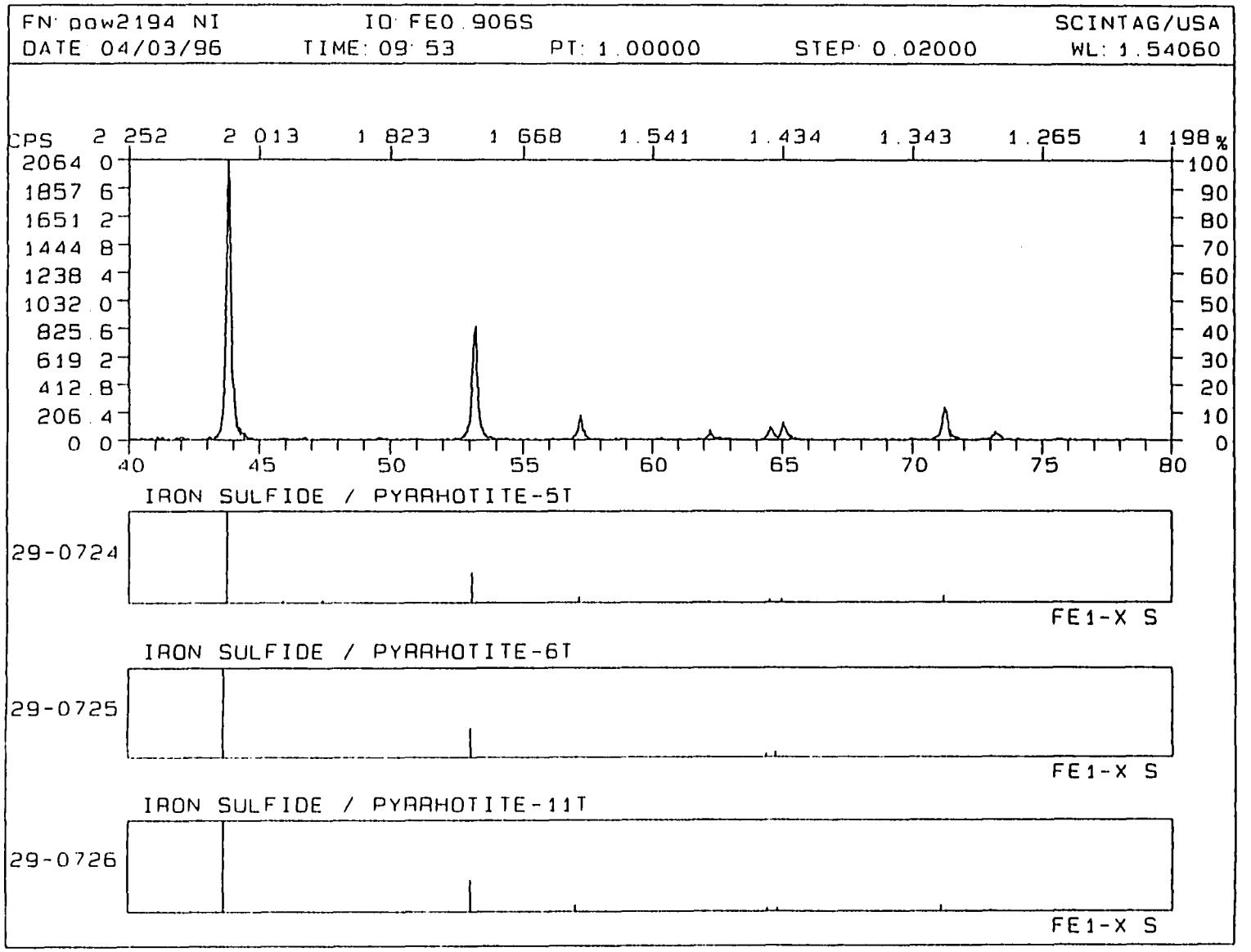
FN: pow2194 NI
IO: FE0.906S
SCINTAG/USA
DATE: 04/03/96
TIME: 09:53
PT: 1.00000
STEP: 0.02000
WL: 1.54060
CPS
2 252
2 013
1 823
1 668
1.541
1.434
1.343
1.265
1 198
%
2064.0
1857.6
1651.2
1444.8
1238.4
1032.0
825.6
619.2
412.8
206.4
0.0
100
90
80
70
60
50
40
30
20
10
0
40
45
50
55
60
65
70
75
80
IRON SULFIDE / PYRRHOTITE-5T
29-0724
FE1-X S
IRON SULFIDE / PYRRHOTITE-6T
29-0725
FE1-X S
IRON SULFIDE / PYRRHOTITE-11T
29-0726
FE1-X S

suggesting that the sample has a mixed NC structure). Furthermore, the subcell parameters a=3.447(7)Å and c=5.742(11)Å were calculated from the substructure diffractions. Consequently, peaks 1(d=5.85Å) and 2 (d= 6.14Å) can be indexed as diffractions $(101)_{5c}$ and $(100)_{5c}$ for the 2Ax2Ax5C hexagonal superstructure. However peak 3 (d=6.79Å) cannot be indexed by any known superstructure type. It is hence proposed that this reflection arises from superstructure that is not integral in *c*. Based upon the TEM results for Fe_7S_8 [1], it is not expected that long-range ordering will be established in the pyrrhotites over the experimental annealing times. For the synthetic samples intergrowth of various stacking sequences inevitably appears, and an incommensurate structure with a non-integral *c* results. Therefore, the ideal NC structure will occur only in domains along with disordered regions and other variants.

In order to relate magnetic properties in peak-type pyrrhotite with vacancy ordering it is necessary to determine the magnetic structure consistent with a given NC structure. First of all, consider the stacking sequences in the experimentally confirmed NC superstructures. The commonly accepted stacking patterns are illustrated in Fig. 16 [21-23]. In these stacking patterns, it is particularly important that the NC structures (N=5, 6, or 11) occur only with the ABCD stacking sequence, as in the well-known monoclinic Fe_7S_8 case, and that if we assume that, as is true for Fe_7S_8, the adjacent iron layers are antiferromagnetically coupled, none of these stacking patterns yields a net ferrimagnetic structure (see column 2 of Fig. 16). Thus the known NC structures are inconsistent with ferrimagnetic ordering as seen in Fe_7S_8.

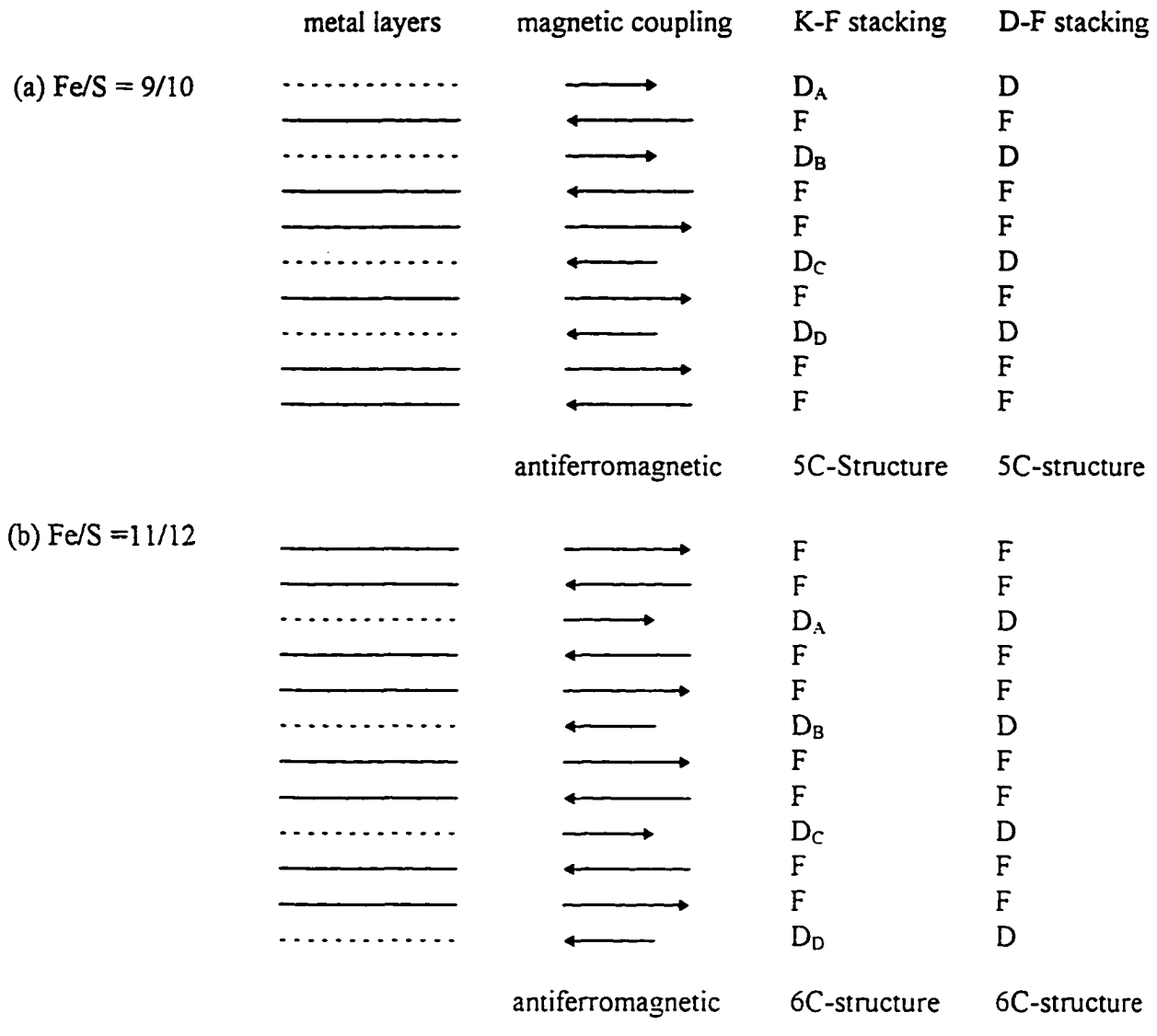

(c) Fe/S = 10/11 11C-structure, that is, 11C=5C + 6C, resulting in an antiferromagnetism as well.

FIGURE 16. Schematic representation of layering patterns and magnetic coupling for intermediate pyrrhotites with NC structures.

Furthermore, a closer inspection of the HTXRD patterns reveals that with increasing temperature the substructure reflections showed no significant change in intensity, but the signature peaks for the 2Ax2Ax5C superstructure (peaks 1 and 2) were found to disappear over the temperature range 150°C - 200°C, then to re-appear after the temperature reached to 250°C and remain until the temperature was above 350°C (Fig. 13). In addition, the reversal behavior in XRD patterns upon heating and cooling is consistent with what was observed in the thermomagnetic and DTA experiments, i.e., when the ultimate heating temperature was lower than 400°C, the original diffraction pattern was exactly recovered, while heating to temperatures higher than 550°C resulted in a high-temperature pattern analogous to the NiAs-type structure. Another observation is that peak 3 which, as suggested above, is associated with non-integral c shifts towards high angle (2θ) with increase of temperature indicating a tendency for the structure to transform towards increase of domain size with increasing temperature.

In order to interpret the behavior observed in the diffractions of the NC structure in accordance with the anti-Curie magnetic behavior, we appeal to the transition sequence model that was proposed for the case of Weiss-type. It is thus suggested that peak-type pyrrhotite with an NC structure has an order-disorder transition sequence similar to Weiss-type, that is, ABCD stacking → ABC stacking → DFDFDF stacking → disordering. It is convenient for this discussion to name the ABCD and ABC stackings as K-F stacking, namely, stacking of alternating Kagome nets and filled layers, and name the alternate stacking of disordered partially occupied layers and filled layers as D-F stacking. It is noteworthy that a D-F stacking sequence arising from an antiferromagnetic parent K-F

stacking is also antiferromagnetic (see Fig. 16). Hence, because ABC stacking is not commensurate with the NC structures, if ABC stacking (or mixed stacking) occurs as an intermediate phase during the vacancy order-disorder transition over the temperature range of 150°C - 250°C, the compensation of magnetic moments between ordered and filled layers in an NC structure is broken. Thus the growth of ABC layering leads to an increase of ferrimagnetization which is followed by a decrease in the magnetization with the growth of D-F layering. In XRD it was observed that the 5C superstructure was lost during the ABC layering or mixed layering, and was re-formed in the D-F layered structure which restored the *c*- modulation. Thus, the following transition sequence is proposed for the peak-type pyrrhotite:

K-F stacking (ABCD) → K-F stacking (ABC + ABCD) → D-F stacking

(antiferromagnetic) (ferrimagnetic) (antiferromagnetic)

The disordered structure between the K-F stacking and D-F stacking is ferrimagnetic, giving rise to the observed anti-Curie transition. Furthermore, in the cooling direction, the incommensurate structure with mixed K-F stackings follows the D-F stacking structure and develops ferrimagnetism at the λ-point (not at the Curie point). However, as the temperature is further decreased, a part of the pyrrhotite with the disordered stacking sequences may not have transformed into regular K-F stacking with ordering of the vacancies within the layers. As result, this portion of the pyrrhotite remains as Weiss-type.

CONCLUSIONS

We have conducted a study on the relationship between the thermomagnetic properties

and structure transitions in pyrrhotites. The results have been interpreted in terms of the known idealized structures in which the vacancies order such as to form the Kagome nets and Kagome nets tend to stack as the ABCD sequence at low temperature. For Fe_7S_8, HTXRD experiments reveal that natural magnetic pyrrhotite can form a stable monoclinic-type structure and follow the previously proposed transition sequence very well. At the Curie transition temperature, this pyrrhotite shows an extraordinarily intense DTA peak, implying a structural modification that is related to the disordering of magnetic spins. As for the so-called peak-type pyrrhotite with compositions over the range Fe_9S_{10} - $Fe_{11}S_{12}$, the ideal ABCD stacking of Kagome nets results in part in NC structures (N=5, 6 or 11). As the ABCD stacking transforms to mixed stacking with ABC components, the NC structure is lost, and along with the accompanying stacking disorder comes a ferrimagnetic contribution from the uncompensated spins in the layers. When the vacancies disorder within the layers to form D-F stacking the NC period is regained, and along with this periodicity comes antiferromagnetic ordering.

REFERENCE

[1] F. Li, H. F. Franzen and M. J. Kramer, *J. Solid State Chem.* **124**, 264 (1996) (Chapter 5).

[2] F. Li and H. F. Franzen, *J. Alloys and Compounds* **238**, 73-80 (1996).

[3] C. B. van den Berg, *Ferroelectics* **4**, 103-116 and 195-212 (1972).

[4] E. F. Bertaut, *Bull. Soc. Fr. Mineral. Cristallogr.* **79**, 276 (1956).

[5] R. H. Carpenter and G. A. Desborough, *Am. Mineral.* **49**, 1350 (1964).

[6] M.E. Fleet, and N. MacRae, *Can. Mineral.* **9**, 699 (1969).

[7] N. Morimoto, H. Nakazawa, K. Nishiguchi and M. Tokonami, *Science* **168**, 964 (1970).

[8]A. Vorma, *Bull. Geol. Soc. Finland* **42**, 3 (1970).

[9] K. Hayase, R. Otsuka and T. Mariko, *Mineralog. J.* **4**, 41 (1963).

[10] F. K. Lotgering, *Z. Phys. Chem* **4**, 238 (1955).

[11]F. K. Lotgering, *Phillips Res. Rep.* **11**, 190 (1956).

[12] J. T. Sparks, W. Mead, A. J. Kirschbaum and W. Marshall, *J. App. Phys.* **31**, 356S (1960).

[13]A. E. Andersen and P. Torbo, *Acta Chem. Scand.* **21**, 2841 (1967).

[14]T. Hirone and N. Tsuya, *Phys. Rev.* **83**, 1063 (1951).

[15]T. Hirone, S. Maeda and N. Tsuya, *J. Phys. Soc. Japan* **9**, 736 (1954).

[16] M. G. Townsend, A. H. Webster and J. L. Horwood, *J. Phys. Chem. Solids* **40**, 183 (1979).

[17]E. J. Schwarz and D. J. Vaughan, *J. Geomag. Geoelectr.* **24**, 441 (1972).

[18]M. Tokonami, K. Nishiguchi and N. Morimoto, *Am. Mineral.* **57**, 1066 (1972).

[19] D. J. Vaughan and J. R. Craig, "Mineral Chemistry of Metal Sulfides", Cambridge University Press, (1978).

[20] JCPDS-ICDD (1992): 29-724, 29-725, and 29-726.

[21] K. Koto, N. Morimoto and A. Gyobu, *Acta Cryst. B* **31**, 2759 (1975).

[22] K.Koto and M. Kitamura, *Acta Cryst. A* **37**, 301 (1981).

[23]I. Dodony and M. Posfai, *Eur. J. Mineral.* **2**, 529 (1990).

CHAPTER 7

GENERAL CONCLUSIONS

With the previous four papers that cover the different compositional regions of pyrrhotite, we have made progress in understanding of structures and phase transitions in this system.

First, we have seen that one transition process, such as crystallographic, magnetic, electric or ferroelectric, may significantly alter the transition path of others when they are entangled. Four transitions, that is, the α-transition (which actually is a ferroelectric transition, and thermodynamically corresponds to a large anomaly), the spin-flip transition (i.e., Morin transition), the electric transition and the crystallographic transition (from P31c to $P\bar{6}2c$), are closely related in near stoichiometric iron monsulfide. When the transition temperatures for the magnetic and ferroelectric transitions decline with increasing defect concentration, the path of the crystallographic transformation is correspondingly altered into one in which the $\sqrt{3} \times \sqrt{3} \times 2$ supercell irreversibly "collapses" into a distorted NiAs-type structure which may be incommensurate with mixing of 1C and 2C structures. The transition from troilite ($P\bar{6}2c$) to NiAs-type structure was observed via a first-order process which is accompanied by the magnetic disordering transition (β-transition) only over a narrow composition range. For the β-transition, the transition temperature is not sensitive to change of composition. However, the vacancy order-disorder process occurring in the defect iron sulfides is associated with

the magnetic disordering transition, and, consequently, this interaction of transitions gives rise to a stronger thermodynamic change at the original magnetic transition temperature.

Second, the formation of Kagome nets is found to be the principal ordering in iron-deficient monsulfide. In order to achieve a maximum separation of iron vacancies, the ABCD stacking is most favorable. At temperatures above which this ideal ordered stacking is the stable form the disordered (or random) stacking of Kagome nets and disordering of vacancies within the layers, both yielding the trigonal symmetry and the former resulting in an incommensurate structure, occur. All the phenomena related to the vacancy order-disorder transition observed in this research, such as the anti-Curie transition, mixing of ABCD and ABC stacking, and formation of CdI_2-type structure, indicate that vacancies disorder preferentially within the iron layers at an early stage, and then reach the complete disordering at temperature above 500°C. It is found that in most of pyrrhotites the structures are distorted in such a way that the [FeS_6] octahedra are stretched along the *c*-direction to form trigonal antiprisms.

Third, figure 1 shows the regions of known phases and their transitions revealed in these studies. At room temperature, ideally, the discrete phases fall near Fe/S=1:1 region, the Fe/S = 10:11 line and the Fe/S = 7: 8 line. In the first region a $\sqrt{3} \times \sqrt{3} \times 2$ superstructure with the troilite symmetry is stable; in the second the stable form is an NC superstructure with ordered vacancies; and in the third another ordered structure with the ABCD stacking and the monoclinic symmetry is formed. Between the regions of Fe/S= 7:8 and 10:11, there is the region where either two phases may co-exist or there occurs

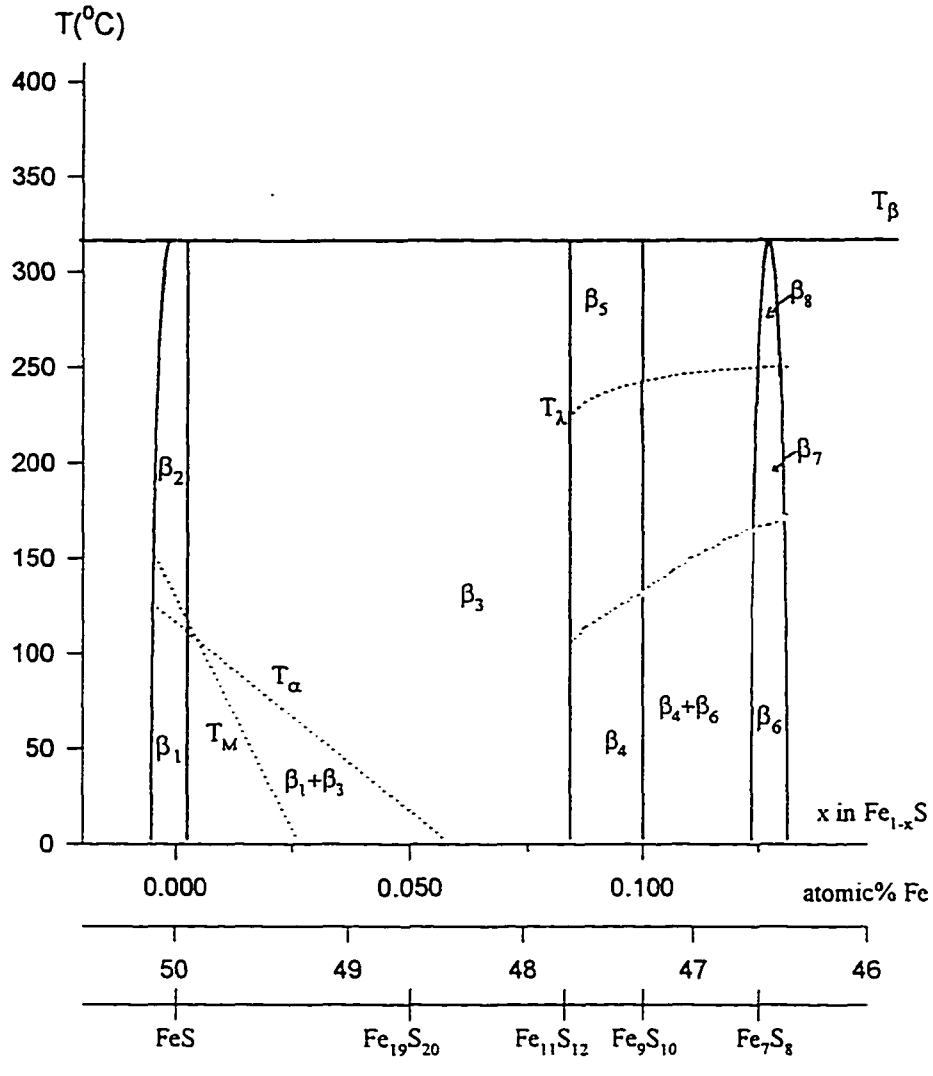

Figure 1. The phases and phase transitions for $Fe_{1-x}S$ (x=0-0.125) studied in this research. T_α—α-transition (ferroelectric transition); T_β— β-transition (disorder transition of magnetic spins); T_M—spin-flop transition; T_λ—anti-Curie transition; β_1—P31c; β_2—P62c; β_3—vacancy-disordered hexagonal structure; β_4—vacancy-ordered NC structure with ABCD stacking; β_5—vacancy-disordered NC structure; β_6—monoclinic structure with ABCD stacking; β_7—trigonal structure with ABC stacking; β_8—vacancy-disordered hexagonal structure; $\beta_4+\beta_6$—incommensurate structure with non-integral *c* length and mixed stacking.

an incommensurate phase with mixed stacking sequences of Kagome nets. Because pyrrhotites with $x < 0.08$ in $Fe_{1-x}S$ essentially show antiferromagnetic characteristics, it is concluded that over this composition range vacancies are not so well ordered to form the Kagome nets. However, there may still exist some discrete phase(s) in the β_3 region arising from the position displacement.

ACKNOWLEDGEMENTS

I would like to express my gratitude to Dr. Franzen, my major professor, for his guidance and education. It was a great experience to study and work under his direction. My special appreciation also goes to Dr. Jacobson, Dr. Miller, Dr. Ng and Dr. Goldman for serving in my committee. They always gave me the valuable suggestions and shared their experiences and time with me.

I also want to thank Dr. Alfred Kracher for the EMP analysis work. Dr. Matthew Kramer and Dr. L. Scott Chumbley for the electron diffraction experiment. Kevin Dennis for the generous assistance and help he offered me in the thermomagnetic and DTA measurements, and to Mr. Hengning Wu and Larry Margulies for their help in the DTA experiments. I am indebted to Dr. Anatoli Frishman for his helpful discussion. I also wish to acknowledge the kindly help from Jim Anderegg, Jerome Ostenson, Michael Sandholm, Dr. Ming Xu and Victor Young. The experience on the third floor of Spedding Hall with solid state chemistry group members was really enjoyable and encouraging. I appreciate the help and friendship they offered to me.

I want to express my deepest appreciation to my lovely wife and daughter. This project would not have been possible without their love, encouragement and devotion. These deepest thanks also go to my parents and my wife's parents who supported and understood me throughout my study abroad. This degree is theirs as much as it is mine.

Support from Inco Limited, Canada, was very important and is gratefully acknowledged. The author wish to thank Dr. Bruce Conard at Inco for his assistance and

encouragement in this project. This research was also supported by the Office of the Basic Energy Sciences, through Materials Sciences Division, Ames Laboratory-operated for the US Department of Energy by Iowa State University under Contract No. W-7405-Eng-82.

APPENDIX A

USING PROJECTION OPERATORS TO CONSTRUCT THE BASIS FUNCTIONS

In Chapter 3, we have seen that a set of appropriate basis functions is very important in consideration of a symmetry-broken structure transformation because the symmetry properties of the solid structure are explicitly defined by the symmetry properties of these basis functions. In the group theory, the fundamental, universally applicable tool for constructing a set of basis functions, essentially for the group which is finite, is the projection operator, i.e.,

$$\hat{P} = \sum_{R} \chi^{\mu}(R) \cdot \hat{O}_R$$

In this appendix, a set of basis functions is found by applying the projection operator into the space group.

As we know, the basis functions are linearly independent (orthonormal), and one can produce the innumerable sets of basis functions by re-combining one set of basis functions.

On the other hand, an arbitrary vector or function in this representation space can always be projected onto the bases. Mathematically, it should therefore be possible to express an arbitrary function as a sum of basis functions as follows

$$\varphi = \Sigma \varphi_i$$

where φ_i's are basis functions.

For the case under consideration in Chapter 3, if we make use of the **k** =(1/3, 1/3, 1/2) and **k*** (= **-k**) to which the transition corresponds to construct this "arbitrary" function, we have

$$\Psi=\exp[2\pi i(\frac{x+y}{3}+\frac{z}{2})]+i\exp[-2\pi i(\frac{x+y}{3}+\frac{z}{2})]$$

By consulting with the character table for this representation under consideration, we acquire the characters that are non-zero as follows

R	$\varepsilon\|000$	$C_{3z}\|000$	$C_{6z}^4\|000$	$\sigma_x\|000$	$\sigma_y\|000$	$\sigma_{x-y}\|000$
χ	2	2	2	-2	-2	-2

Then, the projection operator is employed:

$$\hat{P}\Psi = 2\cdot\{\exp[2\pi i(\frac{x+y}{3}+\frac{z}{2})]+i\exp[-2\pi i(\frac{x+y}{3}+\frac{z}{2})]\}$$
$$+2\cdot\{\exp[2\pi i(\frac{x-2y}{3}+\frac{z}{2})]+i\exp[-2\pi i(\frac{x-2y}{3}+\frac{z}{2})]\}$$
$$+2\cdot\{\exp[2\pi i(\frac{y-2x}{3}+\frac{z}{2})]+i\exp[-2\pi i(\frac{y-2x}{3}+\frac{z}{2})]\}$$
$$-2\cdot\{\exp[2\pi i(\frac{2y-x}{3}+\frac{z}{2})]+i\exp[-2\pi i(\frac{2y-x}{3}+\frac{z}{2})]\}$$
$$-2\cdot\{\exp[2\pi i(\frac{2x-y}{3}+\frac{z}{2})]+i\exp[-2\pi i(\frac{2x-y}{3}+\frac{z}{2})]\}$$
$$-2\cdot\{\exp[-2\pi i(\frac{x+y}{3}-\frac{z}{2})]+i\exp[2\pi i(\frac{x+y}{3}-\frac{z}{2})]\}$$

Let $\varphi_1 = \exp[2\pi i(\frac{x+y}{3}+\frac{z}{2})]-\exp[-2\pi i(\frac{x+y}{3}-\frac{z}{2})]+\exp[2\pi i(\frac{x-2y}{3}+\frac{z}{2})]$
$$-\exp[-2\pi i(\frac{x-2y}{3}-\frac{z}{2})]+\exp[2\pi i(\frac{y-2x}{3}+\frac{z}{2})]-\exp[-2\pi i(\frac{y-2x}{3}-\frac{z}{2})]$$
$\varphi_2 = \exp[-2\pi i(\frac{x+y}{3}+\frac{z}{2})]-\exp[2\pi i(\frac{x+y}{3}-\frac{z}{2})]+\exp[-2\pi i(\frac{x-2y}{3}+\frac{z}{2})]$
$$-\exp[2\pi i(\frac{x-2y}{3}-\frac{z}{2})]+\exp[-2\pi i(\frac{y-2x}{3}+\frac{z}{2})]-\exp[2\pi i(\frac{y-2x}{3}-\frac{z}{2})]$$

Thus we have projected out of the function Ψ onto the two functions φ_1 and φ_2 which form a basis for this representation.

To generate the real functions, we use

$\cos x = (e^{ix} + e^{-ix}) / 2$

$\sin x = -i\cdot(e^{ix} - e^{-ix}) / 2$

and the relations

$\sin(\alpha+\beta) + \sin(\alpha-\beta) = 2\sin\alpha\cdot\cos\beta$

$\cos(\alpha+\beta) - \cos(\alpha-\beta) = -2\sin\alpha\cdot\sin\beta$

Therefore, the functions become

$$\varphi_1 + \varphi_2 = \cos[2\pi(\frac{x+y}{3}+\frac{z}{2})] + \cos[2\pi(\frac{x-2y}{3}+\frac{z}{2})] + \cos[2\pi(\frac{y-2x}{3}+\frac{z}{2})] -$$

$$- \cos[2\pi(\frac{x+y}{3}-\frac{z}{2})] - \cos[2\pi(\frac{x-2y}{3}-\frac{z}{2})] - \cos[2\pi(\frac{y-2x}{3}-\frac{z}{2})]$$

$$= \sin(\pi z)\cdot[\sin 2\pi(\frac{x+y}{3}) + \sin 2\pi(\frac{x-2y}{3}) + \sin 2\pi(\frac{y-2x}{3})]$$

and

$$\varphi_1 - \varphi_2 = \sin[2\pi(\frac{x+y}{3}+\frac{z}{2})] + \sin[2\pi(\frac{x-2y}{3}+\frac{z}{2})] + \sin[2\pi(\frac{y-2x}{3}+\frac{z}{2})] +$$

$$+ \sin[2\pi(\frac{x+y}{3}-\frac{z}{2})] + \sin[2\pi(\frac{x-2y}{3}-\frac{z}{2})] + \sin[2\pi(\frac{y-2x}{3}-\frac{z}{2})]$$

$$= \cos(\pi z)\cdot[\sin 2\pi(\frac{x+y}{3}) + \sin 2\pi(\frac{x-2y}{3}) + \sin 2\pi(\frac{y-2x}{3})]$$

Apparently, the real functions φ_1 and φ_2 are as same as given in Chapter 3.

This projection operator method works for other cases as well. For example, the transition

$P6_3/mmc \rightarrow P\ cmn$ at $\mathbf{k} = (1/2, 0, 0)$ (see Ref.[1])

Since (1/2, 0, 0), (0, 1/2, 0), (1/2, -1/2, 0) in a star, the function

$$\Psi = [e^{i\pi x} + e^{i\pi y} + e^{i\pi(x-y)}] \cdot e^{i2\pi z}$$

is constructed.

For this case, the symmetry operations which have non-zero characters are

R	$\varepsilon\|000$	$C_{2z}\|00\frac{1}{2}$	$C_{2y}\|000$	$C_{2(2x+y)}\|00\frac{1}{2}$	$i\|000$	$\sigma_z\|00\frac{1}{2}$	$\sigma_y\|000$	$\sigma_{2x+y}\|00\frac{1}{2}$
χ	3	3	-3	-3	-3	-3	3	3

Thus, simply, the result is

$$\hat{P}\Psi = \sum_R \chi^{\mu}(R) \cdot \hat{O}_R \Psi$$

$$= (e^{i2\pi z} + e^{-i2\pi z}) \cdot [e^{i\pi x} + e^{i\pi y} + e^{i\pi(x-y)} - e^{-i\pi x} - e^{-i\pi y} - e^{-i\pi(x-y)}]$$

$$= \cos(2\pi z) \cdot [i\sin(x\pi) + i\sin(y\pi) + i\sin\{\pi(x-y)\}]$$

Consequently, we can acquire the three basis functions

$$\varphi_1 = \cos(2\pi z) \cdot \sin(x\pi)$$

$$\varphi_2 = \cos(2\pi z) \cdot \sin(y\pi)$$

$$\varphi_3 = \cos(2\pi z) \cdot \sin[(x-y)\pi]$$

which are same as obtained in the literature.

Reference

1. Franzen, H. F., "Physical Chemistry of Inorganic Crystalline Solid", Springer-Verlag, New York, 1990.

APPENDIX B

THE LOW-TEMPERATURE MAGNETIC TRANSITION IN BULK PYRRHOTITE SAMPLES

Introduction.

As stated in previous chapters, pyrrhotite undergoes a spin rotation transition (also known as Morin transition) from the *c*-plane towards the *c*-axis in the state where the magnetic spins are ordered. This phenomenon seems to be a characteristic feature for NiAs-type compounds. Studies have shown that the transition temperature for troilite with Fe/S ratio = 1:1 is at about 410K, and that this transition temperature declines rapidly as the iron deficiency increases [1, 2]. Horwood et. al studied $Fe_{1-x}S$ single crystal samples for $0 \leq x \leq 0.07$ over the temperature range from 80K to 600K, and confirmed that in $Fe_{0.93}S$ the spin-rotation transition occurs at 170K [3]. By using neutron diffraction, Andreson and Torbo [4] used as evidence for the spin rotation the intensity change of the (001) magnetic reflection which is zero when the spins are $\| c$. They found that there occur two magnetic transitions in $Fe_{1-x}S$ with $x > 0.03$, one at temperatures between 300K and 400K, the other below 200K. These two transitions were also attributed to the co-existence of two phases, one being more deficient of iron than the other. It is also found that this transition when taking place in Fe_7S_8 occurs over a range of temperature instead of abruptly, as happens in near stoichiometric pyrrhotite. Thus, it appears that the composition not only changes the transition temperature, but also alters the transition mechanism. Theoretical model for the spin-rotation transition, which is based on the

consideration of the magnetocrystalline anisotropy energy, was contributed by Adachi [5-7]. The result is expressed as following equation:

$$F(\phi,\theta)= -C_1kT\ \mathrm{In}(\cosh\{[(\lambda l_z S)^2\cos^2\theta + \Delta^2]^{1/2}/kT\}) + C_2K_1\cos^2\theta$$
$$+ C_2' K_2\sin^2\theta\cos 2\phi + C_4K_4\cos^4\theta \qquad (1)$$

where λ is the spin-orbit coupling constant, l_z is the z component of the orbital angular momentum in the orbital doublet state under the trigonal field, Δ is the energy splitting due to the orthorhombic field, θ and ϕ are spin angles with respect to the *c* and *a* axis in the single domain, and K_1, K_2 and K_4, and C_1, C_2 and C_4 are numerical constants which are determined by the population of Fe^{2+} ions on the crystal-lattice site. Given that (cubic field)>> (trigonal field, exchange interaction) >> (orthorhombic field, spin-orbit coupling), Eq. 1 was approximated by Horwood et. al. as follows:

$$F(\theta)= -C_1kT\ \mathrm{In}(\cosh\{[(\lambda l_z S)\cos\theta]/kT\}) + C_2K_1\cos^2\theta + C_4K_4\cos^4\theta \qquad (2)$$

The first term in this equation is the energy due to the ground doublet state in which the spins align preferentially along the *c*-axis; the second term comes from the second-order perturbation in the singlet ground state, in which the spins align preferentially in the *c*-plane; the last term comes from the fourth-order perturbation. This model has been applied to explain the magnetization curves for single crystals of pyrrhotite, although some difficulties exist in qualitative calculation due to lack of information about the constants.

In this report, we present the low-temperature magnetic changes obtained from bulk pyrrhotite samples. These results are analyzed using the Adachi's model, and confirmed to be consistent with those obtained from the single crystals.

Results and Discussion.

Figures 1.(1) -1.(4) display the susceptibility/magnetization curves for the various compositions of synthesized pyrrhotites ($Fe_{0.95}S$, $Fe_{0.93}S$, $Fe_{0.91}S$ and Fe_7S_8) over the temperature range from 300K to 5K. Keep in mind that samples $Fe_{0.95}S$, $Fe_{0.93}S$ and $Fe_{0.91}S$ are antiferromagnetic, $Fe_{0.91}S$ is the sample which shows an anti-Curie transition at about 500K, and Fe_7S_8 is ferrimagnetic arising from the vacancy ordering. For $Fe_{0.96}S$, no magnetic transition was found in this temperature range, as expected because the spin rotation would occur at temperature higher than 300K. For samples with $x > 0.03$, the magnetic changes can be clearly seen. As shown in Fig. 1.(2)-1.(4), the susceptibility/magnetization decreases in the temperature range in which the spin moments have been proved to rotate by neutron diffraction experiments and magnetic measurements on single crystals of pyrrhotite. In Fe_7S_8, the magnetization begins to gradually decrease at 220K - 250K, and then has a rapid drop at $T < 50K$; while for the intermediate pyrrhotites the susceptibility slightly increases at about 100~120K, and then shows a rapid decrease at 50K, and finally reaches a minimum value at about 20K. Furthermore, the magnetization in the magnetic pyrrhotite (Fe_7S_8) decreases by 45% ~ 50% when the temperature drops to 10K; while the intermediate pyrrhotites decrease their susceptibility only by 10% down to this temperature. These characteristics that the course of the transition depends appreciably on the composition has been also observed in the spin rotation transition for $Fe_{1-x}Se$ system. It was found by neutron diffraction and magnetization investigations that the intermediate composition of $Fe_{1-x}Se$ (or for Fe_7Se_8 with the 3C structure) showed an abrupt transition; while for Fe_7Se_8 with the 4C structure a progressive process resulted. It

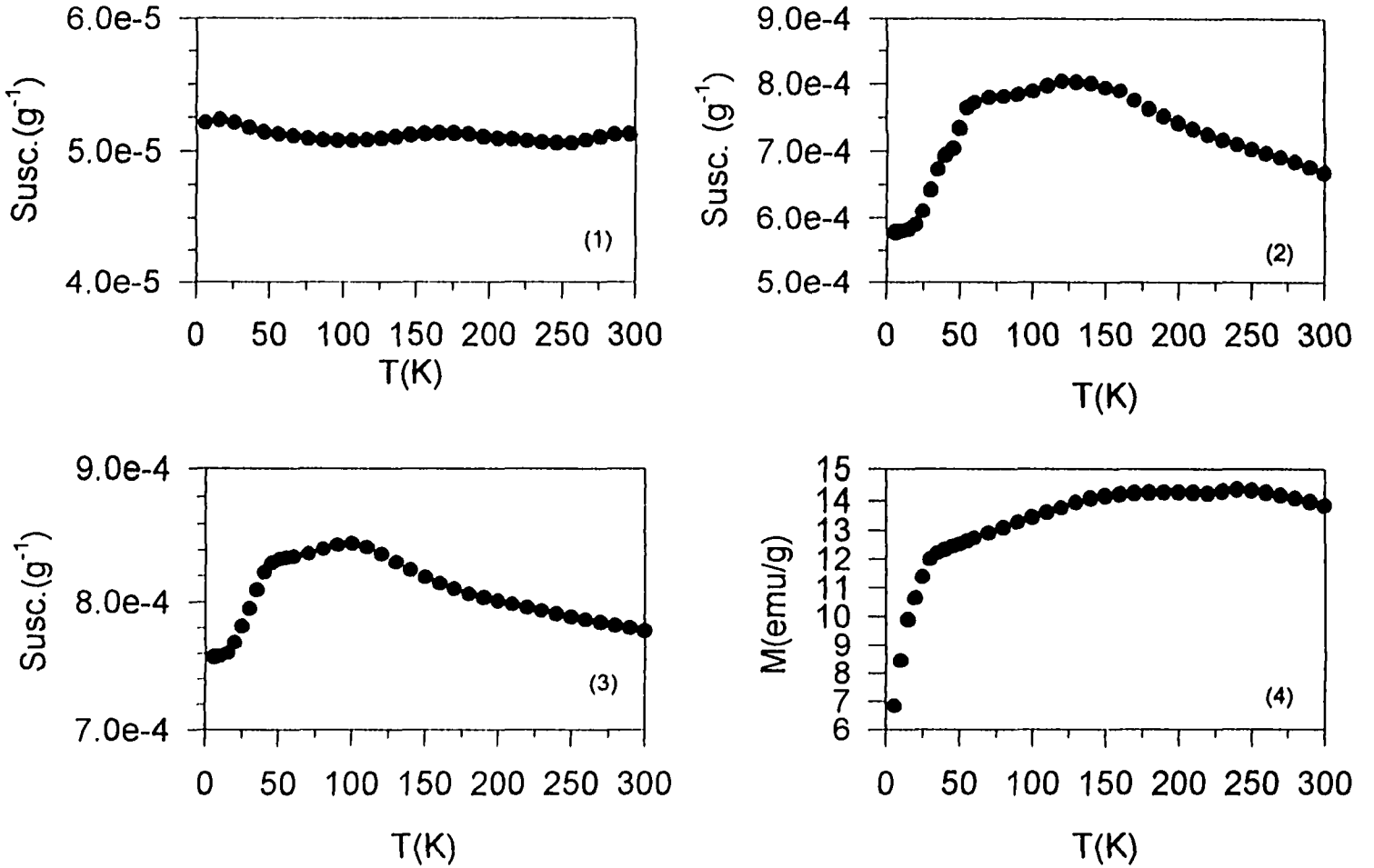

FIGURE 1 The susceptibilities/magnetization for bulk pyrrhotite samples.

(1) $Fe_{0.95}S$ (14) @30,000 Oe, (2). $Fe_{0.93}S$ (22) @1500Oe;

(3). $Fe_{0.91}S$ (19) @1500Oe; (4). Fe_7S_8 (18) @1500Oe.

has also been found that the progressive process in the latter has a higher temperature than the abrupt process in the former [8, 9]. In spite of the lack of more evidence, especially for intermediate pyrrhotites, according to Adachi and Horwood's observations [3, 7], these two distinctive magnetic curves corresponding to different types of pyrrhotite have still been demonstrated.

The previous results from magnetic measurements on the single crystal as well as the calculation by Adachi and Sato showed that the spins "stand up" off the *c*-plane only by 20° even if the temperature is decreased near 12K, and thus, correspondingly, $\cos\theta$ increases by about 0.34 [6, 7]. Because the ferrimagnetism in Fe_7S_8 arises from the uncompensated magnetic moments between the adjacent layers along *c*-axis, the fact that the magnetization in Fe_7S_8 drops by a large ratio rather than restores the original ferrimagnetism even down to 5K suggests that the magnetic spins would rotate from the direction lying within *c*-plane to an angle off the *c*-axis rather than to the direction parallel to the *c*-axis. Another possible configuration of the magnetic structure is that the moments lying within every two adjacent layers turn to a same direction (up or down) off the *c*-plane; while the moments within the next two layers turn to the opposite direction as shown in Fig. 2. As result, the total ferrimagnetic moment is partially canceled due to the interaction between the every two layers with the rotation of the spins.

The mechanism of the composition dependence of the spin "stand up" process is still unclear even for the Fe-Se system where more structure information at low temperature has been derived. According to the literature, for Fe_7S_8 with the 4C structure the splitting energy (Δ) due to the orthorhombic field was estimated to be 19.5 cm^{-1} ~ 21 cm^{-1}. This

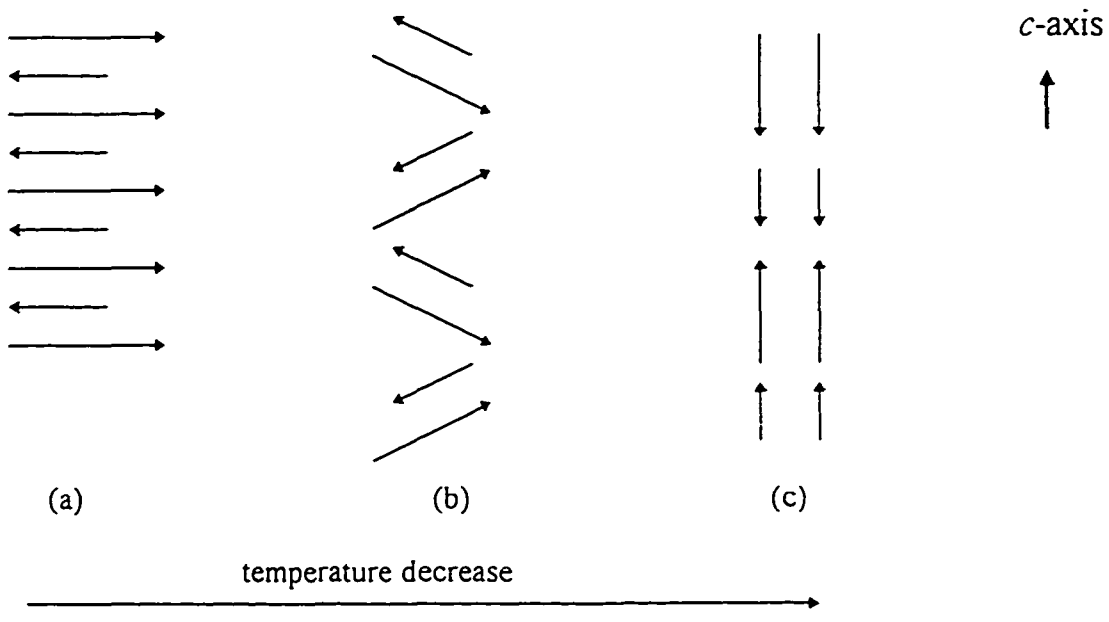

FIGURE 2. One of possible spin rotation mechanisms for which the magnetic spins rotate from the ferrimagnetic structure to the antiferromagnetic structure: (a) c-plane status; (b) rotating status; (c) c-axis status.

value is very compatible with that due to the trigonal field ($\lambda l_z S$) which was calculated to be $50cm^{-1}$. In contrast with the 4C structure, the 3C structure of Fe_7S_8 and intermediate pyrrhotites show a stronger trigonal field effect ($\lambda l_z S \approx 100\ cm^{-1} \sim 200\ cm^{-1}$). It thus seems that the spin rotation angle and rate may be depressed at the earlier stage of the rotation transition for the case of Fe_7S_8 with the 4C structure, where the orthorhombic field becomes significantly important. As the temperature approaches 0K, the orthorhombic field effect is overcome and gives rise to the rapid rotation of spins towards to *c*-axis.

On the other hand, from $\partial^2 F/\partial(kT)^2$ in Eq. (2) we can derive that

$$\frac{\partial^2 F}{\partial(kT)^2} = -\frac{(C_1 D\cos\theta)^2}{(kT)^3}\cdot \operatorname{sech}\left[\frac{D\cos\theta}{kT}\right]$$

where $D = \lambda l_z S$. For the turning point in the F-T curve, $\partial^2 F/\partial(kT)^2 = 0$, that is, $\cos\theta = 0$, $\theta = 90°$; or $\operatorname{sech}\left[\frac{D\cos\theta}{kT}\right] \to 0$, meaning that $D \to \infty$ or $T \to 0$. Obviously, a larger D (= $\lambda l_z S$) will inevitably result in a steeper slope, implying a rapid rotation.

References.

1. J. M. D. Coey, H. Roux-Buisson and R. Brusetti, J. de Physique **C4**, 1 (1976).

2. E. Hirahara and M. Murakami, J. Phys. Chem. Solids 7, 281-289 (1958).

3. J. L. Horwood, M. G. Townsend, and A. H. Webster, *J. Solid State Chem.* **17**, 35 (1976).

4. A. F. Andresen and F. Torbo, *Acta Chem. Scand.* **21**, 2841 (1967).

5. K. Adachi, *J. Phys. Soc. Japan* **16** (11), 2187 (1961).

6. K. Adachi and K. Sato, *J. Appl. Phys.* **39** (2), 1343 (1968).

7. K. Sato, *J. Phys. Soc. Japan* **21** (4), 733 (1966).

8. M. Kawaminami and A. Okazaki, *J. Phys. Soc. Japan* **29** (3), 649 (1970).

9. O. Amcoff, T. Ericsson and A. Gismelseed, *Zeit. fur Krist.* **209**, 197 (1994).